



New Approaches to Help Improving the Interpretation of Frequency Response Analysis (FRA) in Power Transformers

By

Regelii Suassuna de Andrade Ferreira

Under the direction of Issouf Fofana, Hassan Ezzaidi and Patrick Picher

Thesis presented to the University of Quebec at Chicoutimi with a view to obtaining the degree of Philosophiae doctor (PhD) in engineering

Defended on 29 June 2022

Jury:

Issouf Fofana, Professor, UQAC, Research Director

Hassan Ezzaidi, Professor, UQAC, Research Co-director

Patrick Picher, Hydro-Québec Research Institute (IREQ), Research Co-director

Stephan Brettschneider, Professor, UQAC, Jury President

Hossein Hemmatjou, Delta Star, Inc., External Member

Abdellah Chehri, Professor, UQAC, Internal Member

Quebec, Canada

© Regelii Suassuna de Andrade Ferreira, 2022

ABSTRACT

Power transformers are one of the most expensive and critical equipment in power networks. The ever-growing energy demand and the increasing age of power transformers population have expanded the interest in this assets' condition monitoring. The electrical industry has been dealing with many transformers that have reached or even passed their designed lifespan. These circumstances can directly affect the reliability of the network operations. Meanwhile, continuous monitoring allows for preventive repairs, planned replacements and increases system reliability.

Among the diverse monitoring and diagnostic techniques, Frequency Response Analysis (FRA) stands out as an important method widely used in the electric industry for condition assessment of the transformer's active part. FRA has demonstrated its sensitivity for detecting various mechanical and electrical failure modes. The method graphically compares the transfer functions of power transformers over a range of frequencies. The deviations from current and previous traces indicate electrical or mechanical changes inside the transformer.

Even though the FRA technique has been well studied at the international level in various working groups of CIGRÉ, IEC, IEEE and Chinese Standard, the interpretation of deviations up until now needs experts' analysis. Ultimately, the FRA measurement procedure has been well standardized. However, the interpretation of results is still challenging and an interesting subject of study.

The challenge of FRA interpretation lies in the complex structure and the design particularities of power transformers. One of the fundamental shortcomings of experimental investigations is the generation of fault modes in real transformers to collect data in different scenarios and study them. This is especially complex due to the destructive characteristics of the faults. Besides, the availability of data from practical faulty transformers is very scarce. Although there has been more and more FRA testing being conducted worldwide, most of this data is not available and most available data is not released in the literature.

To face these challenges, this research has the investigation and advance of FRA interpretation methods as the primary objective. For this purpose, the main interpretation methods for FRA are considered: numerical indices, artificial intelligence algorithms, and high-frequency models. The numerical indices are studied based on their capacity to well quantify deformations in FRA traces. Different algorithms are evaluated over their performance to automatically detect and classify different fault modes, such as axial displacements, radial deformations and short-circuits. The influence of temperature in FRA traces and its effects on automatic classification algorithms are also explored. In addition, a Finite Element Method simulation is used to develop a high-frequency model aiming at the reproduction of FRA traces.

The research is based on the use of a laboratory winding model. One of the model's main features is the non-destructive interchangeability of its winding sections. This characteristic allows the reproducibility and repeatability of frequency response measurements and the possibility to produce and investigate different mechanical and electrical faults by comparing them to the same reference.

The numerical indices analysis indicated that comparative standard deviation produced good results for evaluating deformations on the winding model. This conclusion is based on the index monotonic behaviour, sensitivity, and linear increase with fault severity.

Additionally, the study of different artificial intelligence algorithms (namely support vector machine learning, radial basis function neural networks and the statistical k-nearest neighbour

method) are supportive and presented good accuracy when classifying winding faults and fault extents.

The temperature influence in FRA traces was evaluated from $-40\text{ }^{\circ}\text{C}$ to $40\text{ }^{\circ}\text{C}$. The results show that if the temperature is not considered in the training dataset, the algorithm misclassifies healthy measurements as mechanical or electrical faults.

Finally, numerical simulations based on the Finite Element method have reproduced FRA traces in good agreement with measured reference. Furthermore, once faults are introduced, and automatic classification algorithms evaluate the traces, the short-circuit faults have good classification scores, while axial displacements only present good classification at their highest extents.

The findings presented in this research contribute to the advancement in FRA interpretation methods. These achievements help support the use of the proposed methods in machine learning algorithms and the generation of faulty frequency responses for classification.

RÉSUMÉ

Les transformateurs de puissance sont l'un des équipements les plus coûteux et les plus critiques des réseaux électriques. La croissante constante de la demande d'énergie ainsi que l'âge croissant de la population de transformateurs de puissance ont accru l'intérêt pour la surveillance de l'état de ces actifs. L'industrie électrique a eu affaire à de nombreux transformateurs qui ont atteint ou même dépassé leur durée de vie prévue. Ces circonstances peuvent affecter directement la fiabilité des opérations du réseau. Pendant ce temps, la surveillance continue permet des réparations préventives, des remplacements planifiés et augmente la fiabilité du système.

Parmi les diverses techniques de surveillance et de diagnostic, l'analyse de la réponse en fréquence (FRA) se distingue comme une méthode importante largement utilisée dans l'industrie électrique pour l'évaluation de l'état de la partie active du transformateur. FRA a démontré sa sensibilité pour détecter divers modes de défaillance mécanique et électrique. La méthode compare graphiquement les fonctions de transfert des transformateurs de puissance sur une gamme de fréquences. Les écarts par rapport aux traces réelles et précédentes indiquent des changements électriques ou mécaniques à l'intérieur du transformateur.

Même si la technique FRA a été bien étudiée au niveau international dans divers groupes de travail du CIGRÉ, de l'IEC, de l'IEEE et de la norme chinoise, l'interprétation des écarts jusqu'à présent nécessite l'analyse d'experts. En fin de compte, la procédure de mesure FRA a été bien standardisée. Cependant, l'interprétation des résultats reste un défi et un sujet d'étude attrayant.

Le défi de l'interprétation FRA réside dans la structure complexe et dans les particularités de conception des transformateurs de puissance. L'une des lacunes fondamentales des investigations expérimentales est la génération de modes de défaut dans des transformateurs réels pour collecter des données dans différents scénarios et les étudier. Ceci est particulièrement complexe en raison des caractéristiques destructrices des failles. En outre, la disponibilité de données provenant de transformateurs défectueux pratiques est très rare. Bien que de plus en plus de tests FRA soient effectués dans le monde, la plupart de ces données ne sont pas disponibles et la plupart des données disponibles ne sont pas en libre accès pour la publication.

Pour faire face à ces défis, cette recherche a pour objectif principal l'investigation et l'avancement des méthodes d'interprétation FRA. À cette fin, les principales méthodes d'interprétation de FRA sont considérées : indices numériques, algorithmes d'intelligence artificielle et modèles de simulation haute fréquence. Les indices numériques sont étudiés en fonction de sa capacité à bien quantifier les déformations dans les traces FRA. Différents algorithmes sont évalués sur ses performances pour détecter et classer automatiquement différents modes de défaut, tels que les déplacements axiaux, les déformations radiales et les court-circuit. L'influence de la température dans les traces FRA et ses effets sur les algorithmes de classification automatique sont également explorés. Et enfin, une simulation par la méthode des éléments finis est utilisée pour développer un modèle de simulation haute fréquence visant la reproduction des traces FRA.

La recherche est basée sur l'utilisation d'un modèle de bobinage de laboratoire. L'une des principales caractéristiques du modèle est l'interchangeabilité non destructive de ses sections d'enroulement. Cette caractéristique permet la reproductibilité et la répétabilité des mesures de réponse en fréquence et la possibilité de produire et d'étudier différents défauts mécaniques et électriques en les comparant à la même référence.

L'analyse des indices numériques a indiqué que l'écart-type comparatif produisait de bons résultats pour l'évaluation des déformations sur le modèle d'enroulement. Cette conclusion est basée sur le comportement monotone de l'indice, la sensibilité et l'augmentation linéaire avec la sévérité du défaut.

De plus, l'étude de différents algorithmes d'intelligence artificielle (à savoir l'apprentissage automatique à vecteurs de support, les réseaux de neurones à fonction de base radiale et la méthode statistique des k plus proches voisins) est favorable et présente une bonne précision lors de la classification des défauts d'enroulement et de l'étendue des défauts.

L'influence de la température dans les traces FRA a été évaluée dans une plage de -40 °C à 40 °C. Les résultats montrent que si la température n'est pas prise en compte dans l'ensemble de données d'apprentissage, l'algorithme considère les mesures saines comme étant des défauts mécaniques ou électriques.

Enfin, l'utilisation de simulations numériques basées sur la méthode des éléments finis a reproduit des traces FRA en bon accord avec la référence mesurée. De plus, une fois les défauts introduits et les traces évaluées par les algorithmes de classification automatique, les défauts de court-circuit présentent une bonne classification, tandis que les déplacements axiaux ne présentent une bonne classification qu'à leurs plus hauts degrés.

Les résultats présentés dans cette recherche contribuent à l'avancement des méthodes d'interprétation FRA. Ces réalisations aident à soutenir l'utilisation des méthodes proposées dans les algorithmes d'apprentissage automatique et dans la génération de réponse en fréquence défectueuse pour la classification.

TABLE OF CONTENTS

ABSTRACT	II
RÉSUMÉ	IV
TABLE OF CONTENTS	VI
LIST OF TABLES	VIII
LIST OF FIGURES	IX
LIST OF ABBREVIATIONS AND ACRONYMS	XI
ACKNOWLEDGEMENTS	XIII
CHAPTER I GENERAL INTRODUCTION	1
1.1. INTRODUCTION.....	1
1.2. RESEARCH MOTIVATION AND OBJECTIVES.....	3
1.3. ORIGINALITY OF THE RESEARCH	4
1.4. THESIS ORGANIZATION	7
CHAPTER II LITERATURE REVIEW	9
2.1. FREQUENCY RESPONSE MEASUREMENTS	10
2.2. FREQUENCY RESPONSE INTERPRETATION METHODS	13
2.2.1. NUMERICAL INDICES.....	13
2.2.2. HIGH-FREQUENCY SIMULATION MODELS	19
2.2.3. ARTIFICIAL INTELLIGENCE ALGORITHMS	22
CHAPTER III FREQUENCY RESPONSE ANALYSIS INTERPRETATION USING NUMERICAL INDICES AND MACHINE LEARNING: A CASE STUDY BASED ON A LABORATORY WINDING MODEL	26
3.1. INTRODUCTION.....	28
3.2. FREQUENCY RESPONSE ANALYSIS	29
3.2.1. FRA INTERPRETATION BASED ON NUMERICAL INDICES	31
3.2.2. FRA INTERPRETATION BASED ON MACHINE LEARNING	33
3.3. LABORATORY WINDING MODEL AND REFERENCE MEASUREMENTS.....	38
3.4. FAULT ANALYSES.....	41
3.5. RECOGNITION PERFORMANCE AND DISCUSSION	52
3.6. CONCLUSION.....	57
CHAPTER IV A MACHINE-LEARNING APPROACH TO IDENTIFY THE INFLUENCE OF TEMPERATURE ON FRA MEASUREMENTS	58
4.1. INTRODUCTION.....	60
4.2. MATERIALS AND METHODS	62
4.2.1. LABORATORY SETUP	62
4.2.2. NUMERICAL INDEX CALCULATION	66
4.2.3. SUPPORT VECTOR MACHINE LEARNING	68
4.3. TEMPERATURE INFLUENCE IN FREQUENCY RESPONSE	70
4.4. NUMERICAL INDEX RESULTS.....	75
4.5. CLASSIFICATION ALGORITHM RESULTS AND DISCUSSIONS.....	77
4.6. CONCLUSIONS.....	81
CHAPTER V REPRODUCING TRANSFORMER'S FREQUENCY RESPONSE FROM FEM SIMULATION AND PARAMETERS OPTIMIZATION	83
5.1. INTRODUCTION.....	85
5.2. MATERIALS AND METHODS	87

5.2.1. LABORATORY WINDING-MODEL.....	87
5.2.2. FINITE ELEMENT METHOD SIMULATION	88
5.2.3. OPTIMIZATION OF CIRCUIT PARAMETERS	91
5.2.4. EVALUATION OF SIMULATION MODEL	91
5.3. SIMULATED FREQUENCY RESPONSE OF WINDING MODEL	93
5.4. WINDING-MODEL FAULT ANALYSIS AND CLASSIFICATION PERFORMANCE.....	98
5.5. CONCLUSIONS.....	102
CHAPTER VI CONCLUSION	104
6.1. SUMMARY AND MAJOR FINDINGS	104
6.2. RESEARCH CONTRIBUTIONS	105
6.3. FUTURE OF THE RESEARCH AND RECOMMENDATIONS	107
REFERENCES.....	108

LIST OF TABLES

TABLE II.1 SUMMARY OF NUMERICAL INDICES USED FOR FRA INTERPRETATION [17, 37, 38].....	15
TABLE II.2 INTERPRETATION CRITERIA USED IN CHINESE STANDARD [22].....	16
TABLE III.1 SUMMARY OF NUMERICAL INDICES USED IN THIS RESEARCH	32
TABLE V.1 INITIAL VALUES FOR CAPACITANCE PARAMETERS IN FREQUENCY RESPONSE SIMULATION.....	97
TABLE V.2 OPTIMIZED VALUES FOR CAPACITANCE PARAMETERS IN FREQUENCY RESPONSE SIMULATION.....	97
TABLE V.3 AUTOMATIC CLASSIFICATION USING SUPPORT VECTOR MACHINE ALGORITHM [56] AND FRA TRACES OBTAINED FROM SIMULATION	102

LIST OF FIGURES

FIGURE I.1 FAILURE MODE BASED ON 799 FAILURES OF SUBSTATION TRANSFORMERS.....	2
FIGURE I.2 FAILURE LOCATION BASED ON 675 FAILURES OF SUBSTATION TRANSFORMERS ABOVE 100 KV	3
FIGURE II.1 FRA MEASUREMENT CONNECTIONS (A) END-TO-END OPEN-CIRCUIT, (B) END-TO-END SHORT-CIRCUIT, (C) CAPACITIVE INTER-WINDING AND (D) INDUCTIVE INTER-WINDING SOURCE: SUASSUNA DE ANDRADE FERREIRA, 2022	11
FIGURE II.2 END-TO-END OPEN-CIRCUIT DETAILS	12
FIGURE II.3 MAIN REGIONS OF A FREQUENCY RESPONSE SOURCE: SUASSUNA DE ANDRADE FERREIRA, 2022, ADAPTED FROM IEC 60076-18, 2012 [20]	17
FIGURE II.4 PRINCIPLE OF SWEEP FREQUENCY WINDOW APPROACH SOURCE: SUASSUNA DE ANDRADE FERREIRA, 2022, ADAPTED FROM TAHIR AND TENBOHLEN, 2019 [31].....	19
FIGURE II.5 LUMPED ELEMENTS FOR A TWO-WINDING TRANSFORMER SOURCE: ABEYWICKRAMA, SERDYUK AND GUBANSKI, 2008. [33]	21
FIGURE III.1 RADIAL BASIS FUNCTION NEURAL NETWORK ARCHITECTURE	35
FIGURE III.2 MODEL FOR LABORATORY TESTS: (A) WINDING PHOTO, (B) DIMENSIONS AND (C) CONNECTIONS SCHEMATIC	39
FIGURE III.3 FRA REFERENCE MEASUREMENTS AT (A) WINDING 1 AND (B) WINDING 2	40
FIGURE III.4 WINDING MODEL REPRESENTATION OF FAULT MODES: (A) HEALTHY STATE; (B) AXIAL DISPLACEMENT; (C) RADIAL DEFORMATION; (D) DISC SPACE VARIATION; AND (E) SHORTED TURNS.....	42
FIGURE III.5 FRA MEASUREMENTS FOR THE DIFFERENT FAULT MODES: (A) AXIAL DISPLACEMENT; (B) RADIAL DEFORMATION; (C) DISC SPACE VARIATION; AND (D) SHORTED TURNS.....	45
FIGURE III.6 FREQUENCY RESPONSE AT A FREQUENCY RANGE AFFECTED IN FAULT MODE: FROM 400 KHZ TO 700 KHZ FOR (A) AXIAL DISPLACEMENT, (B) RADIAL DEFORMATION, (C) DISC SPACE VARIATION AND (D) SHORTED TURNS; AND FROM 20 KHZ TO 50 KHZ FOR (E) SHORTED TURNS.....	48
FIGURE III.7 NUMERICAL INDEX ANALYSES FOR FAULT MODES (A) AXIAL DISPLACEMENT; (B) RADIAL DEFORMATION; (C) DISC SPACE VARIATION; AND (D) SHORTED TURNS.....	50
FIGURE III.8 NUMERICAL INDICES AND FREQUENCY RANGE EVALUATION FOR (A) AXIAL DISPLACEMENT AND (B) SHORTED TURNS FAULTS	52
FIGURE III.9 MACHINE LEARNING ARCHITECTURE PERFORMANCES: (A) RADIAL BASIS FUNCTION NEURAL NETWORK; (B) SUPPORT-VECTOR MACHINE; AND (C) STATISTICAL K-NEAREST NEIGHBOUR	55
FIGURE IV.1 LABORATORY WINDING MODEL USED FOR FRA TESTS: (A) PHOTO AND (B) CONNECTION SCHEMATIC	63
FIGURE IV.2 LABORATORY WINDING MODEL: (A) HEALTHY STATE, (B) AXIAL DISPLACEMENT, (C) RADIAL DEFORMATION, (D) DISC SPACE VARIATION AND (E) SHORTED TURNS.....	65
FIGURE IV.3 WINDING 1 SECTIONS: (A) HEALTHY SECTION: (B) AND (C) RADIALLY DEFORMED SECTIONS.....	66
FIGURE IV.4 FLOWCHART FOR CLASSIFICATION METHODOLOGY	70

FIGURE IV.5 FRA MEASUREMENTS IN WINDING 1 AT DIFFERENT TEMPERATURES: (A) COMPLETE FREQUENCY RANGE; AND (B) ZOOMED-IN PORTION AT THE FIRST ANTI-RESONANCE POINT	71
FIGURE IV.6 CAPACITANCE VARIATION WITH TEMPERATURE CHANGE SOURCE: SUASSUNA DE ANDRADE FERREIRA, 2021	75
FIGURE IV.7 CSD VALUES, CALCULATED FOR FRA MEASUREMENTS AT 40 °C, 20 °C AND -40 °C SOURCE: SUASSUNA DE ANDRADE FERREIRA, 2021	76
FIGURE IV.8 CSD VALUES CALCULATED FOR FRA MEASUREMENTS IN DIFFERENT FAULT MODES AT 20 °C SOURCE: SUASSUNA DE ANDRADE FERREIRA, 2021	77
FIGURE IV.9 CONFUSION MATRICES FOR FAULT DATABASE CLASSIFICATION (CLASSIFICATION SCENARIO 1) USING THE FOLLOWING AS INPUT: (A) CSD VECTOR VALUES, (B) RESONANCE AND ANTI-RESONANCE POINTS (FREQUENCY AND AMPLITUDE) AND (C) COMBINED INPUT	78
FIGURE IV.10 CONFUSION MATRICES USING TEMPERATURE DATABASE TO TEST THE SVM CLASSIFICATION ALGORITHM (CLASSIFICATION SCENARIO 2) WITH THE FOLLOWING AS INPUT: (A) CSD VECTOR VALUES AND (B) COMBINED INPUT WITH CSD VECTOR AND RESONANCES AND ANTI-RESONANCES	80
FIGURE V.1 WINDING- MODEL USED FOR SIMULATION AND MEASUREMENT PURPOSES: (A) MODEL'S PICTURE AND (B) CONNECTIONS SCHEMATIC	88
FIGURE V.2 GEOMETRIC MODEL CREATED FOR SIMULATION OF THE FREQUENCY RESPONSE (A) 2D AXISYMMETRIC GEOMETRY, (B) ROTATIONAL FORM OF 2D AXISYMMETRIC MODEL AND (C) DETAIL OF CONDUCTORS AND INSULATION FROM WINDINGS 1 AND 2 SOURCE: SUASSUNA DE ANDRADE FERREIRA, 2022	89
FIGURE V.3 CURRENT DENSITY IN THE CONDUCTORS' SECTION AREA AT (A) 60 HZ, (B) 10 KHZ AND (C) 1 MHZ, (D) ZOOMED PORTION AT 1 MHZ SOURCE: SUASSUNA DE ANDRADE FERREIRA, 2022	90
FIGURE V.4 FRA MEASUREMENT SCHEMATIC FOR WINDING 1 OPEN CIRCUIT MEASUREMENT SOURCE: SUASSUNA DE ANDRADE FERREIRA, 2022	90
FIGURE V.5 LUMPED ELEMENT CIRCUIT USED TO OBTAIN THE SIMULATED FREQUENCY RESPONSE FOR THE WINDING-MODEL SOURCE: SUASSUNA DE ANDRADE FERREIRA, 2022	94
FIGURE V.6 FREQUENCY RESPONSE MEASUREMENTS (A) INDIVIDUAL WINDING MEASUREMENTS AND (B) CAPACITIVE INTERWINDING MEASUREMENT	96
FIGURE V.7 FRA MEASUREMENT SCHEMATIC FOR INTERWINDING CAPACITIVE MEASUREMENT SOURCE: SUASSUNA DE ANDRADE FERREIRA, 2022	97
FIGURE V.8 FREQUENCY RESPONSE FROM WINDING MODEL MEASUREMENT AND SIMULATION USING INITIAL ESTIMATED VALUES	97
FIGURE V.9 FREQUENCY RESPONSE FROM WINDING MODEL MEASUREMENT AND SIMULATION USING OPTIMIZED CAPACITANCE VALUES	98
FIGURE V.10 WINDING MODEL FREQUENCY RESPONSE SIMULATED FOR: (A) AXIAL DISPLACEMENT AND (B) SHORT-CIRCUIT FAULTS	100
FIGURE V.11 ENERGY DENSITY DISTRIBUTION (J/M3) FOR WINDING MODEL SIMULATION AT 50 KHZ FOR: (A) REFERENCE (NO-FAULT), (B) AXIAL DISPLACEMENT (AD2) AND (C) SHORT-CIRCUIT (SC1) FAULTS	101

LIST OF ABBREVIATIONS AND ACRONYMS

FRA: Frequency Response Analysis	ID: Integral of Difference
LVI: Low Voltage Impulse	MAX: Maximum of Difference
CIGRE: International Council on Large Electric Systems	SDA: Standardized Difference Area
IEC: International Electrotechnical Commission	MM: Minimum-maximum ratio
IEEE: Institute of Electrical and Electronics Engineers	ASLE: Absolute Sum of Logarithmic Error
FEM: Finite Element Method	MAD: Mean Amplitude Deviation
RLC: Resistor, Inductor, and Capacitor	MFD: Mean Frequency Deviation
AI: Artificial intelligence	W_a : Weighted Amplitude Function
LF: Low-Frequency	W_f : Weighted Frequency Function
MF: Medium-Frequency	IAD: Index of Amplitude Deviation
HF: High-Frequency	IFD: Index of Frequency Deviation
R_{XY} : Relative Factor	IFR: Index of Frequency Ratio
CSD: Comparative Standard Deviation	IAR: Index of Amplitude Ratio
CCF: Cross Correlation Factor	VF: Vector Fitting
LCC: Lin's Concordance Coefficient	LVQ: Learning Vector Quantization
SSE: Sum Squared Error	2D: Two-Dimensions
SSRE: Sum Squared Ratio Error	3D: Three-Dimensions
CC: Correlation Coefficient	SVM: Support Vector Machine
ED: Euclidean Distance	RBF: Radial Basis Function
CD: Complex Distance	k-NN: k-Nearest Neighbour
E: Expectation	DT: Decision Tree
SD: Standard Deviation	BP: Backpropagation
σ_e : Standard Deviation	PNN: Probabilistic Neural Network
SDD: Standard Deviation of Difference	ISDA: Iterative Single Data Algorithm
RMSE: Root Mean Square Error	AD: Axial Displacement
	RD: Radial Deformation
	DSV: Disc Space Variation

ST: Short-circuited Turns	$f_{p/d}$: Frequency data points per decade
H_{dB} : Frequency response amplitude in dB	WS: Frequency Window Sweep
CIW_{dB} : Capacitive interwinding frequency response amplitude in dB	W_{step} : Frequency Window Step
Z: Impedance	L: Inductance
Y: Admittance	C: Capacitance
ε : Dielectric permittivity	C_s : Series capacitance
$\hat{\varepsilon}$: Complex dielectric permittivity	C_{12} : Interwinding capacitance
ε' : Real part of the dielectric permittivity	C_g : Ground capacitance
ε'' : Imaginary part of the dielectric permittivity	ω : Angular frequency (rad)
σ : Conductivity	dB: Decibel
T: Temperature	rad: Radian
f_{res} : Resonance frequency	$^{\circ}C$: Degree Celsius
	J/m^3 : Joules per cubic meter
	Ω : Ohm

ACKNOWLEDGEMENTS

This project would not have been possible without the support and collaboration of many people to whom I would like here to express my deepest gratitude.

Thank you to my thesis director Issouf Fofana for welcoming me into his team and guiding me through the past four years. Thank you for your support on this entire project. To my co-director Patrick Picher for his availability, rigour and advice, which allowed me to carry out this thesis. And to my co-director, professor Hassan-Ezzaidi for his supervision and support of the research. Thank you all for believing in the project and my potential to achieve the results.

I would also like to express my gratitude to the professors: Vahid Behjat, Fethi Meghnefi and Christophe Volat, that have been available to discuss and help me on this research project. Thank you for the technical support.

Thanks to the Université du Québec à Chicoutimi for welcoming me, to its administrative staff that helped me over the years and for the financial support.

I am grateful to the Research Chair on the Aging of Power Network Infrastructure (ViAHT), who presented me with great lab friends and supported me financially over this project. To the friends I made in the research team, my most grateful thank you for their cooperation, moral and technical support, and encouragement. Particularly, I would like to extend my thanks to Jaya Sree Thota, Marie Lucia Yapi, Najmeh Seifaddini, Ghada Gmati, Fataneh Zarandi, Mohan Rao Ungarala, Luc Loiselle, Simplicie Akéré, Moise Agouassi, Samson Okikiola, Bekibenan Sékongo and Simon Kassi.

My ultimate gratitude to my family. My parents: Rosangela and Cristovão, for being present throughout my trajectory and always encouraging me to dedicate myself to study. I was able to reach so far because you taught me the virtues of hardworking and perseverance. My sister and brother: Calliandra and Junior, for the company, for the laughs and for listening to me, even when they did not understand me. My boyfriend: Mathieu, for supporting me in my difficulties and for listening to me. I thank them all for always being with open arms to share my dreams. I am grateful for my family's unconditional, unequivocal, and loving support.

Finally, I would like to extend my gratitude to the people in my life, my friends in Brazil, my new friends I made in Québec, my in-law family, and my adoptive family in Quebec. Specially, but not only, to: Joanie Dallaire, Julie Sauvageau, Mario Dallaire, Sophie Lacombe, Felipe Fideles, Filipe Lucena and Ramon Dias. They all help me in different ways to pass through my doctoral studies.

CHAPTER I

GENERAL INTRODUCTION

1.1. INTRODUCTION

Our world has been facing a global challenge: to provide sufficient and reliable energy to its people. On the one hand, the energy demand is constantly growing. On the other, energy resources are limited, and more and more renewable energies should be used in a perspective of sustainable development. In addition, the energy supply for all at an affordable price should be ensured. To meet these challenges, the reliable operation of the existing electricity infrastructure in conciliation with new and more technological equipment must be sought.

In this context, power transformers are one of the most crucial equipment in power transmission and distribution networks. Any malfunction of this equipment can lead to hazardous conditions. Due to their great importance, transformers must be periodically evaluated to ensure the reliable operation of the system. Extreme reliability is required because failures inevitably lead to high repair costs, long downtimes, and possible risks to life safety. According to the CIGRE's guide to the economics of transformer management [1], can reduce the risk of catastrophic failures by 50%, early detection of problems can reduce repair costs by 75% and revenue loss by 60%.

Mechanical failures, as an example, are mainly related to vibration and winding deformations due to high mechanical forces generated by fault currents [2]. These forces can be identified as radial and axial forces [5] and can produce significant mechanical damage on the windings. Once such deformations occur, the transformer's ability to withstand further mechanical forces originating in potential through the fault current is significantly reduced due to localized electromagnetic stresses [6]. In addition, dielectric failures can also be originated from mechanical defects due to dielectric strength loss in insulating materials [3]. Ultimately, major failures must be avoided to maintain the transformer's good system operation conditions.

Thus, the industry has been developing efficient and reliable monitoring and diagnostic techniques to detect incipient failures.

The main causes of power transformers' failures are dielectric, electric, mechanical, chemical, or thermal origins. According to [4], illustrated in Figure I.1, the failure in substation transformers are approximately 38% from dielectric causes, 22% from mechanical causes and 18% from electrical causes. Accounting for almost 80% of all substation transformer failures, dielectric, mechanical and electrical are the most common conditions monitored in transformers.

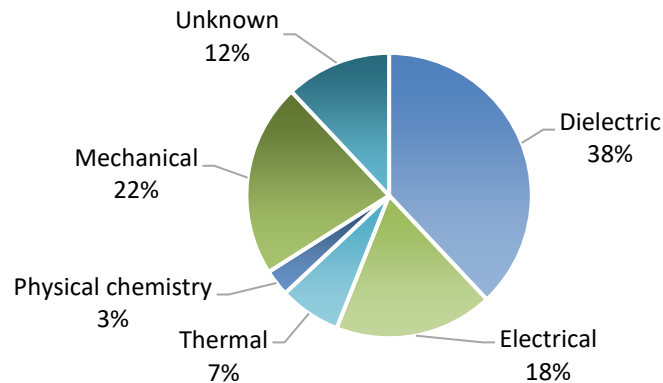


Figure I.1 Failure mode based on 799 failures of substation transformers
Source: Suassuna de Andrade Ferreira, 2022, adapted from Tenbohlen et al., 2017 [4]

In relation to the failure location in power transformers, the windings have the most significant contribution (40%), along with the tap changer (30%) and the bushings (17%). This data is based on a survey on transformers' reliability from CIGRE's working group A2.37 [5]. The statistics presented in the mentioned survey are illustrated in Figure I.2.

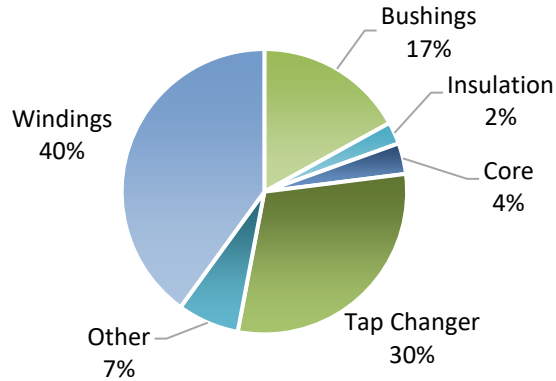


Figure I.2 Failure location based on 675 failures of substation transformers above 100 kV
 Source: Suassuna de Andrade Ferreira, 2022, adapted from CIGRE Technical Brochure 642, 2015 [5] and Islam, Lee and Hettiwatte [6]

Based on the data presented in these surveys, it is possible to notice that transformer integrity depends on multiple factors. Hence the importance of using monitoring and diagnostic methods to evaluate different components.

Frequent methods used for monitoring and diagnostics of fault conditions in power transformers are dissolved gas analysis [7], capacitance and power factor measurements [6], excitation current measurement [8], partial discharge measurement [9], polarization and depolarization current measurement [10], Frequency Response Analysis (FRA) [11-14], among others. Each of these methods is used for the analysis of specific conditions. FRA is currently well known and used in the electrical industry for condition assessment of transformer windings.

1.2. RESEARCH MOTIVATION AND OBJECTIVES

From the first studies [15], FRA has demonstrated its sensitivity for detecting mechanical and electrical failure modes [16, 17]. The method is very sensitive to changes in the transformer windings [18, 19]. Comparing two frequency response measurements can present deviations from changes inside the transformer. For example, frequency response measurements are used to detect mechanical defects during transformer transportation; a

measurement is taken at the manufacturer, and another is taken at the installation site. The comparison of measurements can indicate if mechanical changes have occurred. Therefore, FRA must compare two measurements: a reference and an after-event.

The interpretation of frequency response measurements can lead to identifying the deformation type, its magnitude, and its location in the transformer. Even though the FRA measurement procedure has been discussed and well standardized at the international level in working groups of CIGRE [16], IEC [20], IEEE [21] and Chinese Standards [22], the literature review has shown that objective interpretation is still unresolved [17]. In fact, FRA interpretation is usually performed with the aid of experts since there is no reliable algorithm for its interpretation [23, 24].

FRA objective interpretation is a concern that requires more investigation. The present research aims to study and improve FRA interpretation by analyzing different influences in FRA measurements and developing methods for automatic interpretation of FRA in power transformers. To attain this main goal, the following objectives are defined:

- Identify indices suitable for assessing the mechanical deformation severity;
- Investigate machine learning algorithms for automatic faults classification;
- Study the impact of temperature on FRA traces for automatic fault classification;
- Develop a new approach for modelling frequency response from Finite Element Method simulation using lumped elements circuit and parameters' optimization.

1.3. ORIGINALITY OF THE RESEARCH

The main advantage of the proposed approach is the opportunity to investigate a large number of failure modes and different failure extents on the same unit, compared to past studies that used limited databases and real transformers, which can be problematic to

interpret. It, therefore, seems reasonable to affirm that this research paves the way for improvement in the diagnostic methods.

Based on these premises and to the best knowledge of the author, the following contributions are original to the field of research:

- The use of a winding model that allows the introduction of faults without physical damage to the structure.

Due to the limited availability of real case transformer studies, researchers have been working with the generation of FRA data from laboratory winding models that can be physically modified to simulate failures [24-26]. However, the main advantage of the winding model used in this research is the possibility of introducing faults such as mechanical deformations and electrical faults and returning the model to its healthy state.

- The investigation of FRA measurements under a wide range of temperatures (-40 °C to 40 °C).

The literature has studied the influence of temperature on FRA measurements [27, 28]. Still, the use of a climatic chamber allowing the entire winding model to be exposed to temperatures as low as -40 °C has not yet been investigated.

- The evaluation of the performance of automatic classifiers in discriminating among different faults (axial displacement, radial deformation, disc-space variation, and short-circuit) and healthy measurements taken at different temperatures.

Automatic fault classifiers are well used in the literature [29, 30]. However, the impact of temperature measurements on the fault's classification has never been explored.

- The new study of numerical indices and machine learning algorithms optimization applied to an FRA measurements database.

This project studied numerical indices, machine learning algorithms, and the optimization of different parameters. The study focused on the advance in fault classification. It included: the evaluation of the best numerical index suitable for the FRA database, the use of numerical indices individually or in a combination, and the optimization of algorithms parameters. The combination of these studies in developing improved algorithms for faults classification using FRA traces has not been previously found in the literature.

- The application of the sweep frequency window approach for numerical index calculation is used in algorithms for automatic faults classification.

The sweep frequency window approach presented in [31] is used to obtain a numerical index vector to characterize FRA traces and then as input for faults' classification. This approach has not been previously used as input to automatic classification algorithms.

- The novel approach for FEM simulation of transformer's frequency response tailored for generating infinite and unique database for the training of classification algorithms with the potential impact on FRA interpretation improvements.

High-frequency models for FRA in transformers using FEM simulation and RLC lumped circuit elements have been already explored in the literature individually [25, 32] and combined [33]. Nonetheless, the parameters optimization for capacitance calculations allows the simplification of calculations and has not yet been investigated.

The present research contributes to the electrical industry by supporting decision-making tools for maintenance, repair, or replacing power transformers. This is timely and potentially impacts both academic and industrial levels. Therefore, it seems reasonable to affirm that this research paves the way for improvement in the diagnostic methods.

1.4. THESIS ORGANIZATION

The structure of the present research work focuses on the accomplishment of the objectives detailed earlier. The specific objectives were achieved by the publication of two research articles in renowned journals in the electrical engineering field and by a third article that is currently under revision before submission. This thesis is organised as follows to present the results accomplished and discuss the literature review on the research topic.

The first chapter presents a general introduction to the power transformer's monitoring and diagnostic subject along with the motivation, the main objectives and the originalities of the work.

In the second chapter, a literature review comprising the background on frequency response analysis and frequency response interpretation is present.

Chapter 3 presents the two first objectives of this research: identify indices suitable for assessing the mechanical deformation severity and investigate machine learning algorithms for automatic faults classification. These objectives were presented in publication 1 for the IEEE Access journal: "Frequency Response Analysis Interpretation using Numerical Indices and Machine Learning: A case study based on a Laboratory Winding Model".

Chapter 4 presents the third objective of this research: to study the impact of temperature on FRA traces for automatic fault classification. This objective was presented in publication 2 for the MDPI Energies journal: "A Machine Learning Approach to Identify the Influence of Temperature on FRA Measurements".

Chapter 5 presents the fourth objective of this research: to develop a new approach for modelling frequency response from Finite Element Method simulation using lumped elements circuit and parameters' optimization. This objective is presented in publication 3 to be submitted to the MDPI Energies journal: "Reproducing Transformer's Frequency Response from FEM simulation and Parameters Optimization".

Finally, in Chapter 6, the findings and contributions of the research are summarized, and the scope for future development of the research is presented.

CHAPTER II

LITERATURE REVIEW

During their lifetime, power transformers can experience atmospheric discharges, short-circuits, energizations, and overloads. Those occurrences can cause the transformer's thermal, chemical, dielectric, and mechanical failures. The study in [34] identified that these failures' main locations are in the transformers' components such as bushings, windings, tank, on-load tap-changer, core, oil and insulation. For example, mechanical failures usually occur due to movements and vibrations within the transformers and affect the windings and the solid insulation of the power transformer. The main cause for winding movements is the mechanical forces generated at current-carrying conductors. Any current-carrying conductor in the presence of alternating magnetic flux density will be affected by forces. Thus, deformations are a result of elevated forces due to overcurrent. Transportation of transformers is also a concern for mechanical deformations. Usually, windings deformations during transports occur due to loosening conditions that lead to the displacement of windings or insulation damage.

Due to the failures that can occur in the power transformer, its importance to the electric industry, and its high financial cost, power transformers' reliable and efficient operation are topics of constant concern. Modern monitoring and diagnostic methods aim to ensure optimal power transfer and lifetime of the transformers. Monitoring procedures to detect mechanical deformations are Frequency Response Analysis (FRA) or the time domain low-voltage impulse (LVI) method. FRA has been proven more efficient [15] and is more widely used today than the LVI method. In industry, FRA is one of the most commonly used techniques to detect and identify faults in the active part of power transformers [35].

The FRA method can detect faults based on the changes caused to internal inductances, resistances and capacitances of the transformer equivalent RLC circuit. Since a transformer can be considered a complex network of RLC components representing the resistances of windings, inductances of coils and capacitance from the insulation layers, a

variation in the frequency response may indicate a physical change in these parameters. Thus, once a fault occurs, deviations will be present in the frequency response of the transformer allowing the fault detection and, further, its identification.

2.1. FREQUENCY RESPONSE MEASUREMENTS

The first studies for detecting mechanical deformations with transfer function methods date from the 1960s with the LVI method proposed by Lech and Tyminski in Poland [36]. In the late 1970s, Dick and Erven at Ontario Hydro (Canada) pioneered the FRA method by injecting a frequency sweep sinusoidal signal and directly measuring the frequency response [15]. The main advantage of the method proposed by Dick and Erven is that the same voltage is applied at all frequencies ensuring less influence from external electromagnetic disturbances. The method is also less dependent on the test set-up, leading to simplified interpretation of results and better repeatability. In the 1990s, the FRA technique was developed internationally. It was presented at international conferences and technical meetings along with the development of the first commercially built systems for FRA measurements on-site.

As Dick and Erven [15] proposed, the FRA obtains a measurement at each frequency by injecting a sinusoidal waveform with constant amplitude to one of the terminals of the transformer (input point). The frequency response is measured in terms of its amplitude (dB) and phase (degrees) at another available terminal (output point). There are four main and standardized connections to obtain different responses regarding the transformer windings [16, 20, 21]. These connection types are divided into two groups: end-to-end measurements and inter-winding measurements. Figure II.1 presents the standard FRA connections.

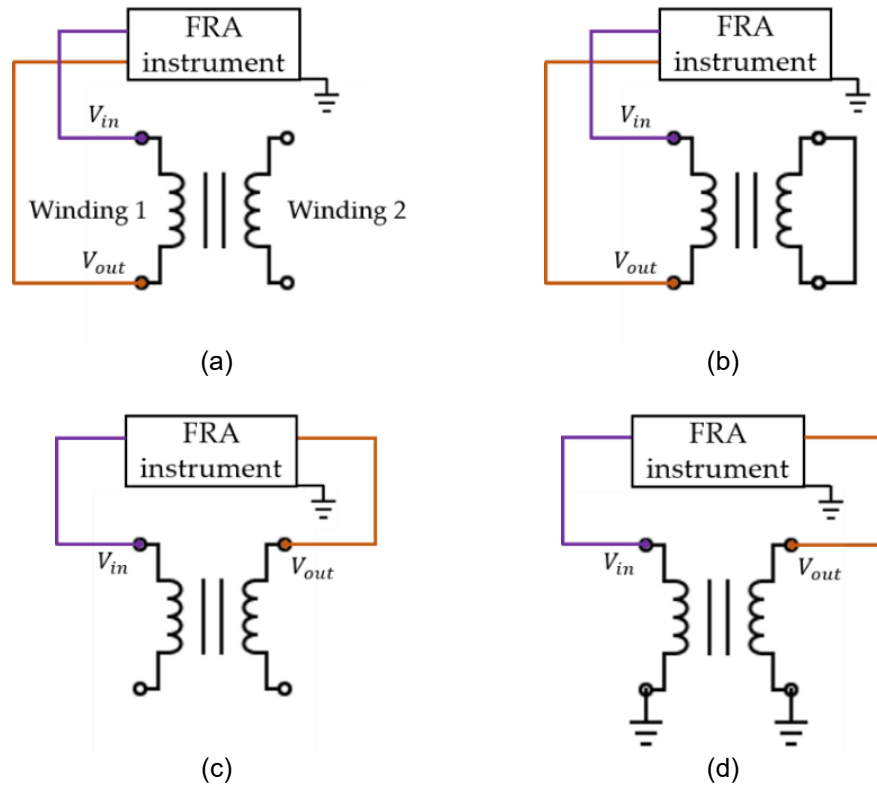


Figure II.1 FRA measurement connections (a) end-to-end open-circuit, (b) end-to-end short-circuit, (c) capacitive inter-winding and (d) inductive inter-winding
Source: Suassuna de Andrade Ferreira, 2022

The end-to-end measurements apply the input signal (V_{in}) to one end of the winding and read the output signal (V_{out}) at the other end on the same winding. In the case of end-to-end open circuit measurement, the other windings in the same phase are left open (Figure II.1a). For this connection, the magnetizing inductance is the main parameter to characterize the low-frequency region (before the first resonance). For the end-to-end measurement group, the other windings can also be shorted for a short-circuit measurement (Figure II.1b). At this configuration, the core influence is removed and the leakage inductance characterizes the low-frequency region. As a result, the first resonance is displaced to higher frequencies. The end-to-end measurements group is more commonly used in FRA interpretation due to the possibility of individual winding analysis [16].

The inter-winding measurements apply V_{in} to one winding and read the V_{out} at another winding on the same phase. The low-frequency region of these measurements is characterized

depending on the conditions of the other endings of the windings. If the windings are left open (Figure II.1c), the low-frequency region represents the inter-winding capacitances. When both windings are grounded (Figure II.1d), the same frequency region is now characterized by the windings turn ratio.

To illustrate the details of the FRA measurement, Figure II.2 shows the representation of the electrical circuit used to obtain the frequency response. The impedance measurement is represented as a $50\ \Omega$ resistance as this value is frequently observed in commercial FRA instruments.

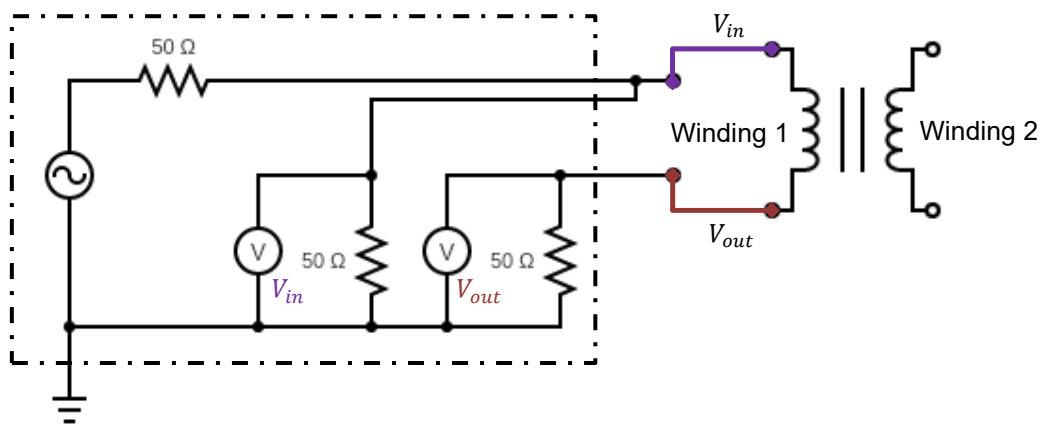


Figure II.2 End-to-end open-circuit details
Source: Suassuna de Andrade Ferreira, 2022

After the measurements are taken, the frequency response can be presented in terms of amplitude (H_{dB}) and phase (φ). To calculate the response from the measured voltages, equations (II.1) and (II.2) are used,

$$H_{dB} = 20 \cdot \log_{10} \left(\frac{V_{out}}{V_{in}} \right), \quad (II.1)$$

$$\varphi = \varphi(V_{out}) - \varphi(V_{in}). \quad (II.2)$$

The interpretation of frequency response is then accomplished by comparing current and reference measurements. The reference measurement is ideally from the same transformer in a previous time (before fault). However, in the absence of previous measurements, comparing different phases for a three-phase transformer or between sister

unit transformers can provide FRA interpretation [16]. In addition, both measurements (current and reference) should use the same measurement connections and similar conditions.

The challenge when utilizing FRA to diagnose the transformer active part lies mainly in correctly interpreting deviations from current and reference measurements. Previous studies have resulted in a well-standardized FRA procedure; thus, measurements comparison should not face problems [16, 20-22]. Nonetheless, a comparison needs to result in the identification of the current condition of the transformer. The interpretation should be able to provide a decision on whether the transformer can continue its reliable operation, should be repaired, or has achieved its end-of-life. Moreover, in the case of a defect, it should be able to point to its type, extent, and location.

2.2. FREQUENCY RESPONSE INTERPRETATION METHODS

The currently available FRA interpretation methods are based on subjective visual inspection of curves and need experts' decisions to determine the transformer conditions [23, 24]. Thus, research studies have been focused on investigating FRA interpretation methods to overcome experts' dependency and develop an objective interpretation of trace deviations. The main interpretation methods are based on: numerical indices [37, 38], high-frequency simulation models [25, 33], artificial intelligence algorithms [29, 39-41], or a combination of different methods. Moreover, the traces used in FRA interpretation research are predominantly obtained from real case transformers [24, 42], laboratory experiments [43] or simulation studies [44-46]. The main interpretation methods are further described in the following topics.

2.2.1. NUMERICAL INDICES

Numerical indices are one of the most common and intuitive methods for quantification of variation between two frequency response measurements. There are two main groups for

indices: indices calculated directly from FRA vectors (amplitude and sometimes phase) and indices based on resonance and anti-resonance points [17, 37, 38]. Moreover, indices can exhibit different sensitivities regarding amplitude and frequency variations. For example, correlation coefficients are not influenced by constant amplitude deviations. Table II.1, presents examples of numerical indices with their abbreviation and some references that used them for FRA interpretation.

A good numerical index should present characteristics such as monotonicity, linearity and sensitivity [35]. A monotonous index will present a higher value for higher faults extent. The linear relation between the deformation degree and the index value is desired. The sensitivity should be related to the type of defect under analysis; different indices will be more suitable for specific defects.

Moreover, to be able to well identify faults in transformers' active part, the interpretation should be based on thresholds to determine the limits from no-fault and slight deformation index values. One of the most well-known applications of numerical indices using defined index limits is the Chinese Standard [20]. The standard calculates a relative factor (R_{XY}) based on variance and covariance and sets thresholds for winding deformation assessment. The interpretation is based on the values calculated for three frequency ranges: low-frequency (LF) from 1 to 100 kHz; medium-frequency (MF) from 100 to 600 kHz; and high-frequency (HF) from 600 to 1000 kHz. The thresholds proposed by the Chinese Standard [20] are presented in Table II.2.

Nonetheless, these limits are unclear in describing the differences between the deformation levels [36]. Namely, a slight deformation identified using the Chinese Standard limits does not indicate whether the power transformer needs to be taken out of operation for repairs or its reliable operation can continue.

Table II.1 Summary of numerical indices used for FRA interpretation [17, 37, 38]

Indices Definition	Abbreviation	References
Cross Correlation Factor	CCF	[22, 47-49]
Correlation Coefficient	CC	[41, 50, 51]
Euclidean Distance	ED	[41, 52]
Complex Distance	CD	[53, 54]
Expectation	E	[48]
Standard Deviation	SD, σ_e	[48, 50, 55]
Standard Deviation of Difference	SDD	[31]
Comparative Standard Deviation	CSD	[53, 56]
Sum Squared Ratio Error	SSRE	[41, 52, 57]
Sum Squared Error	SSE	[41, 52, 53, 57]
Root Mean Square Error	RMSE	[58]
Integral of Difference	ID	[59]
Maximum of Difference	MAX	[52, 59]
Standardized Difference Area	SDA	[19]
Minimum-maximum ratio	MM	[53, 60]
Absolute Sum of Logarithmic Error	ASLE	[50, 57]
Mean Amplitude Deviation	MAD	[48]
Mean Frequency Deviation	MFD	[48]
Weighted Amplitude Function	W_a	[19, 59]
Weighted Frequency Function	W_f	[19, 52]
Index of Amplitude Deviation	IAD	[19, 61]
Index of Frequency Deviation	IFD	[19, 61]
Lin's concordance coefficient	LCC	[24, 62]

Source: Suassuna de Andrade Ferreira, 2022

Studies such as those presented in [43, 48, 51] have researched the application of Chinese Standard for the detection of axial displacement [43, 48] and radial deformation [51] on real case transformers [48, 51] or laboratory models [43].

Table II.2 Interpretation criteria used in Chinese Standard [22]

Relative Factor (R_{XY})	Winding Deformation Degree
$R_{LF} < 0.6$	Severe Deformation
$0.6 \leq R_{LF} < 1.0$ or $R_{MF} < 0.6$	Obvious Deformation
$1.0 \leq R_{LF} < 2.0$ or $0.6 \leq R_{MF} < 1.0$	Slight Deformation
$R_{LF} \geq 2.0$ and $R_{MF} \geq 1.0$ and $R_{HF} \geq 0.6$	Normal Winding

Source: The Electric Power Industry Standard of People's Republic of China, DL/T 911 2016 [22]

As the Chinese Standard [22] demonstrates, the numerical index calculation frequency band is of great importance in determining the faults' classification. Different methods can be used to determine such frequency divisions. The simplest is to evaluate the entire frequency range. For example, using one frequency band from a few Hz, usually 10 or 20 Hz, up to 1 or 2 MHz, as described in [30, 50, 51], or from 100 kHz up to 1 MHz, presented in [63, 64]. This approach, however, can result in a lack of sensitivity to deviations concentrated in small ranges of the frequency response. The division of the frequency range into sub-bands is, accordingly, usually explored [20].

The literature shows that different frequency sub-bands can be influenced by different transformer structures [20]. Thus, the frequency response can be divided into sub-bands according to their different structure influences. The first subdivisions for frequency response were presented in [19, 65, 66]. These studies defined the frequency sub-bands at low-frequency (from 10 kHz till 100 kHz), medium-frequency (from 100 kHz till 600 kHz) and high-frequency (from 600 kHz till 1 MHz). However, researchers have used other limits for the frequency divisions that can vary greatly. For example, the low-frequency band can go up to 10 kHz [53], 20 kHz [67, 68], 50 kHz [69] or 350 kHz [70]. The medium and high-frequency bands will also have different limits in consequence.

Furthermore, other studies have considered four sub-bands for FRA interpretation [71-74]. This division was also used in the IEC 60076-18:2012 standard [20], such as presented in Figure II.3.

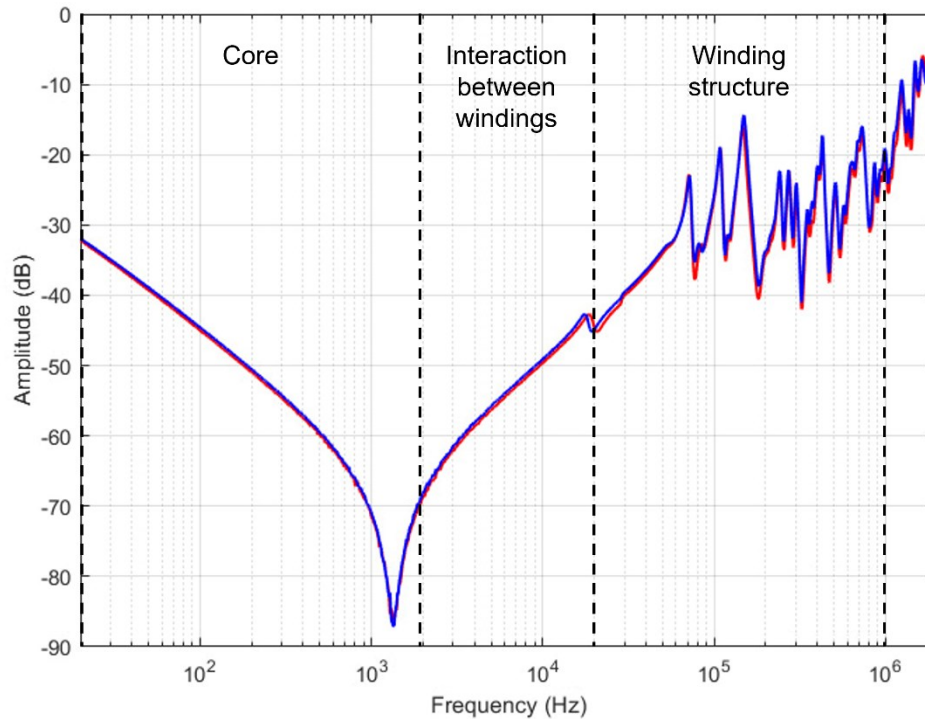


Figure II.3 Main regions of a frequency response

Source: Suassuna de Andrade Ferreira, 2022, adapted from IEC 60076-18, 2012 [20]

The lower frequency region (usually below 2 kHz) is mainly influenced by the core magnetizing inductance (for end-to-end open circuit measurements), or by the leakage inductance (for end-to-end short-circuit measurements). The coupling between windings affects the response for medium frequencies (between 2 kHz and 20 kHz). At higher frequencies (from 20 kHz to 1 MHz) the measurement is influenced by the winding structure, such as winding leakage inductance and windings series and shunt capacitances. For frequencies above 1 MHz, the measurement set-up affects the response, so this region shows less reproducibility in measurements [17]. Moreover, studies have also used more than four frequency sub-bands. For example, in [64], six sub-bands are used; in [41], 10 ranges are defined between 20 Hz and 1 MHz.

As the frequency regions are related to transformer structures (core, windings, leads, and others), it seems misleading to establish generally fixed frequency sub-bands. A variable selection for frequency sub-bands was proposed by Velasquez in [75, 76]. The proposed frequency response division is similar to the one presented in [74], with the low-frequency

region divided into two sub-regions (LF1 and LF2). The method is based on the locations of poles and zeros in the frequency response.

Similarly, Tahir and Tenbohlen proposed in [77] an adaptive frequency division based on different features present in FRA traces. The method is characterized by the location of resonances, anti-resonances, and phase zero-crossings. The entire frequency band is divided into four sub-bands according to the different physical components of the transformer. Two low-frequency sub-bands are related to the core, where magnetizing inductance and equivalent capacitances dominate the response. One medium-frequency sub-band corresponds to the mutual inductances between windings and inter-winding capacitances. Moreover, a high-frequency sub-band coincides with the region dominated by the winding inductance and series and ground capacitances.

An alternative method to frequency sub-band divisions is explored in [31]. The authors proposed using a sweep frequency window approach, illustrated in Figure II.4, where X and Y are the amplitude of frequency response traces used in the numerical index calculation and $\overline{Xw(i)}$ and $\overline{Yw(i)}$ are the mean values of the i^{th} window.

The frequency window (WS) is determined from the number of data points per decade ($f_{p/d}$) in the measured traces using equation (II.3),

$$WS=10+6\left(\frac{f_{p/d}-200}{200}\right). \quad (II.3)$$

The frequency window is then swept over the complete frequency range in predefined steps (W_{step}). In this method, a vector of index values is obtained. The index values vector allows the better characterization of the trace deviations without relying on predefined frequency bands.

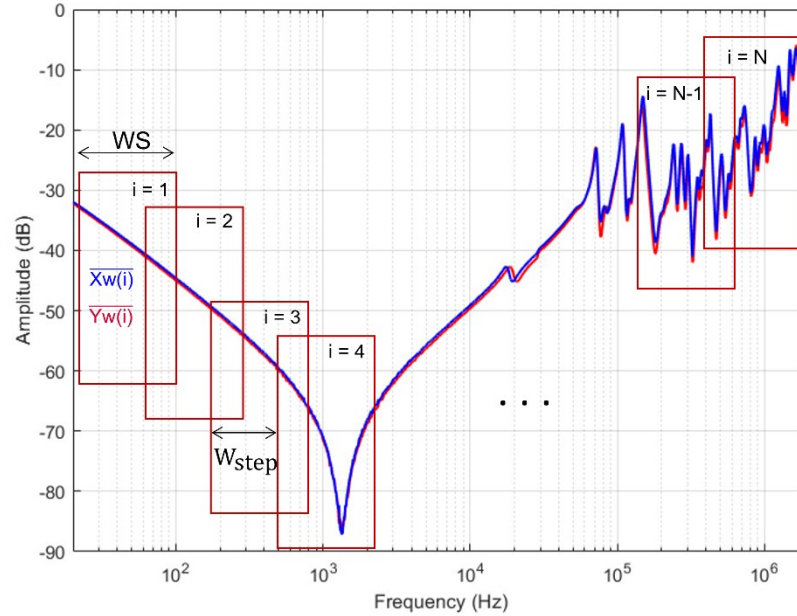


Figure II.4 Principle of sweep frequency window approach
 Source: Suassuna de Andrade Ferreira, 2022, adapted from Tahir and Tenbohlen, 2019 [31]

2.2.2.HIGH-FREQUENCY SIMULATION MODELS

High-frequency simulation models are used as frequency response interpretation methods due to their capability to reproduce FRA traces. In addition, the simulation allows the study of FRA measurements in different situations without damaging the power transformer's physical conditions, such as mechanical deformations, electrical faults, insulation properties changes and others.

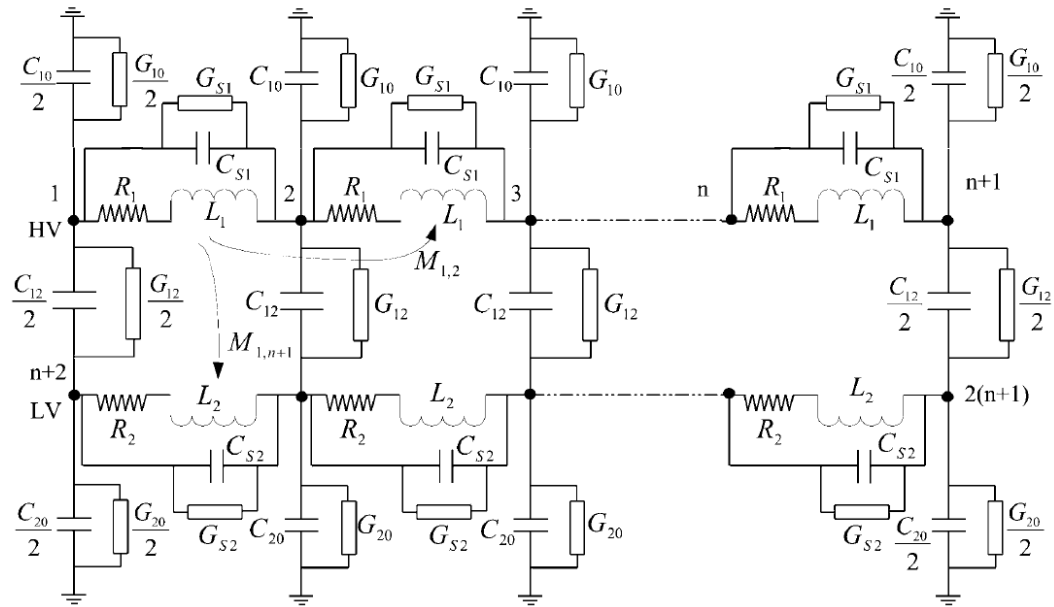
The finite element method (FEM) and the RLC equivalent circuit method are the two main approaches to developing high-frequency simulation models. The equivalent RLC circuits use lumped elements such as resistances, self and mutual inductances and capacitances estimated from analytical calculations or FEM simulations. RLC estimations were used by studies such as [18, 26, 65-67]. Alternatively, simulation models can also detect changes to lumped circuit elements and correlate them to fault identification [61, 68]. With the improving computational capacity, FEM simulations have been well employed for RLC estimations [27, 69-71]. FEM simulations have advantages over analytical formulas, such as the possibility to

extract parameters from complex and anisotropic structures. The more detailed design data is introduced in FEM simulations; the more accurate estimations the model will present. However, detailed models will also demand higher computational performances. Thus, a compromise between accuracy and computational cost should be made when using simulations.

FEM simulations are explored, for example, in [25, 78]. In the first study [25], FRA traces are calculated directly from the FEM model, and axial displacement faults in different levels are used to evaluate the simulation results. Later, this study evaluates the numerical indices calculated from simulated and measured traces demonstrating that they present good agreement. The second study [78] explores the use of FEM simulation in the calculation of high-frequency inductances. The investigation has shown that the high-frequency inductance calculated is sensitive to detect disc space variation faults and even its extents on transformer windings.

The RLC equivalent circuit method for high-frequency simulation of FRA traces is explored in [32, 33, 79]. The authors in [33] investigated the modelling of transformers from lumped parameters circuits. This study has used geometrical details and frequency-dependent material properties to explore its influence in obtaining a good match between simulated and measured responses. The published paper also uses FEM simulations to obtain the inductances and resistances of its lumped parameter circuit. Figure II.5 presents the RLC lumped parameter circuit used in reference [33]. This circuit model is also widely used in research exploring high-frequency transformer models.

In [79], the circuit parameters for frequency response reproduction are estimated from artificial intelligence techniques. The authors use finite element analysis to estimate reference values for the circuit parameters for later comparison with the artificial intelligence algorithms calculations. The results have shown that the fault type can be identified from circuit parameter model changes. For example, self and mutual inductance changes are related to winding or core deformations and shorted turns, while series-capacitance changes are associated with disk movements and insulation degradation [79].



- C_{10}, C_{20} earth capacitance of HV and LV windings, respectively
- G_{10}, G_{20} conductance to earth of HV and LV
- C_{12}, G_{12} capacitance and conductance between HV and LV
- C_{S1}, C_{S2} series capacitance of HV and LV
- G_{S1}, G_{S2} series conductance of HV and LV
- L_1, L_2 inductances of HV and LV
- R_1, R_2 resistances of HV and LV
- $M_{i,j}$ mutual inductance between i^{th} and j^{th} winding elements

Figure II.5 Lumped elements for a two-winding transformer
Source: Abeywickrama, Serdyuk and Gubanski, 2008. [33]

Alternatively, the authors in [32] have used complex equations based on the transformer's physical dimensions to calculate the circuit parameter for the high-frequency model. Further, a study is conducted on faults analysis using numerical indices such as CC, ASLE, SD, and SSE (Table II.1). Three fixed sub-bands are used for the calculation of indices: $100 \text{ Hz} < \text{Low-Frequency} < 2 \text{ kHz}$, $2 \text{ kHz} < \text{Medium-Frequency} < 20 \text{ kHz}$, and $\text{High-Frequency} > 20 \text{ kHz}$. The study's conclusions have remarked that although ASLE presented a good performance on the fault analysis, the use of a single index is not suitable for detecting all faults.

Further, the use of circuit models can also provide information by correlating circuit parameter changes and fault analysis. This is the case presented in [80, 81]. Both studies have

differently varied circuit parameters. The first reference, [80], is based on analytical calculation and circuit simulation. A winding model is used to compare deviations from FRA traces and determine the correlation of these deviations with the variation in circuit elements, for instance, series capacitance, shunt capacitances or self-inductances. The method can also indicate if the deviation originated from an increase or a decrease of the circuit parameters reference values. The second study, [81], has demonstrated the effects of the non-uniform distribution of capacitances, inductances and resistances in the FRA traces. The authors have demonstrated that, depending on how the circuit parameter is affected by non-uniformity, the diagnostic algorithms can be improved by considering re-weighting its rules based on the non-uniformity.

Another approach using RLC circuit representation and natural frequency analyses was employed by Larin in [82, 83]. The natural frequencies largely depend on the windings' electrical and physical parameters, contributing to a more transformer-specific interpretation. The report [83] studies the detection and location of winding internal short-circuit based on identifying winding natural frequencies.

Moreover, researchers such as [84, 85] study the sensitivity of equivalent circuit parameters in the FRA traces. First, an equivalent circuit model was developed, and its parameters were varied according to the mechanical faults that influenced them. In [84], the sensitivity of parameters variation is evaluated in relation with the shift of resonance frequencies and in [85], a fault analysis was also presented. The latter found that radial displacement parameters affected FRA in its entire frequency range while axial displacements affected only frequencies above 200 kHz.

2.2.3.ARTIFICIAL INTELLIGENCE ALGORITHMS

Machine learning and neural networks are artificial intelligence (AI) algorithms frequently used to classify patterns by learning from examples. Given their adaptive

characteristic, these classifiers have been widely used for FRA interpretation of fault diagnostics in power transformers [29, 56, 86, 87].

The AI approach supports the previously mentioned interpretation methods and can have different applications. For example, the algorithms can automatically classify FRA traces [29, 88] or estimate circuit parameters of high-frequency models [79, 89]. More recently, AI algorithms have also been used with image processing methods to compare FRA traces and identify shorted turns faults based on image deviations [26].

Common AI algorithms used in FRA interpretation are decision tree (DT), radial basis function (RBF), k-nearest neighbour (k-NN), and support vector machine (SVM). A decision tree is a classification tool presenting its classification in a tree-like graphical form. The structure follows a flowchart with a root node and intermediate nodes. Each node is a test, and each class is presented in one tree leaf [24].

The k-NN is a non-parametric algorithm that uses classification and regression. Based on similarity measures, the k-NN algorithm assigns the category's test pattern to the class with the majority of nearest neighbours. The k-NN function is only approximated locally, and the only parameter of the algorithm is the number of neighbours (k) considered for classification, where k is a positive integer. If k=1, the input is assigned to the class of that single nearest neighbour. For the best algorithm performance, a normalization of the database is often required. A data set with different physical units or different scales can seriously undermine the accuracy of the algorithm [90].

RBF is a feed-forward algorithm with multilayer structures. The architecture of RBF neural networks comprises an input layer, a hidden layer and an output layer. The output node is a decision based on a linear combination of the RBF outputs computed by the hidden layer neurons. Each RBF neuron stores a prototype information vector and then compares the input vector to its prototype. The output of each neuron is a value between zero and 1, a similarity measure. If the input is equal to the prototype, then the output of that neuron will be 1. The

response tends to zero as the difference between the input and the prototype increases. The RBF neuron's response shape is a bell curve [91].

The SVM method is a supervised learning model with associated learning algorithms. Firstly, developed for solving binary classification problems, SVMs can also be adapted for multiclass problem applications. The adaption is performed with the help of one-versus-one or one-versus-all heuristic methods. The SVM algorithm allows the classification of linearly separable patterns. However, real-world data are frequently not linearly separable, so the SVM does a kernel trick to transform the input space into a higher-dimensional space where the data is linearly separable. This transformation is made possible using kernel functions [92]. Many different functions can be used as kernel functions in SVMs, some of the most common being linear, polynomial and Gaussian.

Support Vector Machine algorithm is used in different studies to detect faults in transformers using features such as Index of Frequency Ratio (IFR), Index of Amplitude Ratio (IAR) or Vector Fitting (VF) methods as input [30]. This study uses about 20 FRA measurements. SVM has also been employed for winding type recognition [40, 46]. Other references, such as [93, 94], have also used SVM techniques to interpret frequency responses to mechanical faults and short-circuits.

Different algorithms are compared over their performances using mainly numerical indices as input. For example, reference [29] compares over 20 numerical indices based on the performance of intelligent classifiers such as Probabilistic Neural Network (PNN), DT, SVM, and k-NN. This study is based on using a limited database of 36 instances distributed over five classes of faults. Reference [77] uses a Backpropagation (BP) neural network to compare the performance of CCF, LCC, SD, CSD, and SE numerical indices. The latter study has a more extensive database using at least 139 FRA measurement cases.

Analyzing the topics addressed in this literature review, it is possible to conclude that many studies have been conducted regarding frequency response use and interpretation.

Nowadays, the main challenge to the application of AI in FRA interpretation lies in the necessary database for algorithm training. Most of the studies reported in the literature are based on limited data.

CHAPTER III
FREQUENCY RESPONSE ANALYSIS INTERPRETATION USING NUMERICAL INDICES
AND MACHINE LEARNING: A CASE STUDY BASED ON A LABORATORY WINDING
MODEL

Article published in IEEE Access, April 2021

doi: [10.1109/ACCESS.2021.3076154](https://doi.org/10.1109/ACCESS.2021.3076154)

FREQUENCY RESPONSE ANALYSIS INTERPRETATION USING NUMERICAL INDICES AND MACHINE LEARNING: A CASE STUDY BASED ON A LABORATORY MODEL

Abstract

Frequency response analysis is a powerful tool for mechanical fault diagnostics in power transformers. However, interpretation schemes still today depend on expert analyses, mainly because of the complex structure of power transformers. One of the fundamental shortcomings of experimental investigations is that mechanical deformations cannot be managed on real transformers to obtain data for different scenarios because they are too destructive. To address this issue in a systematic way, the current research used a specially designed laboratory transformer model that allows mechanical defects to be introduced so its frequency response can be evaluated under different conditions. The key feature of this model is the non-destructive interchangeability of its winding sections, allowing reproducibility and repeatability of frequency response measurements. Numerical indices were compared over key performance indicators (linearity, sensitivity and monotonicity). The analysis indicated that comparative standard deviation offered promising results for evaluation of mechanical deformations on the laboratory winding model given its monotonic behaviour, sensitivity and linear increase with fault severity. Additionally, support vector machine learning, radial basis function neural network and the statistical k-nearest neighbour method were used for fault classification with different strategies and configurations. While limited data from different transformers are used in the available literature, the approach discussed here considers 371 measurements from the same transformer model. The test results are supportive and demonstrate great accuracy when machine learning is used for winding fault classification.

3.1. INTRODUCTION

Power transformers are essential assets of electrical power networks, and monitoring their operating condition is crucial for functional and economic reasons. Regular monitoring to ensure incipient failure is detected at the earliest stage is vital. Power transformers are vulnerable to through faults, which can result in significant mechanical forces on the active part. In addition, insulation degradation due to ageing may cause a reduction in clamping pressure, increasing the risk of mechanical damage [16, 85]. Mechanical forces beyond the design limits of the transformer may cause deformations in the windings. Once such deformations occur, the transformer's ability to withstand further mechanical forces originating in a potential overcurrent is greatly reduced due to localized electromagnetic stresses [2].

Nowadays, there are many non-intrusive monitoring and diagnostic techniques available to detect incipient power transformer failures. These techniques evaluate the effects of different faults and can be implemented without requiring transformer disassembly. Frequency response analysis (FRA) is one of these methods, and it is currently commonly used in the electrical industry for condition assessment of transformer windings. From the very first studies [15], FRA has demonstrated its sensitivity for detecting mechanical and electrical failure modes [16, 17].

FRA compares current and reference frequency response measurements of a power transformer. Ideally, the reference measurements are obtained just before transformer energization, and subsequent monitoring over the years provides a continuous evaluation of the condition of the windings. Whenever reference traces are unavailable, traces from sister units (identical transformers) or other phases of the same transformer (in the case of three-phase transformers) can also be used. Deviations between current and reference measurements can indicate electrical or mechanical damage to transformer active part.

Though FRA measurement procedures have been thoroughly studied at the international level in working groups of the IEEE [21], CIGRE [16] and the IEC [20], result

interpretation still depends on expert analyses. Some of the quantitative interpretation methods proposed so far fall into three groups: numerical indices, white box physical models and artificial intelligence algorithms [24].

The frequency response of a transformer depends to a large extent on the type of transformer and its power rating, voltage rating, phase connections, winding design, etc. This means basic and fundamental principles using simple geometrical models, to guide the quantitative analyses.

This paper explores different measurements taken on a laboratory transformer model to study FRA interpretation. The model allows different deformations to be introduced and their influence on frequency response can then be evaluated. Four different fault modes (the fault extent varying) were introduced to the winding model: axial displacement (AD), radial deformation (RD), disc space variation (DSV) and short-circuited turns (ST). Numerical indices were then computed for quantitative interpretation of the different arrangements. The research also considered different frequency bands for application of the numerical indices, evaluating the sensitivity of the frequency range for numerical index calculations.

Machine learning classifiers were also compared over different architectures for an improved and objective fault classification. The classifiers use index calculation at target frequency bands as input for diagnosis of winding faults. Three main diagnostic categories were investigated: detection of fault occurrence; determination of fault type; determination of the fault type and extent.

3.2. FREQUENCY RESPONSE ANALYSIS

FRA is a powerful tool for detecting mechanical changes in the active part of a power transformer. Since a transformer can be considered a complex network of RLC components [95] (resistance of the winding, inductance of the coils and capacitance of insulation layers and

to the ground), variation in frequency response may indicate a physical change inside the transformer.

A frequency response is obtained by injecting a sinusoidal waveform at the reference point and measuring the amplitude and phase shift at the response point [16]. FRA traces can be represented in terms of amplitude (H_{dB}) (dB) and phase shift (φ) (degrees), as shown in (III.1) and (III.2),

$$H_{dB}=20 \cdot \log_{10}(V_m/V_r), \quad (III.1)$$

$$\varphi=\varphi(V_m)-\varphi(V_r), \quad (III.2)$$

where, V_m is the response voltage and V_r is the reference voltage [16]. Amplitude (H_{dB}) is widely used for interpretation purposes and numerical indices calculations.

There are also multiple measurement types depending on where the reference and response points are connected. The measurement types can be separated into two main groups: end-to-end measurements and interwinding measurements. End-to-end measurements are obtained when the signal is applied to one end of the winding and the response is measured at the other end of that same winding. Interwinding measurements are obtained when the signal is applied to one winding and the response is measured at another. The frequency response traces discussed in this paper were produced by an end-to-end open circuit measurement configuration and in some cases by an end-to-end short-circuit measurement, as described in [21].

The challenge when utilizing FRA to diagnose transformer active part is mainly in the correct interpretation of deviations from current and reference measurements. Studies investigating FRA interpretation use numerical indices [37, 38], white-box modelling [25, 33] and artificial intelligence algorithms [29, 39-41] to objectively assess frequency response traces obtained from real cases [24, 42], laboratory experiments [43] and simulation studies [44-46]. Different approaches for the interpretation of FRA measurements are reported in recent

literature on the application of intelligent classifiers. For instance, the combination of numerical indices and intelligent classifiers is explored in [29, 30, 86, 96, 97]. References [29, 30], use numerical indices as input to neural networks and discuss the use of support vector machine (SVM) for fault type recognition in power transformers. Reference [96] presents a method for locating shorted turns with FRA interpretation again based on numerical indices and SVM. However, the databases on which most of the studies reported in the literature are based are limited and the transformers types diverse.

The components of a transformer (tank, core, winding type, insulation type and so forth) also have an impact on its frequency response. Accordingly, the effects of transformer structures are explored in the literature [24, 45]. Reference [46] examines the identification of winding type by SVM. Transformer insulation plays a major role in frequency response, with liquid insulation changing the permittivity of the material, increasing capacitances and, as a result, shifting resonances to lower frequencies [98]. Meanwhile the migration of moisture into solid insulation has been reported to shift resonances to higher frequencies [28].

Nonetheless, the most common method of frequency response interpretation remains the visual comparison of reference and faulty traces. Numerical indices are applied to obtain a better quantitative interpretation. In the approach proposed in this paper, frequency bands of interest (those where measurements deviate) were determined by visual inspection of the traces, and numerical indices were evaluated over these frequency bands. The frequency bands of interest and the best-performing numerical index were subsequently used as machine-learning input to achieve an objective interpretation of fault modes in FRA measurements.

3.2.1. FRA INTERPRETATION BASED ON NUMERICAL INDICES

Frequency response interpretation based on numerical indices is used to quantify differences between investigated and reference traces. Different indices [17, 37] evaluated

over key performance indicators (such as linearity, monotonicity and sensitivity [99]) are suggested in the literature.

This research used some of the most promising numerical indices to evaluate frequency response measurements [24]. A description of these indices is presented in Table III.1.

Table III.1 Summary of numerical indices used in this research

Index	Description	Equation
CCF	The cross-correlation factor quantifies the linear dependence between two data sets. Its value is closer to 1 if there is large positive correlation between the data sets and closer to zero in case of a weak correlation.	(III.3)
LCC	Lin's concordance coefficient measures the agreement between two variables. A value near 1 indicates a strong concordance, a value close to zero denotes a weak concordance, and a value near -1 denotes strong discordance.	(III.4)
CSD	Comparative standard deviation is zero in case of a complete match of traces, and there is no upper limit value. For amplitude deviations, this index has lower sensitivity [24, 53].	(III.5)
SSE	The sum squared error calculates the square of the distance between two traces. A value close to zero means a good match of traces, and there is no upper limit value. The index has shown low sensitivity for amplitude deviations [24], though its sensitivity is improved when amplitude deviations occur around resonance points [38].	(III.6)
SSRE	The sum squared ratio error uses the squared ratio error between two traces. A value of zero indicates a good match of data, and there is no upper limit value. Like other squared sums, this index presents less linear behaviour [24].	(III.7)

Source: Suassuna de Andrade Ferreira, 2021

The numerical indices described in Table 1 and used in this paper are calculated in equations (III.3) to (III.7), where, X and Y are the magnitude vectors of reference and investigated frequency responses respectively, X(i) and Y(i) are the i^{th} element of these vectors and N is the number of data points.

$$CCF = \frac{\sum_{i=1}^N (X(i) - \bar{X})(Y(i) - \bar{Y})}{\sqrt{\sum_{i=1}^N (X(i) - \bar{X})^2 \sum_{i=1}^N (Y(i) - \bar{Y})^2}} \quad (III.3)$$

$$LCC = \frac{\frac{2}{N} \sum_{i=1}^N (X(i) - \bar{X})(Y(i) - \bar{Y})}{(\bar{Y} - \bar{X})^2 + \frac{1}{N} \sum_{i=1}^N (X(i) - \bar{X})^2 + \frac{1}{N} \sum_{i=1}^N (Y(i) - \bar{Y})^2}} \quad (III.4)$$

$$CSD = \sqrt{\frac{\sum_{i=1}^N [(X(i) - \bar{X}) - (Y(i) - \bar{Y})]^2}{N-1}} \quad (III.5)$$

$$SSE = \frac{\sum_{i=1}^N (Y(i) - X(i))^2}{N} \quad (III.6)$$

$$SSRE = \frac{\sum_{i=1}^N \left(\frac{Y(i)}{X(i)} - 1\right)^2}{N} \quad (III.7)$$

where, $\bar{X} = 1/N \sum_{i=1}^N X(i)$ and $\bar{Y} = 1/N \sum_{i=1}^N Y(i)$.

Not only must the numerical index that will be used to evaluate the frequency response traces be selected, but the frequency band to which this index is applied must be determined as well, and this can be challenging. Different methods can be used, the simplest being to evaluate the entire frequency range in the same way, as described in [64, 100]. This approach, however, can result in a lack of sensitivity to deviations in a small range of the frequency response. Division of the frequency range into sub-ranges is, accordingly, usually explored [20, 22]. To achieve an independent frequency range subdivision, the study described in [99] suggests a frequency window that sweeps the total frequency range, evaluating some of the traces at each window step.

3.2.2. FRA INTERPRETATION BASED ON MACHINE LEARNING

Machine learning and neural networks are intelligence algorithms frequently used to classify patterns by learning from examples. Given their adaptive characteristic, these classifiers have been widely used for fault diagnostics in power transformers [29, 30, 101].

Two approaches are used for network learning by example: unsupervised and supervised learning. With unsupervised learning, there is no need to supervise the network and provide target outputs to match inputs. With supervised learning, the network is provided with a target output for each input vector injected. Based on the computed output error (difference between the target output and the estimated output), the network adjusts its synaptic weights using heuristic algorithms at each iteration.

This paper compares several well-known and widely used machine learning classifiers: radial basis function (RBF) neural network, support vector machine (SVM) and the statistical k-nearest neighbour (k-NN). These models have become very popular in recent years because of their ability to solve problems in classification, regression and other applications in different areas.

A) RADIAL BASIS FUNCTION

RBFs are feed-forward multilayer structures. The output node is a decision based on a linear combination of the RBF outputs computed by the hidden layer neurons. Each RBF neuron stores a prototype information vector and then compares the input vector to its prototype. The output of each neuron is a value between zero and 1, which is a similarity measure. If the input is equal to the prototype, then the output of that neuron will be 1. The response tends to zero as the difference between the input and the prototype increases. The shape of the RBF neuron's response is a bell curve, as illustrated in the network architecture diagram in Figure III.1.

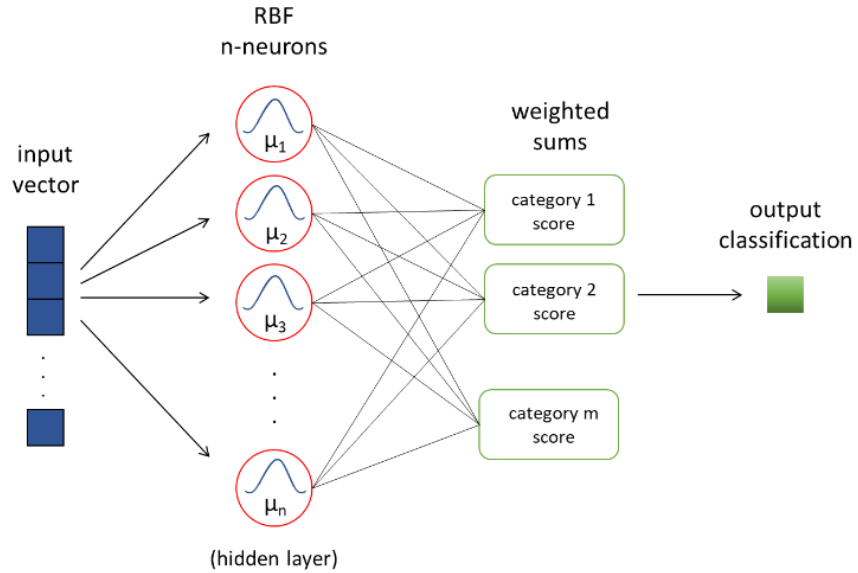


Figure III.1 Radial basis function neural network architecture
 Source: Suassuna de Andrade Ferreira, 2021 adapted from McCormick, 2013 [91]

B) SUPPORT VECTOR MACHINE

The SVM is a supervised learning model with associated learning algorithms. Even though SVMs were first applied to binary class problems, they can also be applied to multiclass problems by using one-versus-one and one-versus-all heuristic methods to split and transpose the multiclass into a binary classification problem. The SVM model is considered a generalization of linear classifiers when classifying a set of linearly separable patterns (x_i) from two classes: C_1 and C_2 . This is achieved by positioning an appropriate hyperplane as a decision boundary satisfying the equation $g(x)=w^t x + b=0$, where w is the weight vector and b is the bias or threshold. All pattern data x_i with $g(x_i)>0$ are assigned to C_1 and those with $g(x_i)<0$ are assigned to C_2 . However, SVMs choose the linear separator with the largest margin, centered between two hyperplanes described by equations (III.8) and (III.9):

$$h_1(x_i)=w^t x_i + b \geq 1, \text{ for } x_i \in C_1 \quad (\text{III.8})$$

$$h_2(x_i)=w^t x_i + b \leq -1, \text{ for } x_i \in C_2 \quad (\text{III.9})$$

The distance between the hyperplanes h_1 and h_2 is the margin, and all points that lie on h_1 or h_2 are called support vectors. To take into account the non-separable data x_i , a slack

variable ξ_i is incorporated to give more relaxation at the constraints, yielding a compact form of the previous equations as follow:

$$y_i(w^t x_i + b) \geq 1 - \xi_i, \text{ for } i=1, 2, \dots, N \quad (\text{III.10})$$

with $y_i=1$ if $x_i \in C_1$ and $y_i=-1$ if $x_i \in C_2$.

The margin to be maximized is then equal to $1/\|w\|$, and the primal formulation of the SVM task is to find the optimal weights and bias that will minimize the cost function defined in (III.11)

$$\varphi(w, b, \xi) = \frac{1}{2} w^t w + \rho \sum_{i=1}^N \xi_i, \quad (\text{III.11})$$

while satisfying the constraints in (III.10), with $\xi_i \geq 0$ for $i=1, 2, \dots, N$. The parameter ρ , referred to as the regularization parameter, controls the penalty of non-separable points.

Using the method of Lagrange multipliers and formulating the optimization problem from a dual problem perspective, the objective function (III.12) to be maximized is obtained [102].

$$Q(\alpha) = \sum_{i=1}^N \alpha_i - \frac{1}{2} \sum_{i=1}^N \sum_{j=1}^N y_i y_j \alpha_i \alpha_j x_i^T x_j. \quad (\text{III.12})$$

The equation (III.12) is subjected to the constraints $\sum_{i=1}^N y_i \alpha_i = 0$ and $0 \leq \alpha_i \leq \rho$ for all i , where α_i is a set of Lagrange multipliers.

The SVM algorithms use a set of mathematical functions that are defined as kernel functions. In SVM models, kernel functions are used to transform the non-linear space into a higher dimensional linear space, changing the objective function as follows:

$$Q(\alpha) = \sum_{i=1}^N \alpha_i - \frac{1}{2} \sum_{i=1}^N \sum_{j=1}^N y_i y_j \alpha_i \alpha_j \text{kernel}(x_i, x_j). \quad (\text{III.13})$$

The software used to train the SVM model is based on the iterative single data algorithm (ISDA) solver [103]. The cost p applied to the misclassification in training data is defined as 1. The regularization parameter for smoothing is fixed at $1/N$, where N is the number of observations. Each class is then centered by its mean value and scaled by its standard deviation. Before evaluation of the kernel(x_j, x_k), where x_j and x_k are the training datasets, an appropriate factor is selected automatically by the software to scale the data and 0.1 is added as kernel offset.

For this research, three popular kernel functions were considered: linear, Gaussian and polynomial. A one-versus-one heuristic method (or coding design) and a one-versus-all method were tested for SVM classification algorithms. The kernel functions were investigated and compared using default SVM methods. The functions explored in this paper are shown in equations (III.14) to (III.16). The linear kernel function is defined as:

$$G(x_j, x_k) = x_j^T x_k, \quad (III.14)$$

the polynomial kernel function with order $p=3$, is defined as:

$$G(x_j, x_k) = (1 + x_j^T x_k)^p, \quad (III.15)$$

the Gaussian kernel function is defined as:

$$G(x_j, x_k) = e^{-\frac{\|x_j - x_k\|^2}{\sigma_e^2}}, \quad (III.16)$$

where the standard deviation (σ_e) is set to 1.

C) K-NEAREST NEIGHBOUR

In machine learning, k-NN is a non-parametric algorithm used for classification and regression. Based on similarity measures, the k-NN algorithm assigns the test pattern in the category to the class which has the majority of nearest neighbours. Though k-NN is considered the simplest algorithm, in practice the learning vector quantization (LVQ) algorithm seems more

appropriate and simpler. LVQ is based on a reduced number of prototypes that can be estimated using the k-means algorithm. LVQ classification is based on the similarity measure of the test pattern and the prototypes representing each category.

The k-NN function is only approximated locally, and the only parameter of the algorithm is the number of neighbours (k) considered for classification, where k is a positive integer. If $k=1$, the input is assigned to the class of that single nearest neighbour. For the best algorithm performance, a normalization of the database is often required. A data set with different physical units or different scales can seriously undermine the accuracy of the algorithm [90].

3.3. LABORATORY WINDING MODEL AND REFERENCE MEASUREMENTS

Measurements were taken from 1 kHz to 1 MHz on a laboratory winding model with removable sections using a commercially available FRA instrument. The model was designed and manufactured to enable short-circuits and different mechanical deformations [43].

The laboratory winding model used for this study is of uniform structure, that is, same conductor throughout the winding and an equal number of turns per winding section. The model has solid, non-grated insulation and was designed specifically for FRA testing: that is, there are no power or voltage ratings for the model.

Figure III.2 shows the model and its connection schematic. The transformer model is composed of two windings, the outer coil (winding 1) with 448 turns divided into 16 sections (28 turns per section) and the inner coil (winding 2) divided into three concentric and fixed layers with 76 turns each, a total of 228 turns in this winding.

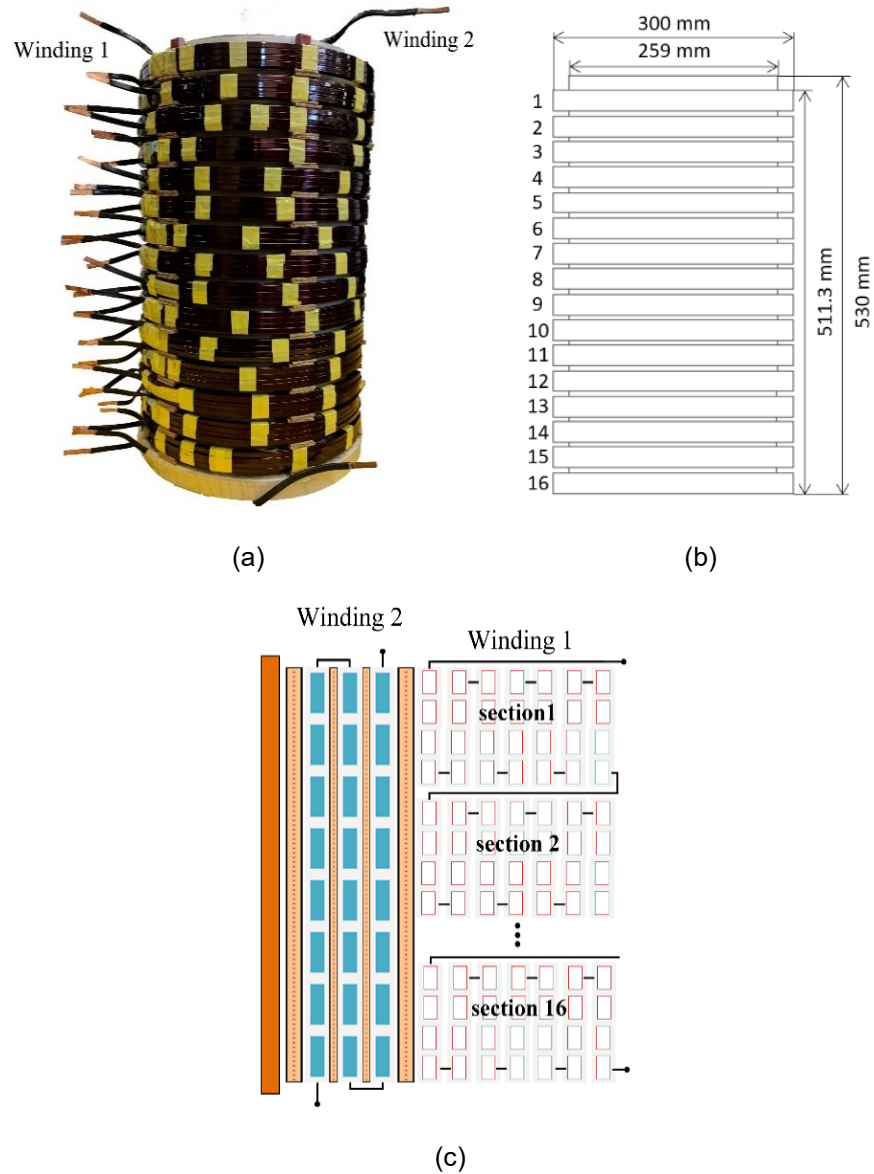


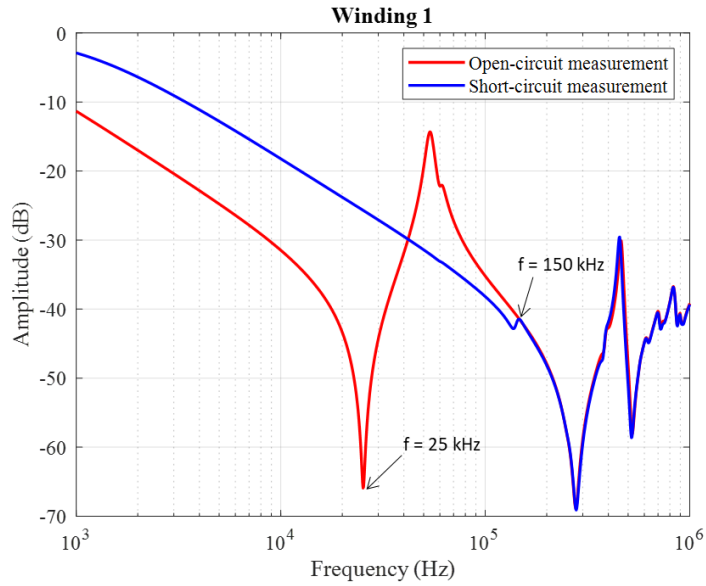
Figure III.2 Model for laboratory tests: (a) winding photo, (b) dimensions and (c) connections schematic

Source: Suassuna de Andrade Ferreira, 2021

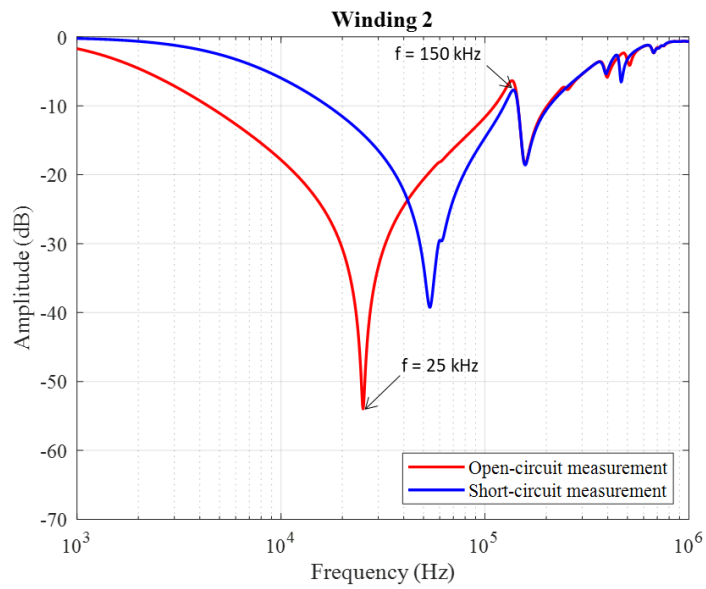
The inner diameter of winding 1 is 300 mm, its radial dimension is 8.5 mm and its height is 511.3 mm. Winding 2 has an inner diameter of 259 mm, a radial dimension of 9 mm and a total height of 530 mm. The outer winding of the transformer model has 16 sections. These sections facilitate defect introduction at different locations.

All FRA measurements discussed in this paper were taken with an air core and concentrically arranged coils, as shown in Figure III.2. The reference measurements (healthy

winding) for windings 1 and 2 are presented in Figure III.3. The curves in Figure III.3 serve as reference for comparison with fault modes.



(a)



(b)

Figure III.3 FRA reference measurements at (a) winding 1 and (b) winding 2
Source: Suassuna de Andrade Ferreira, 2021

As Figure III.3 shows, the first anti-resonance for the open circuit measurement appears at a frequency around 25 kHz for both windings. A magnetic core, not present in this laboratory model, would create a high-magnetizing inductance and a first anti-resonance frequency below 1 kHz. The short-circuit measurement matches the open circuit measurement at over 150 kHz, in both windings. Since the faults were introduced on winding 1, the open-circuit measurement taken from winding 1 was used in this research to compare faulty and healthy states.

3.4. FAULT ANALYSES

For this research, four different fault modes were introduced in winding 1: three mechanical deformations and one electrical fault. Six levels of each fault were tested to verify the evolution of the fault in the frequency response. Figure III.4 is a sketch representation of the fault modes.

A) AXIAL DISPLACEMENT

Axial displacement (AD) faults were created by adding spacers at the bottom of winding 1, resulting in vertical displacement between winding 1 and winding 2. The AD fault started with 6 mm spacer (AD 1) and increased the spacers in steps of approximately 5.4 mm up to 34 mm (AD 6). Figure III.5a shows the frequency response for reference and the AD fault steps.

B) RADIAL DEFORMATION

Radial deformation (RD) faults were created by replacing healthy sections of winding 1 by deformed ones. The model has sixteen identical healthy sections. Six radially deformed sections were used to replace healthy sections and introduce radial deformation to the model. The RD fault started by replacing one healthy section with a deformed one, and then replaced one more for each fault step in the positions indicated in Figure III.4c., such that RD 1 has one

deformed section and RD 6 has six. Figure III.5b shows the frequency response for reference and RD faults.

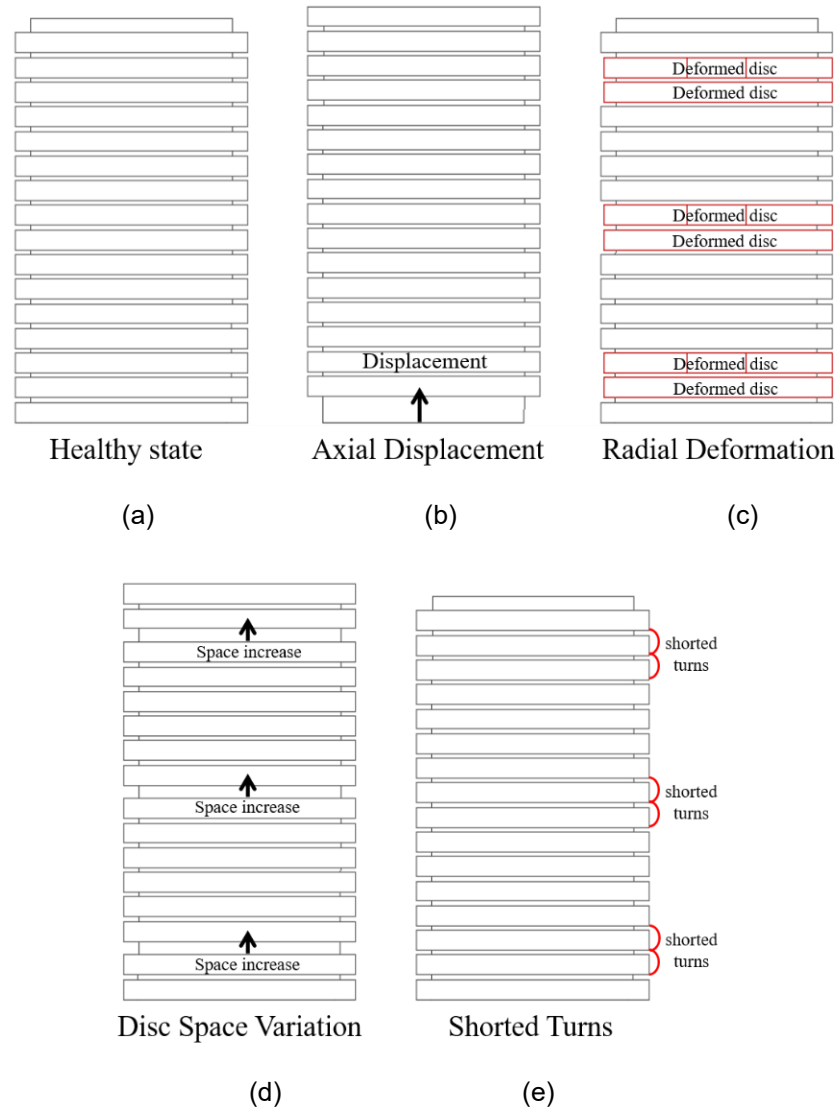


Figure III.4 Winding model representation of fault modes: (a) healthy state; (b) axial displacement; (c) radial deformation; (d) disc space variation; and (e) shorted turns
Source: Suassuna de Andrade Ferreira, 2021

C) DISC SPACE VARIATION

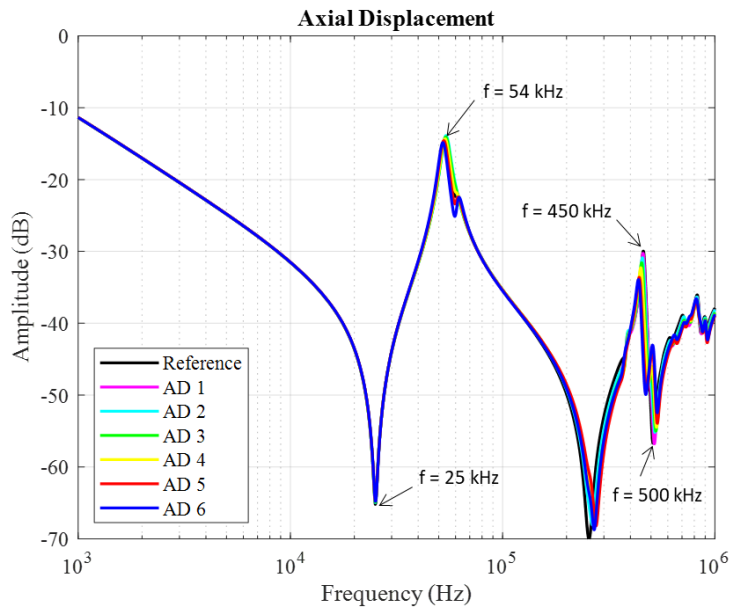
Disc space variation (DSV) faults were created like the AD faults, but the spacers were added between sections at three different positions, as shown in Figure III.4d. The first DSV fault level (DSV 1) has 6 mm spacer between sections 2 and 3. DSV 2 has 11.4 mm spacer between the same sections. The next DSV fault steps were created by adding first 6 mm and

then 11.4 mm spacers between sections 8 and 9. The last two steps were created by adding 6 mm (DSV 5) and then 11.4 mm (DSV 6) spacers between sections 14 and 15. Spacers were always added without removing those for the previous levels, increasing the fault extent at each step. Figure III.5c shows the frequency response for reference and DSV faults.

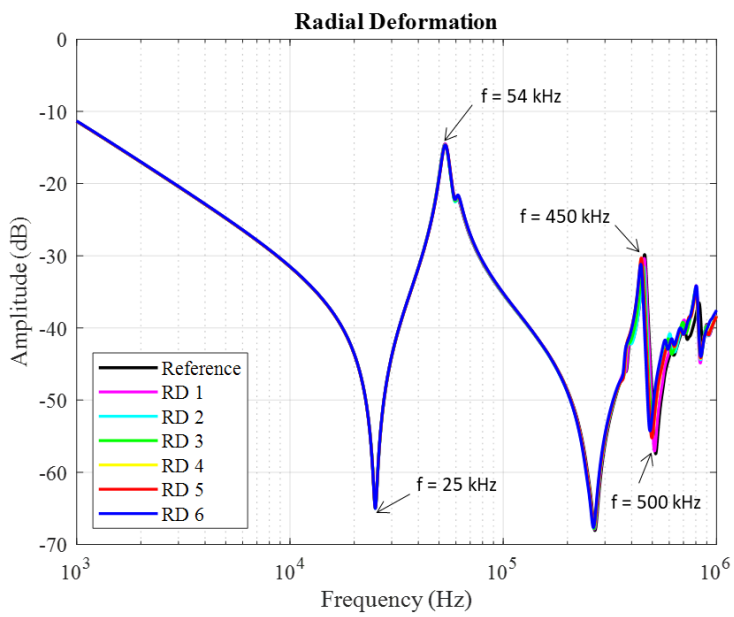
D) SHORT-CIRCUITED TURNS

The final fault, the shorted turns (ST) fault, is an electrical fault created by generating a short-circuit between turns of winding 1. The ST fault started with a short-circuit of section 2 of winding 1 (ST 1), for a total of 28 turns shorted. For ST 2 the turns of sections 2 and 3 were shorted, for a total of 56 turns shorted. Shorted turns continued to be added to winding 1 until sections 2, 3, 8, 9, 14 and 15 (ST 6) were all shorted, for a total of 168 turns shorted. At each level, the shorted sections were added without correcting those of the previous levels, so the impact of shorted turns all along winding 1 could be observed. Figure III.5d shows the frequency response for reference and the six ST fault levels.

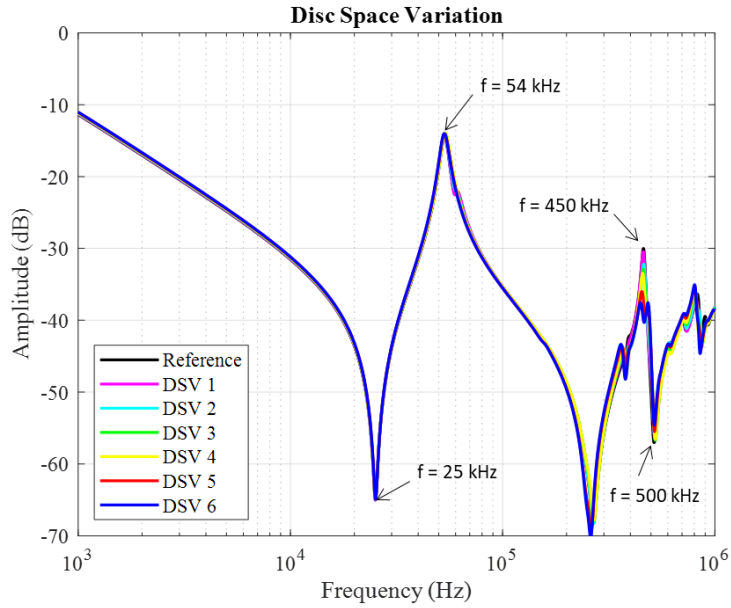
Figure III.5 shows frequency responses for the different faults analyzed in this study. As the figure demonstrates, the faults have different impacts on frequency response. The first resonance at 25 kHz was not affected by the mechanical deformations, but the shorted turns had a substantial effect in this region. This is mainly because the lower frequency region is dominated by the main inductance of the transformer and the ST fault reduces this inductance significantly. Reducing coil inductance results in frequency response displacement towards higher frequencies, as clearly shown in Fig. 6.e. The next anti-resonance point along the frequency response curve, at around 54 kHz, is less affected by the faults. In fact, this point is not even much affected by the ST fault, though the entire frequency range (1 kHz to 1 MHz) is greatly affected by this electrical fault.



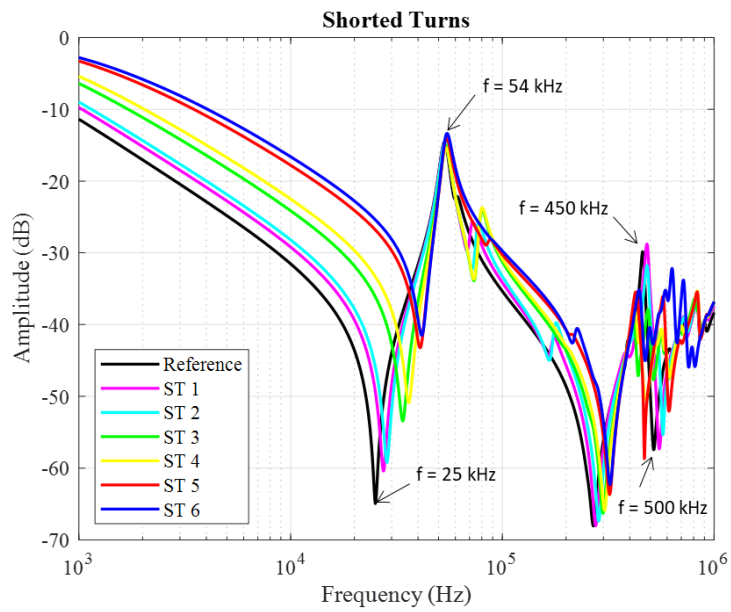
(a)



(b)



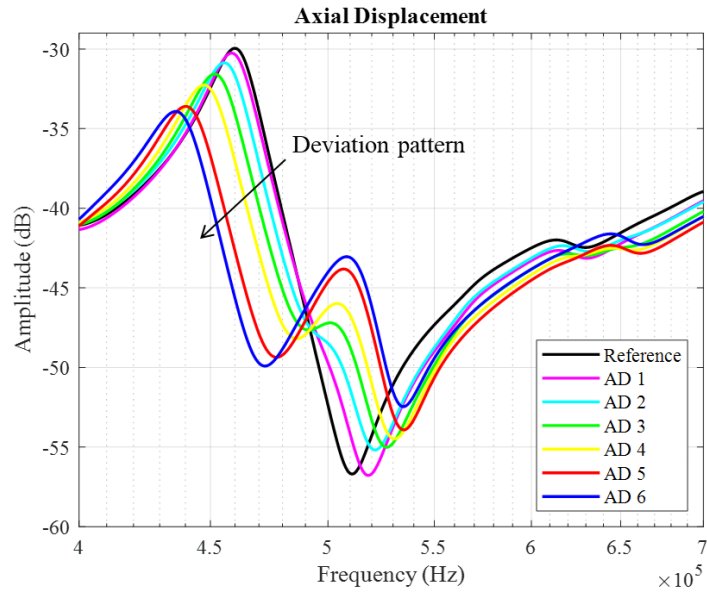
(c)



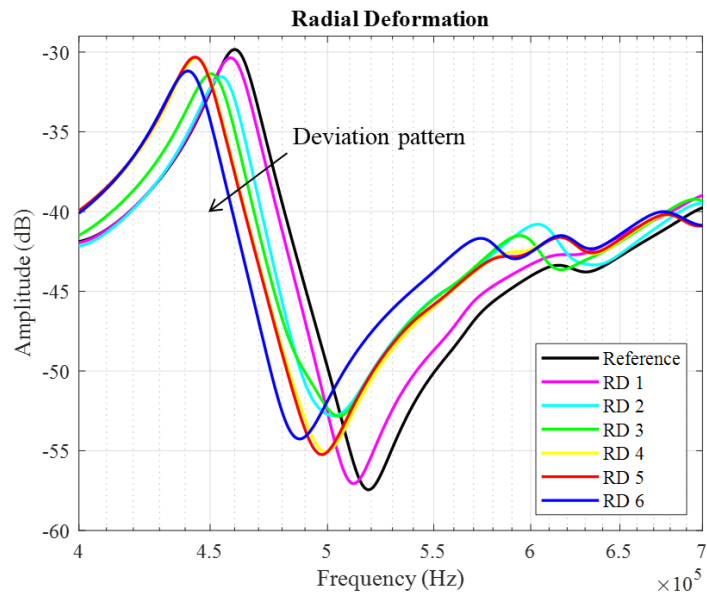
(d)

Figure III.5 FRA measurements for the different fault modes: (a) axial displacement; (b) radial deformation; (c) disc space variation; and (d) shorted turns
Source: Suassuna de Andrade Ferreira, 2021

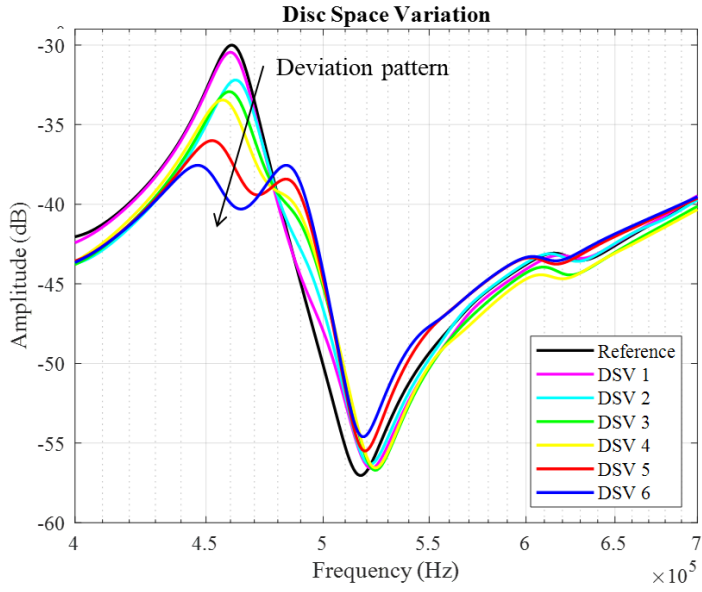
The last frequency region of interest is 400 kHz to 700 kHz, where a resonance at 450 kHz and an anti-resonance at 500 kHz are present (these resonance frequencies are observed in the healthy winding). This particular frequency range (400 kHz to 700 kHz) was affected by all faults (mechanical and electrical), as shown in Figure III.6.



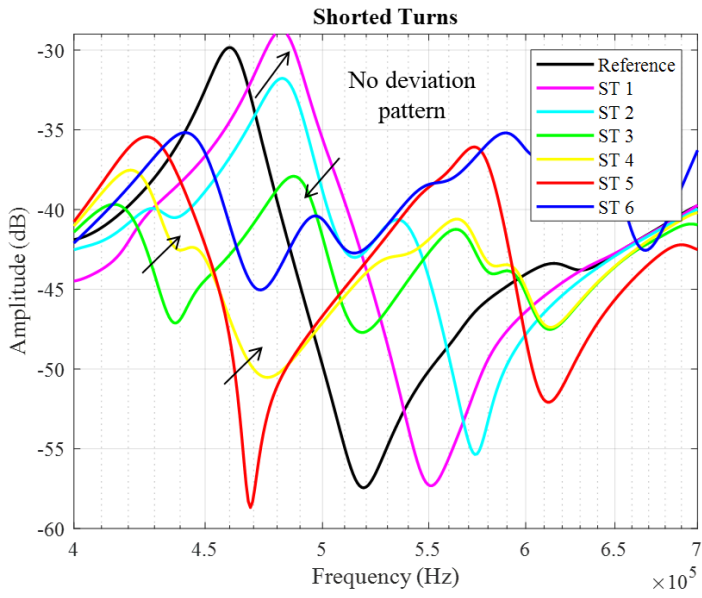
(a)



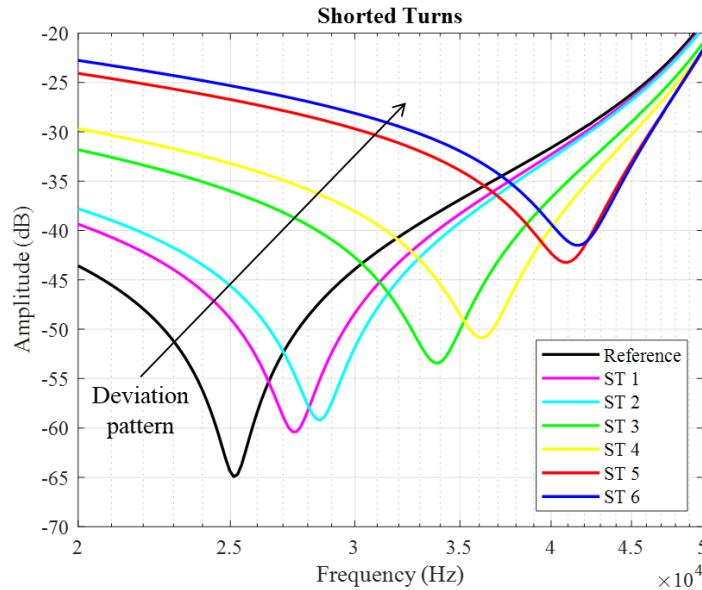
(b)



(c)



(d)

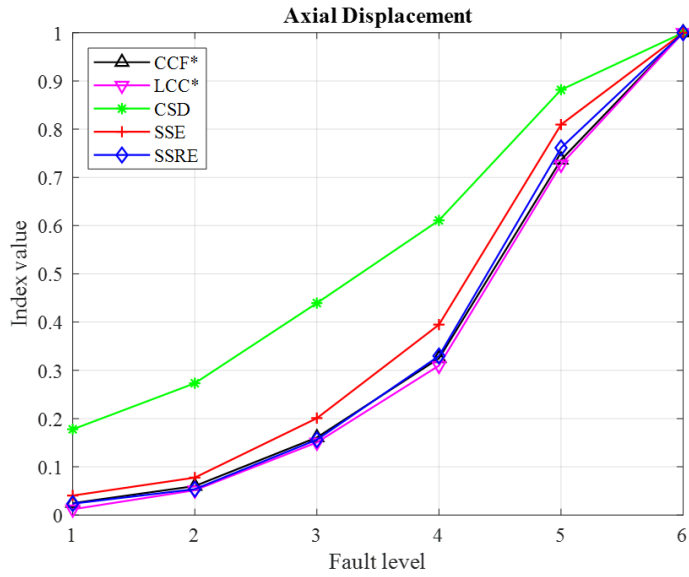


(e)

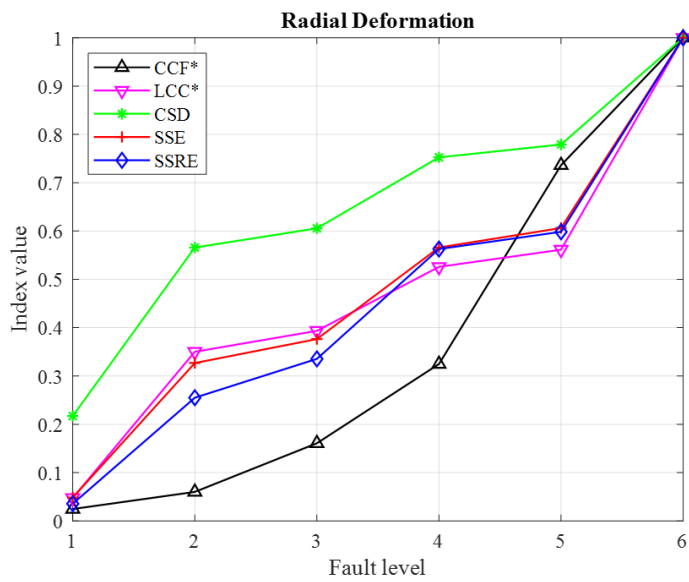
Figure III.6 Frequency response at a frequency range affected in fault mode: from 400 kHz to 700 kHz for (a) axial displacement, (b) radial deformation, (c) disc space variation and (d) shorted turns; and from 20 kHz to 50 kHz for (e) shorted turns
Source: Suassuna de Andrade Ferreira, 2021

Each of the faults affected the frequency range from 400 kHz to 700 kHz differently. As a result, this frequency was used to calculate indices for quantitative evaluation of the faults. However, unlike the mechanical faults, the ST fault did not present a clear deviation pattern at this frequency band, as shown in Figure III.6. The frequency range from 20 kHz to 50 kHz was thus used to evaluate ST faults, since the deviation pattern is clearer in this region.

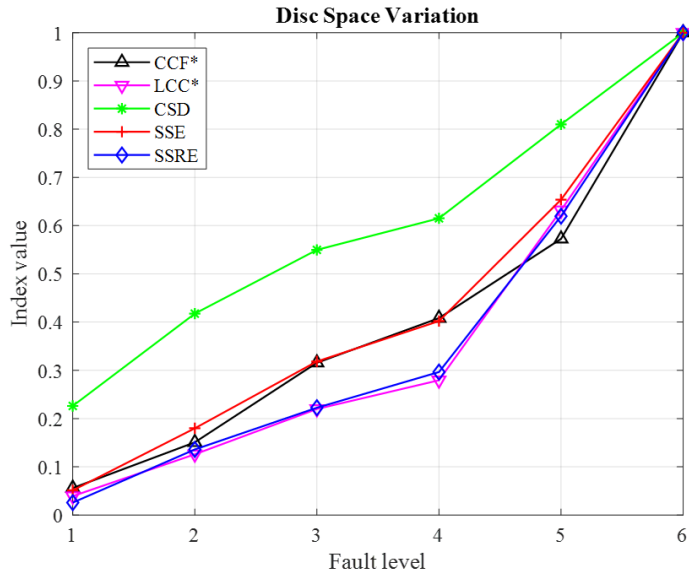
The curves in Figure III.7 show the numerical indices calculated from equations (III.3) to (III.7) for the different levels of fault in the frequency range from 400 kHz to 700 kHz for the mechanical faults and the range from 20 kHz to 50 kHz for the ST fault. Note that the indices CCF and LCC are evaluated as $CCF^* = 1 - CCF$ and $LCC^* = 1 - LCC$ to simplify comparison with other indices. Also, to facilitate indices comparison, a normalization was performed, each index value being divided by the maximum value of its group to obtain a rescale between zero and 1.



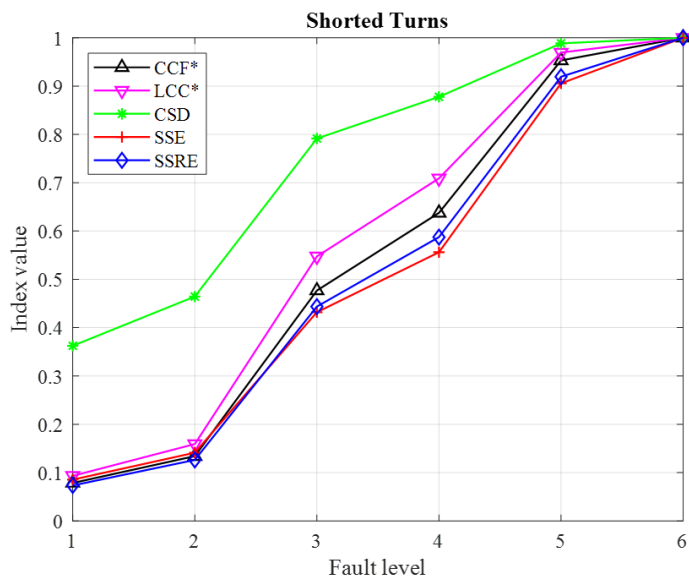
(a)



(b)



(c)



(d)

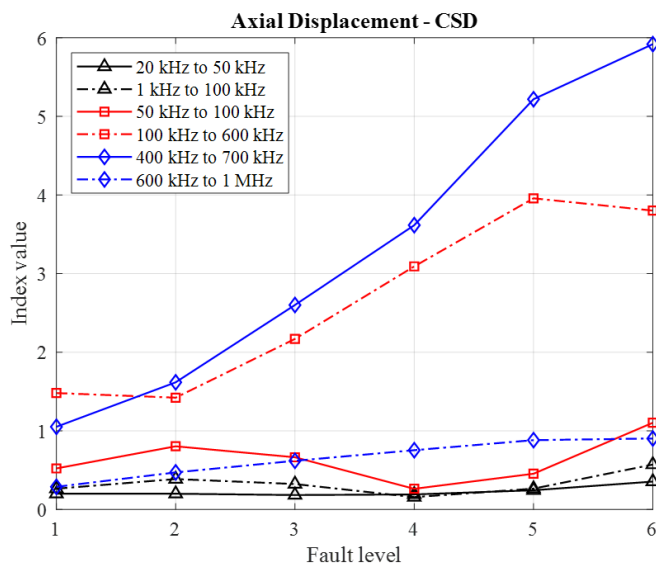
Figure III.7 Numerical index analyses for fault modes (a) axial displacement; (b) radial deformation; (c) disc space variation; and (d) shorted turns
Source: Suassuna de Andrade Ferreira, 2021

All the indices evaluated presented monotonic behaviour for the different faults; that is, for higher levels of the fault, the indices presented their highest value. In addition, the indices all appeared to be linear, though some indices in general are not linear: for example, when the indices include squared calculations. The sensitivity of the indices was not consistent,

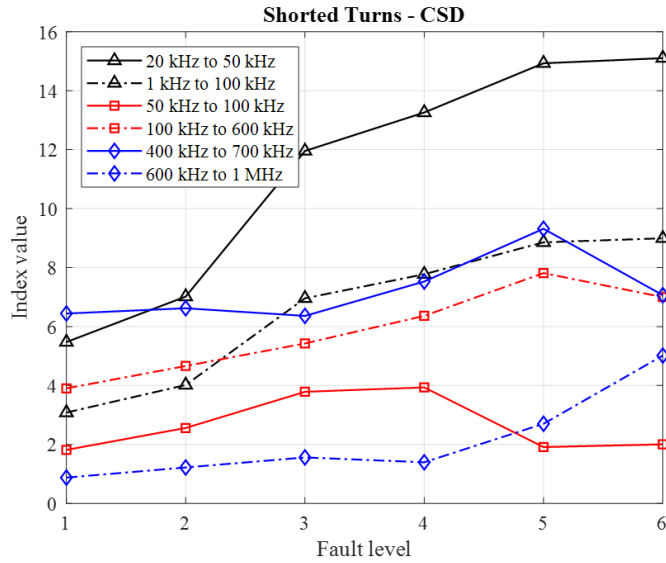
especially at the lowest fault level, which most indices were unable to detect. The CSD index, however, showed good sensitivity, even at the lowest fault level, for all faults, with a value of at least 18% when comparing the first deformation step with the last step up in all cases. Furthermore, the CSD index showed the best overall results for this analysis given its monotonic, linearity and sensitivity behaviour.

Figure III.8 shows an analysis of the frequency ranges used for the index calculations. Frequency ranges from the first resonance (20 kHz to 50 kHz), the first anti-resonance (50 kHz to 100 kHz) and the deviations in fault analysis (400 kHz to 700 kHz) are compared to the Chinese standard [22] frequency band divisions: 1 kHz to 100 kHz; 100 kHz to 600 kHz; and 600 kHz to 1 MHz.

To simplify this last comparison, only the AD and the ST faults were evaluated, the other mechanical faults demonstrating results similar to the AD fault. In addition, only the CSD index was used for this comparison, since it offered the best overall performance for fault evaluation in this laboratory winding model. The CSD index was not normalized for this comparison.



(a)



(b)

Figure III.8 Numerical indices and frequency range evaluation for (a) axial displacement and (b) shorted turns faults

Source: Suassuna de Andrade Ferreira, 2021

Figure III.8a shows that the monotonic behaviour of the CSD index disappeared in most frequency ranges and linearity was observed only from 400 kHz to 700 kHz. This indicates that the frequency range analyzed has a substantial impact on index results and that the frequency bands suggested in [22] are not suitable for the winding model studied. In Figure III.8b, on the other hand, monotonic behaviour appears in the frequency bands suggested by [22] but there is less linearity, mainly due to this fault's characteristics, once again confirming the need for care in determining the frequency bands to be used for index calculation.

3.5. RECOGNITION PERFORMANCE AND DISCUSSION

Three machine learning classifiers were investigated in an effort to obtain a more objective interpretation for fault diagnostics in a winding model: radial basis function (RBF), support vector machine (SVM) and k-nearest neighbour (k-NN).

The measurements shown in Figure III.5 were replicated under very similar conditions, providing a large database of measurements. After disassembling and reassembling sections of winding 1, small deviations were noted in the winding frequency response, giving slight differences in index values. A total of 371 measurements (with and without faults) were taken. For the proposed classifiers, 80% of the measurements were used for training, leaving 20% for testing and validation.

The input vectors were composed of CSD index values in the three main frequency bands of interest (20 kHz to 50 kHz; 50 kHz to 100 kHz; and 400 kHz to 700 kHz).

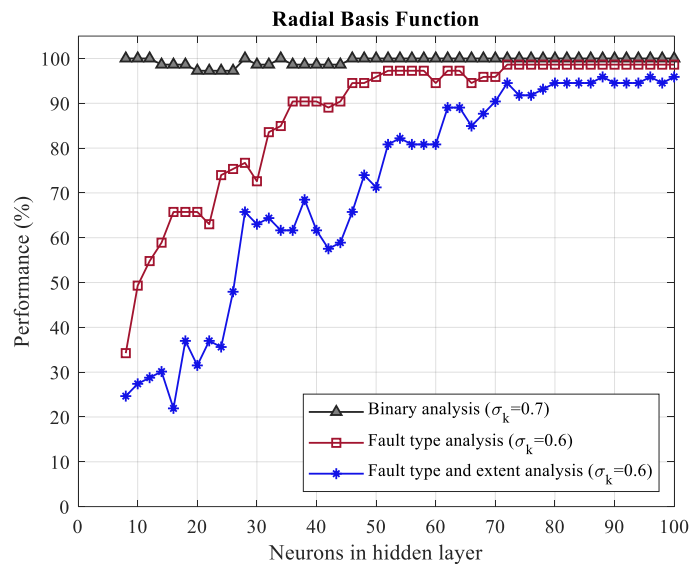
Three types of fault identification were investigated. In the first scenario, the intelligent classifiers were trained and tested to issue a binary decision on the presence or absence of a fault regardless of fault type or nature. Since the learning was qualified as supervised, all fault data were assigned to class C1 and data without fault were assigned to class C2 (binary analysis).

Determination of fault type was introduced in the second scenario. The intelligence algorithms were asked to identify fault type (5 classes): no-fault detected, AD, RD, DSV or ST.

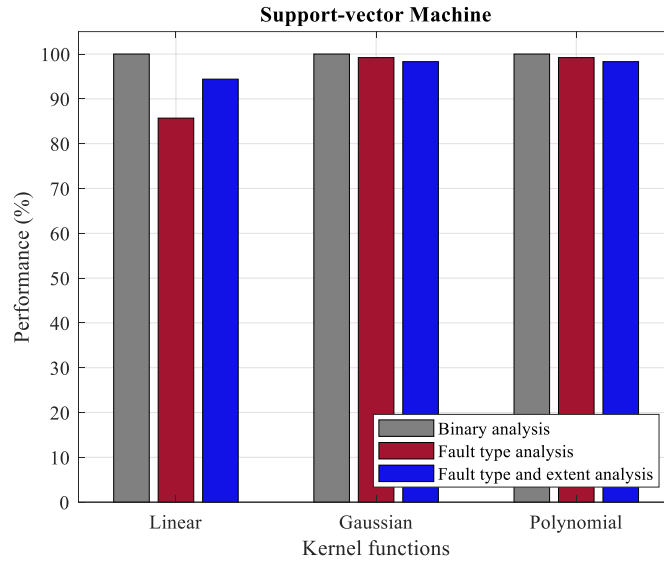
In the third and last scenario, the classifiers were requested to identify fault type (as above) along with fault extent (1 to 6). This calls for discrimination between 25 classes, considerably reducing the amount of data per class and possibly negatively affecting statistical convergence of the network.

The architecture of the suggested RBF neural network comprises an input layer, a hidden layer and an output layer. The neurons in the hidden layer contain Gaussian activation functions whose outputs are inversely proportional to distance from the centre of the neuron. The neurons in the second layer contain a linear activation function (purelin) for categorization purposes. Both layers have biases. The smoothing parameter (spread) of radial basis functions was fixed at 1.

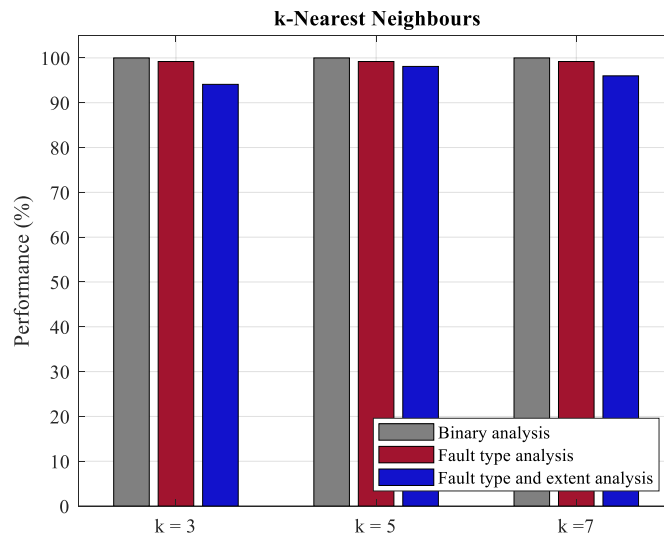
Figure III.9 shows the results for the machine learning classifiers in all the suggested scenarios. The optimization problem in RBF neural network structures is to find the optimal number of hidden layer neurons and their corresponding spread σ_k and centroids μ_k . To find the best value for these parameters, several architectures were considered, trained and tested using 80% and 20% of the measurements, respectively, as described above. For each architecture, the number of neurons in the hidden layer was increased from eight to 100 neuron cells in increments of two. The impact of spread was also investigated, varying σ_k from 0.6 to 1 in increments of 0.1. In normal distributions, variation of the standard deviation impacts the spread of the distribution curve; higher standard deviations spread out the distribution, while lower ones mean a less spread distribution and a more pronounced peak.



(a)



(b)



(c)

Figure III.9 Machine learning architecture performances: (a) radial basis function neural network; (b) support-vector machine; and (c) statistical k-nearest neighbour
Source: Suassuna de Andrade Ferreira, 2021

As Figure III.9a shows, the RBF neural network demonstrated high accuracy (above 98%) in the binary analysis (determining presence or absence of fault) even when using only 8 neurons in the hidden layer. For this analysis, the spread value of $\sigma_k = 0.7$ showed the best performance, though results were very close for all spread values verified. The RBF network's performance in determining fault type was good, more than 90% accurate when at least 40

neurons were used and more than 80% accurate when at least 32 neurons were used. For this analysis, the best performance was obtained with the spread value $\sigma_k = 0.6$. When the RBF neural network was asked to determine fault type and extent, accuracy only exceeded 80% with at least 52 neurons; for 90% accuracy or more, it took at least 70 neurons—considered disproportionate given the size of the database. To overcome this problem, the amount of data available to train the network would have to be increased. For fault type and extent analysis, the best performance was obtained with spread value $\sigma_k = 0.6$.

As Figure III.9b shows, all SVM kernel functions performed well (accuracy > 85%) in the three analyses. The figure also indicates that the performance of the Gaussian and polynomial functions was very close. In fact, these functions are, overall, the best kernel function choice for analysis of the suggested data set, achieving 98% accuracy for fault type and extent detection. Meanwhile, SVM using Gaussian or polynomial kernel functions obtained above 99% accuracy in determining presence or absence of fault. Comparison of the one-versus-one and one-versus-all heuristic methods for SVM algorithms did not show significant variation in their results. To simplify the results, the one-versus-all heuristic method was selected for the graphic presentation.

For the statistical model k-NN, the impact of the number of neighbours was evaluated, that is, $k = 3, 5$ and 7 . The performance of this model was also above 94% for the three classification models studied. These results are shown in Figure III.9c.

The research described in this paper is a proof of concept study. The main advantage of the approach taken was the opportunity to investigate a large number of failure modes and different failure extents on the same unit, as compared to past studies that used limited databases and real transformers, which can be problematic to interpret. A three-phase transformer model that is closer to the real model is being developed so this research can continue in the near future. With this approach and the new model, it should be possible to obtain results that can be more closely generalized to real-case transformers.

3.6. CONCLUSION

This paper reports on frequency response interpretation using numerical indices and machine learning applications. Used for the study was a specially designed laboratory transformer model that allows mechanical defects to be introduced so its frequency response under different circumstances can be evaluated. This model has removable sections and is designed and manufactured to enable short-circuits and deformations (axial and/or radial), allowing reproducibility and repeatability of frequency response measurements. Numerical indices were used to evaluate deviations derived from axial displacements, radial deformations, disc space variations and short-circuited turns integrated into the outer winding.

The results of the index evaluations showed that while all the indices were able to identify the highest levels of deformations in the frequency range of interest (400 kHz to 700 kHz), best overall results were obtained in this study with the CSD, given its monotonic behaviour, linear increase with fault severity and sensitivity even to the smallest deformations.

Results for use of machine learning classifiers for fault diagnostics were promising. The RBF, SVM and k-NN networks performed well classifying faults using the CSD index and targeted frequency bands as input. An automatic- interpretation for fault extent detection in addition to fault classification would be a major asset in power transformer condition monitoring. This remains one of the challenges of our research activities.

CHAPTER IV
A MACHINE-LEARNING APPROACH TO IDENTIFY THE INFLUENCE OF
TEMPERATURE ON FRA MEASUREMENTS

Article published in *Energies*, September 2021

doi: [10.3390/en14185718](https://doi.org/10.3390/en14185718)

A MACHINE-LEARNING APPROACH TO IDENTIFY THE INFLUENCE OF TEMPERATURE ON FRA MEASUREMENTS

Abstract

Frequency response analysis (FRA) is a powerful and widely used tool for condition assessment in power transformers. However, interpretation schemes are still challenging. Studies show that FRA data can be influenced by parameters other than winding deformation, including temperature. In this study, a machine-learning approach with temperature as an input attribute was used to objectively identify faults in FRA traces. To the best knowledge of the authors, this has not been reported in the literature. A single-phase transformer model was specifically designed and fabricated for use as a test object for the study. The model is unique in that it allows the non-destructive interchange of healthy and distorted winding sections and, hence, reproducible and repeatable FRA measurements. FRA measurements taken at temperatures ranging from $-40\text{ }^{\circ}\text{C}$ to $40\text{ }^{\circ}\text{C}$ were used first to describe the impact of temperature on FRA traces and then to test the ability of the machine learning algorithms to discriminate between fault conditions and temperature variation. The results show that when temperature is not considered in the training dataset, the algorithm may misclassify healthy measurements, taken at different temperatures, as mechanical or electrical faults. However, once the influence of temperature was considered in the training set, the performance of the classifier as studied was restored. The results indicate the feasibility of using the proposed approach to prevent misclassification based on temperature changes.

4.1. INTRODUCTION

Power transformer monitoring is crucial to prevent unplanned service interruptions and maintain electric power system stability. Frequency response analysis (FRA) is a well-known method for condition monitoring in power transformers that can identify changes in a transformer's active part. From early studies of the technique in the late 1970s [15] to the present, FRA has demonstrated an ability to detect mechanical and electrical faults in power transformers.

FRA is a non-intrusive monitoring and diagnostic technique that can be implemented without requiring transformer disassembly. As recommended by the principal FRA standards [20, 21], a small sinusoidal voltage waveform is applied over a large frequency band (from a few Hz up to a couple of MHz) to one of the terminals of the transformer (input point), and the response is measured in terms of its amplitude (dB) and phase (degrees) at another available terminal (output point).

The current and reference FRA traces are compared to interpret the FRA measurements, identify changes in the transformer's active part and relate these changes to faults. Ideally, reference measurements are taken just before energization, and subsequent FRA measurements can then show the evolution of the mechanical condition of the transformer over the years. When a reference trace is not available, comparisons between phases in a three-phase transformer or between identical transformers (sister units) can allow the identification of mechanical deformations [16].

In recent studies of FRA interpretation, there has been an increase in the use of machine learning algorithms to help in developing objective interpretations and to reduce dependency on expert analyses [40, 77, 86]. The main challenge now is building a sufficient database to train and test these algorithms. Although more and more FRA testing has been conducted worldwide, data for machine-learning training is still scarce [24].

Another key point in objective FRA interpretation is the method's sensitivity to small changes in the active parts of the power transformers. Alterations in winding geometry, for example, directly influence winding inductance and capacitance and are therefore reflected in FRA traces as frequency shifts and/or amplitude variations. FRA traces are also susceptible to other factors, such as core magnetization, insulation type, and aging, moisture, and temperature [27, 28, 98, 104]. Since the interpretation algorithms can be affected by these conditions, they must be considered in the training sets of the machine learning algorithms.

This study used a laboratory model to build the database necessary to train and test machine learning algorithms. The model allows fault modes to be introduced and FRA measurements to be replicated to generate a large database. A support vector machine (SVM) method with demonstrably good performance in fault identification [105] was tested. The SVM algorithm's ability to distinguish fault measurements from healthy measurements at different temperatures was evaluated. The main goal was to determine the influence of temperature variation on the SVM algorithm used for the automatic classification of FRA measurements. The comparative standard deviation (CSD) index was used to quantify deviations between healthy and faulty FRA traces. Frequencies and amplitudes of the main resonance and anti-resonance points were also obtained to characterize each FRA measurement. The CSD and the resonance points served as input to the SVM algorithm, both individually and combined.

When on-site FRA measurements are taken, temperature can lead to misinterpretation. This study presents a systematic investigation of the influence of temperature on FRA measurement results. A series of experiments were performed on a laboratory model under controlled temperature conditions. The contributions of this study are as follows:

Investigation of FRA measurements in a laboratory winding model under a wide range of temperatures ($-40\text{ }^{\circ}\text{C}$ to $40\text{ }^{\circ}\text{C}$);

Comparative analysis of machine learning algorithm performance with a large database of fault modes, considering the effects of temperature on automatic classification.

Recommendations that will minimize the influence of temperature variation on automated FRA traces interpretation.

The research was not intended to evaluate the numerical index used to quantify deviations between traces or the performance of the classification algorithms. The CSD index and the SVM were selected because they have been widely used in previous studies concerning FRA interpretation [24, 53, 86, 105]. Other numerical indices and/or classification algorithms should offer similar conclusions.

4.2. MATERIALS AND METHODS

The study had three parts: (1) FRA measurements were performed on a laboratory winding model; (2) the numerical CSD index was calculated to quantify deviations between reference measurements, and frequencies and amplitudes of resonance and anti-resonance points were determined; and (3) an SVM algorithm was used to automatically classify the measurements.

4.2.1. LABORATORY SETUP

Measurements were taken on a laboratory transformer model specifically designed for FRA testing, the model having no specifications for power or voltage ratings. The model has a uniform conductor structure (same conductor throughout the windings and an equal number of turns per winding section), and solid, non-graded insulation. The model has two windings that are arranged concentrically. The outer winding (winding 1) has 16 separable sections, each with 28 turns, for a total of 448 turns. The outer diameter of winding 1 measures 317 mm, its

inner diameter measures 300 mm, and it is 511.3 mm high. The inner winding (winding 2) consists of three fixed layers with 76 turns per layer, for a total of 228 turns. The outer diameter of winding 2 measures 277 mm, its inner diameter measures 259 mm, and it is 530 mm high. Figure IV.1 shows the laboratory winding model and its connection schematic.

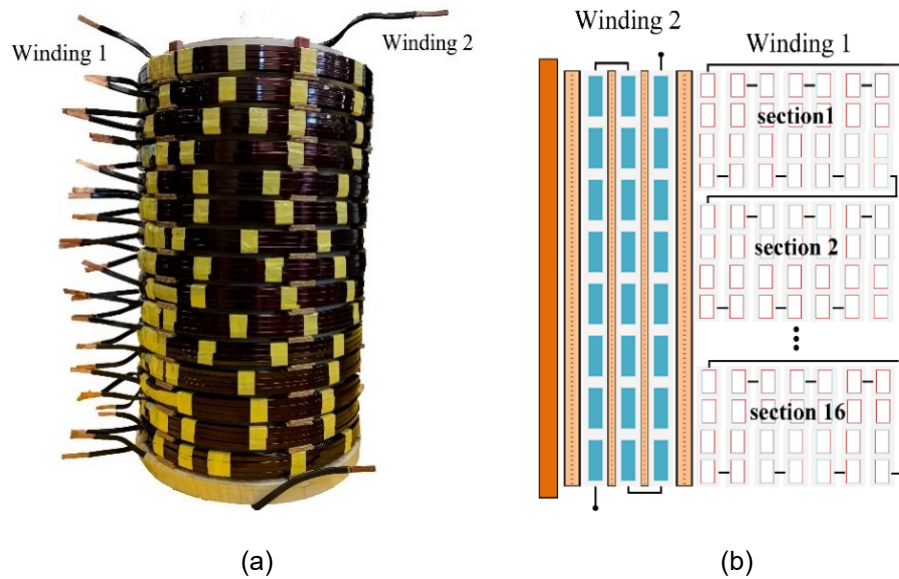


Figure IV.1 Laboratory winding model used for FRA tests: (a) photo and (b) connection schematic

Source: Suassuna de Andrade Ferreira, 2021

A commercial instrument was used to measure FRA traces in the laboratory winding model. For this study, the minimum number of data points per decade was 200, as specified in the IEC standard 60076-18 [20]. Measurements were taken from 1 kHz up to 1 MHz. Two databases of measurements were used for the study: a database with four fault modes and a database with measurements taken at a variety of temperatures.

A) FAULT DATABASE

The fault database was created by introducing four different faults in the laboratory winding model, as well as taking healthy state measurements to serve as reference measurements. The faults include one electrical fault, shorted turns (ST), and three mechanical

deformations: axial displacement (AD), radial deformation (RD), and disc space variation (DSV). Figure IV.2 illustrates the faults and the healthy state of the laboratory winding model.

The AD fault was created by inserting spacers at the bottom of winding 1 to displace it relative to winding 2, resulting in a loss of magnetic coupling between the windings. The fault was incremented in six steps, AD 1 to AD 6. For the first step (AD 1), 6-mm spacers were inserted under winding 1. Spacers were then added in steps of 5.4 mm, to a maximum of 34.4 mm of displacement (AD 6). Figure IV.2b illustrates the winding model as winding 1 is displaced vertically upwards.

The RD fault was generated by replacing healthy sections of the winding with deformed sections. Figure IV.3 shows examples of both healthy and deformed sections used for the measurements. This fault was also incremented in six steps, RD 1 to RD 6. At RD 1, only one deformed section was introduced, to replace section 2 (top to bottom). The sections highlighted in Figure IV.2c were replaced one by one in each subsequent step with a deformed section until six sections were deformed (RD 6).

The DSV fault was created by adding spacers in three different positions between the sections of winding 1, as shown in Figure IV.2d. For DSV 1, a 6-mm spacer was inserted between Sections 2 and 3, and for DSV 2, a 5.4-mm spacer was inserted between these same sections, for a total displacement of 11.4 mm. Next, first a 6-mm spacer (DSV 3) and then a 5.4-mm spacer (DSV-4) were added between Sections 8 and 9, and finally, DSV 5 and DSV 6 were created by adding 6-mm and then 5.4-mm spacers between Sections 14 and 15. In incrementing the DSV fault, the new spacers were added as described without removing the spacers already added for the preceding steps.

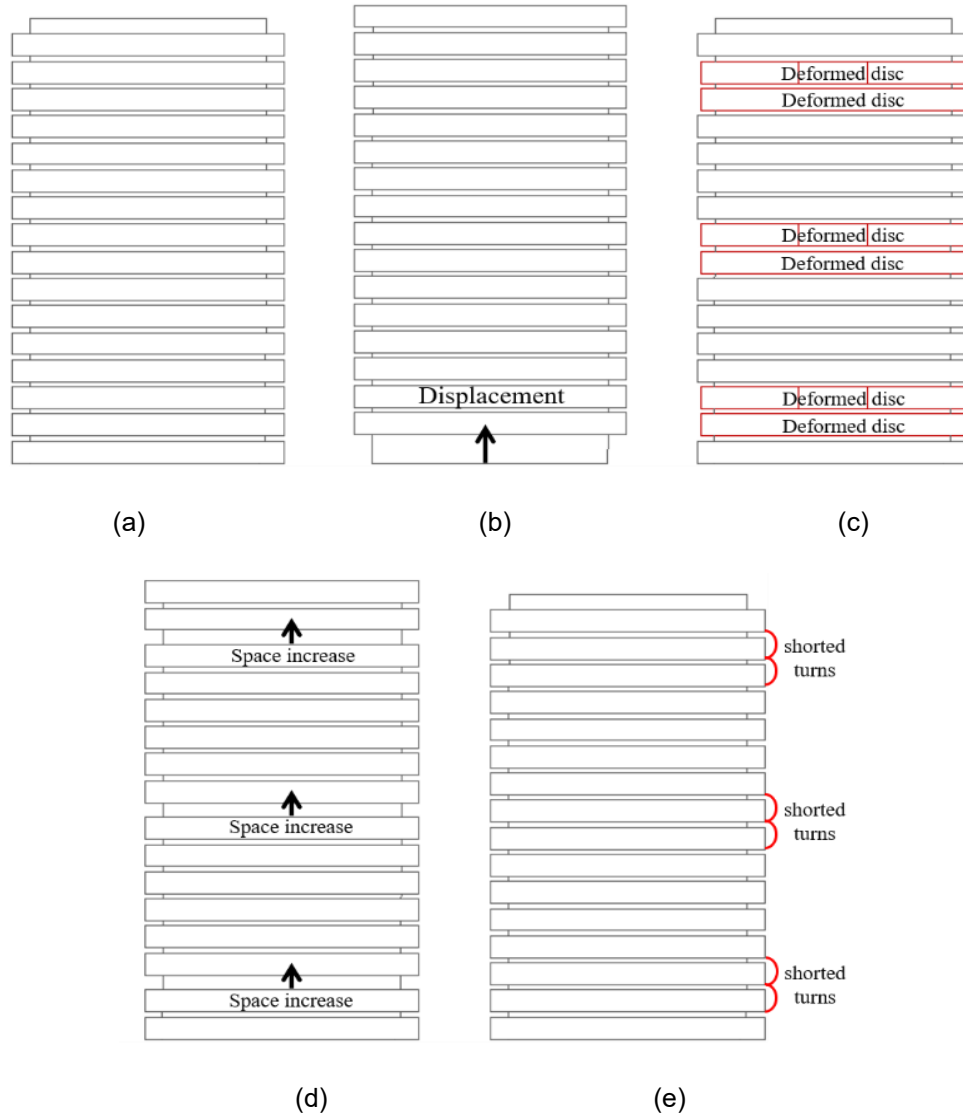


Figure IV.2 Laboratory winding model: (a) healthy state, (b) axial displacement, (c) radial deformation, (d) disc space variation and (e) shorted turns
 Source: Suassuna de Andrade Ferreira, 2021

The shorted turns (ST) fault was created by short-circuiting sections of winding 1. For ST 1, the turns of Section 2 were shorted, for a total of 28 shorted turns. For ST 2, the turns of Section 3 were also shorted, for a total of 56 shorted turns, and so forth, with ST 6 having Sections 2, 3, 8, 9, 14, and 15 shorted, for a total of 168 shorted turns. In incrementing the ST fault, the shorted turns were added without correcting those shorted for the preceding step. Figure IV.2e shows the locations of the shorted turns.

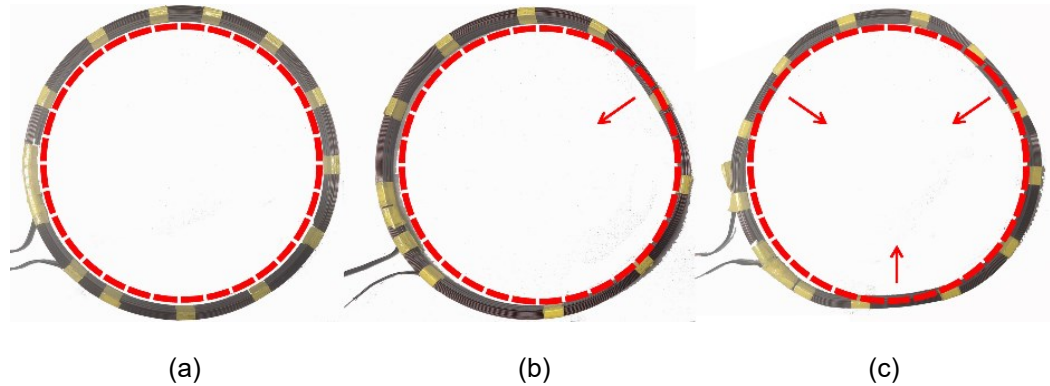


Figure IV.3 Winding 1 sections: (a) healthy section: (b) and (c) radially deformed sections
Source: Suassuna de Andrade Ferreira, 2021

All measurements in the database were taken at 20 °C. A total of 343 FRA traces were used. Details of the FRA traces in the database are given in reference [105].

A) TEMPERATURE DATABASE

The second database created in this study was a temperature database. The FRA measurements were taken with the laboratory winding model placed inside a climatic chamber that can simulate temperatures ranging from -40 °C to 30 °C. For testing at 40 °C, portable heaters were added inside the chamber. The chamber was first heated to 40 °C using the portable heaters and the temperature was then decreased in steps of 10 °C, down to -40 °C. This was done to prevent condensation from forming on the winding model. Once the room temperature was stable (not varying more than ± 1 °C), the FRA trace was obtained. At least four measurements were taken at each temperature to ensure a sufficient database of measurements. A total of 42 measurements were included in the temperature database.

4.2.2. NUMERICAL INDEX CALCULATION

The numerical CSD index was used to quantify deviations between the reference measurement at 20 °C and measurements for other temperatures and faults. CSD values range from zero (perfect match) to infinity, increasing as the deviations between traces

increase. The index works well for frequency deviations, but its sensitivity is not as good for amplitude deviations [24, 53]. In a comparison with other numerical indices, the CSD was deemed to offer good performance in evaluating deviations in FRA traces, given its monotonicity, linearity, and sensitivity [24, 105].

The following equation is used to calculate the CSD:

$$\text{CSD} = \sqrt{\frac{\sum_{i=1}^N [(X(i)-\bar{X}) - (Y(i)-\bar{Y})]^2}{N-1}}, \quad (\text{IV.1})$$

$$\bar{X} = 1/N \sum_{i=1}^N X(i) \quad \text{and} \quad \bar{Y} = 1/N \sum_{i=1}^N Y(i),$$

where X and Y are, respectively, the reference and investigated amplitude vectors of measured frequency responses; $X(i)$ and $Y(i)$ are the i^{th} element of these vectors; and N is the number of data points in vectors X and Y at the frequency window under evaluation.

It is important to note that the frequency range of the index calculation has a significant impact on the calculated value. Many different methods are thus used to select the frequency band for the index calculation. One of the simplest approaches is to evaluate the entire frequency spectrum, as described in [64, 100]. However, if the frequency range is too wide, deviations between traces might be suppressed or may overlap, resulting in a lack of sensitivity in the numerical index evaluation. The frequencies may then be divided into sub-bands, as explained in [20, 22]. To overcome the problem of frequency band division, this study used a sweep frequency window approach, a method based on the study described in [106]. A frequency window (WS) is determined from the number of data points per decade ($f_{p/d}$) in the FRA traces, using Equation (IV.2). Then, the frequency window is swept over the complete frequency range (1 kHz to 1 MHz) in steps of WS/4 to obtain a vector of CSD values:

$$\text{WS} = 10 + 6 \left(\frac{f_{p/d} - 200}{200} \right). \quad (\text{IV.2})$$

4.2.3. SUPPORT VECTOR MACHINE LEARNING

A support vector machine (SVM) is a supervised learning model with associated learning algorithms. SVMs were first developed for solving binary classification problems. They can, however, be adapted for multiclass problem applications with the help of one-versus-one or one-versus-all heuristic methods. These heuristic methods split and transpose a multiclass problem into a binary classification problem. The SVM algorithm allows the classification of linearly separable patterns (x_i) from two classes: C_1 and C_2 . The discrimination between classes is achieved by positioning a hyperplane as a decision boundary. SVMs choose the maximum margin linear separator centered between the hyperplanes h_1 and h_2 , described in Equations (IV.3) and (IV.4):

$$h_1(x_i) = w^t x_i + b \geq 1, \text{ for } x_i \in C_1, \quad (\text{IV.3})$$

$$h_2(x_i) = w^t x_i + b \leq -1, \text{ for } x_i \in C_2, \quad (\text{IV.4})$$

where w is the weight vector and b is the bias or threshold. The support vectors, which give the name to the method, are all the points lying on h_1 or h_2 . The main task of SVM algorithms is to find the optimal weights and biases that minimize the cost function [102].

However, real-world data are frequently not linearly separable, so the SVM does a kernel trick to transform the input space into a higher-dimensional space where the data is linearly separable. This transformation is made possible by the use of kernel functions [92]. Many different functions can be used as kernel functions in SVMs, some of the most common being linear, polynomial and Gaussian.

For the database for this research, the polynomial kernel function was found to perform well and was used for classification. A polynomial function with order p was used, as defined in Equation (IV.5).

$$G(x_j, x_k) = (1 - x_j x_k)^p. \quad (IV.5)$$

A 10-fold cross-validation method can be used to train and test SVM algorithms to prevent overfitting in the data used for model validation. In this method, the data set is divided into 10 parts. One part is then left out of the training and is used instead as the test set, and the classification is performed 10 times, with a different part used each time as the test set. The average deviation of the repeated classifications is then returned as the classification error.

To optimize the study results, grid search optimization [107, 108] was used to determine the best SVM parameters and hence improve algorithm accuracy. The polynomial kernel of order $p = 2$ was found to be the best fit for the dataset classification, together with a one-versus-one heuristic method.

The described SVM algorithm was used to automatically classify the data and obtain an objective interpretation of trace deviation. The machine learning algorithm was implemented using Weka, an open-source software developed at the University of Waikato in New Zealand [107].

Three classification scenarios were produced. For the first, the algorithm was trained and tested as described above, using the fault database. For the second, the same already trained algorithm was tested using the temperature database. For the third classification scenario, the SVM algorithm was trained and tested using a combined database that included faults and temperature measurements.

Three inputs were considered in the SVM classification. First, the CSD values calculated for the frequency windows were used. Then, the frequencies and amplitudes of resonance and anti-resonance points were also used as classification input. Lastly, the combination of these two inputs was used to produce the classification scenarios.

Frequencies and amplitudes of resonance and anti-resonance points were detected by a maxima and minima search of the frequency response traces. Five main resonances and anti-resonances for each measurement were identified using an automatic search.

Figure IV.4 shows a flowchart of the methodology. It is important to note the colors of the arrows in the chart: each classification scenario is presented in a different color.

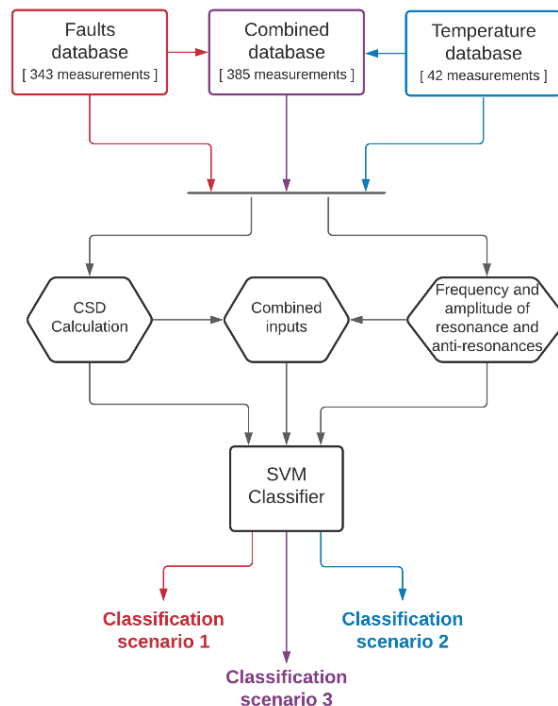
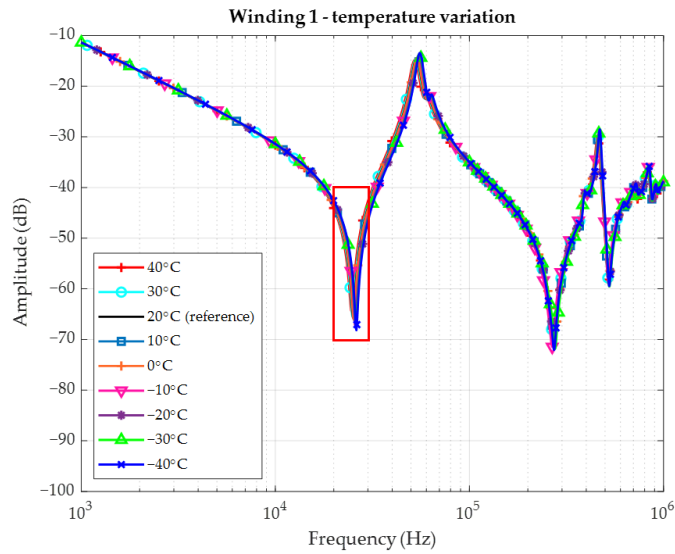


Figure IV.4 Flowchart for classification methodology
Source: Suassuna de Andrade Ferreira, 2021

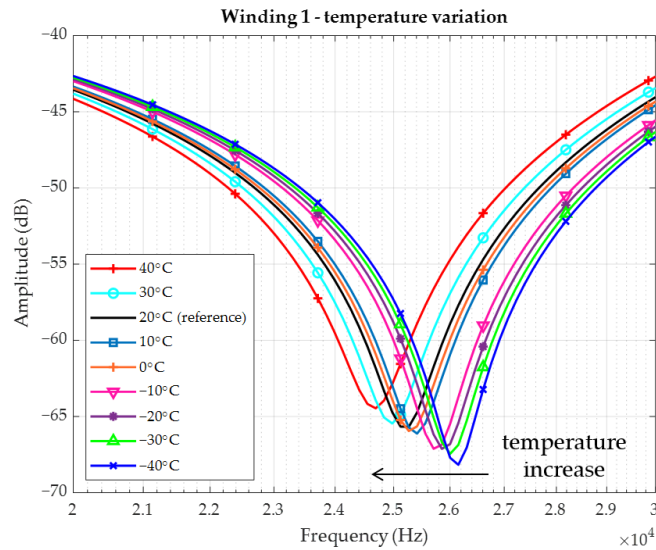
4.3. TEMPERATURE INFLUENCE IN FREQUENCY RESPONSE

Figure IV.5 shows the FRA measurements taken at temperatures from $-40\text{ }^{\circ}\text{C}$ to $40\text{ }^{\circ}\text{C}$, in increments of $10\text{ }^{\circ}\text{C}$. As the figure shows, although deviations are more perceptible at the first anti-resonance and resonance points for the complete frequency range, even higher frequencies also present slight frequency shifts. Zooming in on the first anti-resonance frequency region allows better visualization of the deviations influenced by temperature changes. As the temperature increases, the resonance points shift to lower frequencies. The

zoomed-in portion of Figure IV.5b also shows that resonance amplitudes are damped as the temperature increases.



(a)



(b)

Figure IV.5 FRA measurements in winding 1 at different temperatures: (a) complete frequency range; and (b) zoomed-in portion at the first anti-resonance point
Source: Suassuna de Andrade Ferreira, 2021

The deviations in the FRA traces, such as those seen in Figure IV.5, are definitely from alterations in transformer elements, as demonstrated in previous FRA studies [15, 21, 24].

Changes to winding inductances, series and shunt capacitances, resistances and insulation conductance are the main causes of deviations. Temperature can influence FRA traces by modifying material parameters, such as magnetic permeability, resistivity, electrical permittivity, etc. [33, 109, 110]. Changes to geometry due to temperature changes (thermal expansion of conductors, for example) might also be present and affect self and mutual inductances, as well as capacitances between turns. However, in the temperature range considered in this study ($-40\text{ }^{\circ}\text{C}$ to $40\text{ }^{\circ}\text{C}$), copper dilation can be assumed to be negligible [111]. and, hence, changes to geometry were not considered as possibly affecting the FRA traces.

Coil inductances can be affected by changes in magnetic permeability due to temperature variation. However, the studies in [28] show only small inductance variations (less than 1.1%) under similar conditions for a temperature shift of $60\text{ }^{\circ}\text{C}$. In addition, there is no magnetic core in the tested model. Hence, the impact of inductance variation on the FRA traces due to temperature change can be considered insignificant.

The complex model for high-frequency studies of a transformer winding can be overviewed as a series impedance ($Z(\omega)$) and a dielectric shunt capacitance ($Y(\omega)$). These elements are presented as:

$$Z(\omega) = R(\omega) + j\omega L(\omega), \quad (\text{IV.6})$$

$$Y(\omega) = G(\omega) + j\omega C(\omega), \quad (\text{IV.7})$$

where ω is the angular frequency, R and L are the equivalent resistance and equivalent inductance of the conductors, respectively, and G and C are the equivalent conductance and equivalent capacitance of the insulation system, respectively.

The model under study presents dielectric materials, such as pressboard, paper, and air. The response of these materials in the presence of alternating fields can be described by a complex permittivity frequency dependent presented in Equation (IV.8):

$$\hat{\epsilon}(\omega) = \epsilon'(\omega) - j\epsilon''(\omega), \quad (\text{IV.8})$$

where ϵ' and ϵ'' are the real and imaginary parts of the dielectric permittivity, respectively. The admittance can then be re-written, in terms of the dielectric response [27];, as Equation (IV.9):

$$Y = \omega\epsilon''C + j\omega\epsilon'C. \quad (\text{IV.9})$$

The dielectric response is a function of both frequency and temperature. The dependency of the permittivity to temperature can be described by its relation to the medium conductivity (σ), which is highly temperature (T)-dependent. The imaginary part of the dielectric response related to the conductivity is then presented by:

$$\epsilon''(\omega) = \frac{\sigma(T)}{\omega}, \quad (\text{IV.10})$$

and the temperature dependence of the conductivity can be described by the Arrhenius equation, as in Equation (IV.11) [112]:

$$\sigma(T) = \sigma_0 e^{(-E_a/k_B T)}, \quad (\text{IV.11})$$

where σ_0 is the pre-exponential factor, E_a is the activation energy, and k_B is the Boltzmann's constant. Finally, the increase in the complex permittivity of the insulation, due to the increase in temperature, has an impact on the conductance loss, and this loss can be identified by the damping effect present in the resonances in the FRA traces, as illustrated in Figure IV.5b.

Furthermore, the shift of resonances to lower frequencies, as the temperature increases, can be associated with an increase in the capacitances of the model [112]. The capacitance changes can be calculated from the first resonance point (Figure IV.5b). Local resonances and anti-resonances are characterized by the interaction between inductive and capacitive reactances [95]. Every resonance or anti-resonance considered independently can be interpreted through Equation (IV.12):

$$f_{res} = \frac{1}{2\pi \sqrt{L_i C_i}}, \quad (IV.12)$$

where f_{res} is the resonance frequency, and L_i and C_i are the inductance and capacitance corresponding to the resonance point under consideration.

It is well established that winding inductances are not significantly affected by temperature variation [27, 28].; the main hypothesis is that temperature primarily influences the resonance frequency points due to moisture migration/dynamics and electrical permittivity changes. Based on this hypothesis, capacitance variation with temperature can be estimated using Equation (IV.12), with the inductance value estimated from Equation (IV.13). This equation is derived from the FRA transfer function in (IV.14) with a 50 Ω measurement impedance for the measuring instrument [16]:

$$L_i = \frac{50 \sin(-\varphi)}{10^{H_{dB}/20} 2\pi f}, \quad (IV.13)$$

$$H_{dB} = 20 \log_{10} \left(\frac{V_{out}}{V_{in}} \right), \quad (IV.14)$$

where V_{in} is the input voltage applied at the input point, V_{out} is the output voltage measured at the response terminal, and φ is the phase difference between input and output voltages [21].

The inductance value is then calculated at the linear descendent part of the FRA trace leading to the first anti-resonance. In this region (around 4 kHz), the inductances are very close to each other, demonstrating that the inductance is not significantly influenced by temperature. The average value is 28 mH. Capacitance values are calculated using a rearranged Equation (IV.12), solving for C_i , and using the first anti-resonance frequencies at each temperature point. The results are shown in Figure IV.6, along with the polynomial fitted curve for the data points of the capacitance calculation.

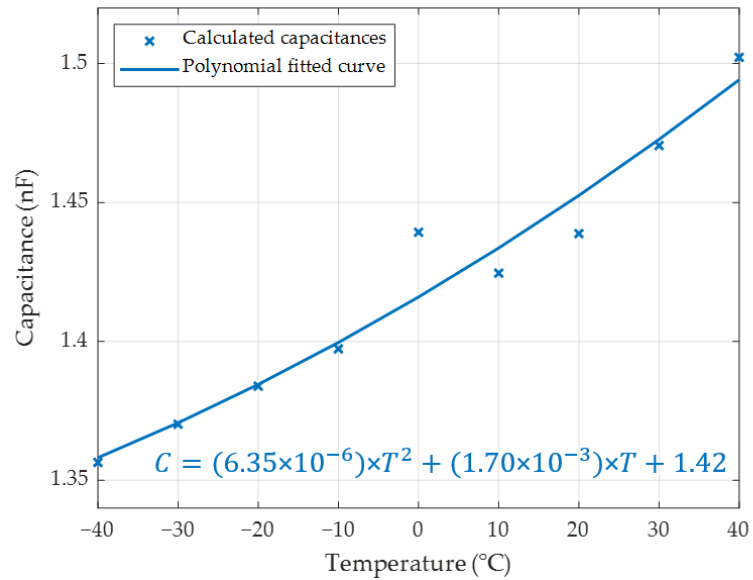


Figure IV.6 Capacitance variation with temperature change
 Source: Suassuna de Andrade Ferreira, 2021

As shown in Figure IV.6, distributed capacitance increases as the temperature increases. This is mainly due to the electrical permittivity change in the test environment. Since the model has air insulation, any change in the testing chamber temperature directly affects the temperature of the insulation, which in turn displaces the resonant frequencies.

4.4. NUMERICAL INDEX RESULTS

The CSD index was used to quantify deviations according to temperature change. The index was calculated over the complete frequency range, from 1 kHz to 1 MHz, in frequency windows calculated from (2). Figure IV.7 illustrates CSD values for the different temperatures. To avoid overloading the figure, only the two extreme temperatures (40 °C and -40 °C), plus the curve at reference temperature (20 °C), are included in the figure. The CSD index indicated higher values around the first anti-resonance and resonance points, and lower but significant values at higher frequencies (above 200 kHz), as can be seen in Figure IV.7.

CSD values were similarly calculated for the different fault modes (axial displacement, radial deformation, disc space variation, and shorted turns) for further comparisons and classification algorithm implementation. Figure IV.8 provides a sample (only one step of each fault) of the results and the calculated CSD vectors.

As Figure 8 shows, the different faults affected the frequency response at different frequency ranges. A comparison of Figure IV.7 and Figure IV.8 shows that the shorted turns fault had an impact similar to that of temperature variation on the first anti-resonance, with smaller CSD values. Temperature variation caused significant deviations at higher frequencies (above 250 kHz), as was the case with the different fault modes. As this comparison indicates, an automatic algorithm might have difficulty distinguishing simple temperature variation in FRA measurements from a fault mode.

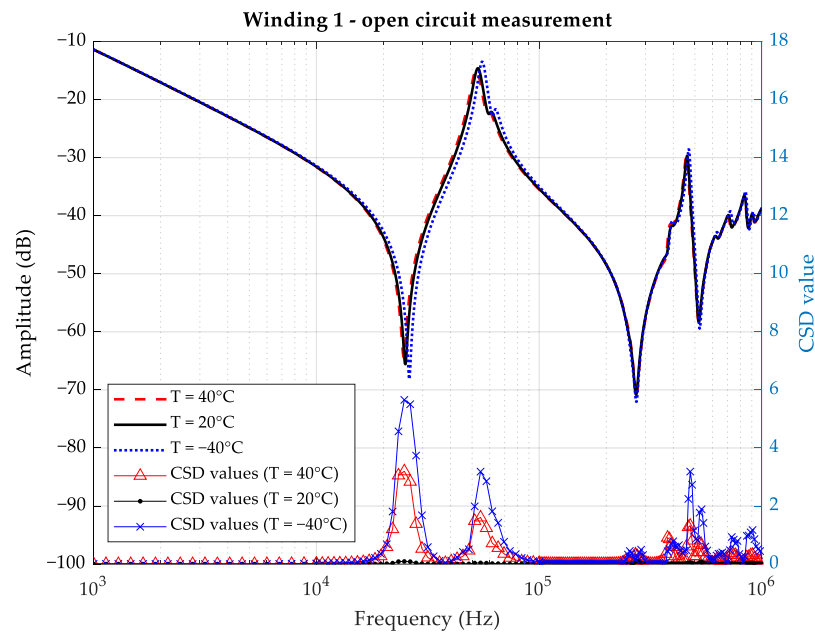


Figure IV.7 CSD values, calculated for FRA measurements at 40 °C, 20 °C and -40 °C
Source: Suassuna de Andrade Ferreira, 2021

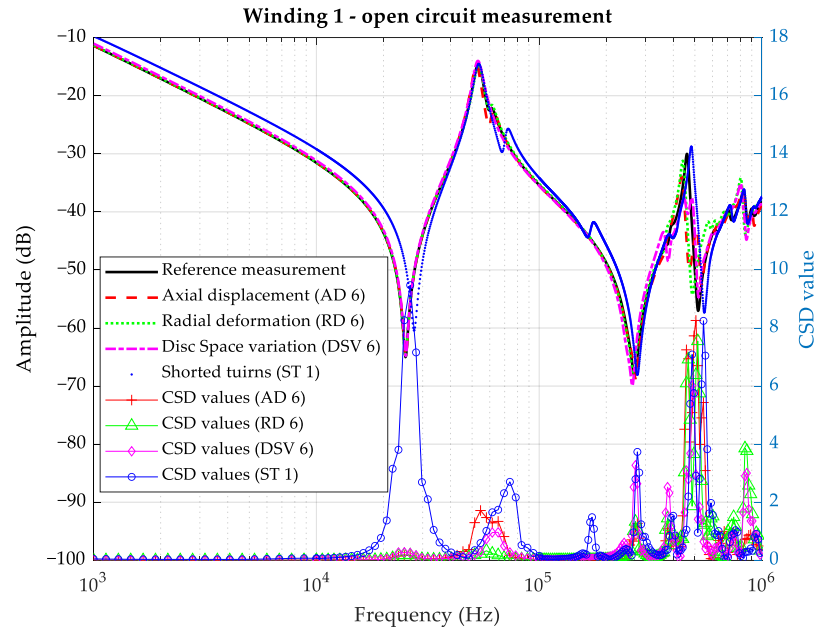


Figure IV.8 CSD values calculated for FRA measurements in different fault modes at 20 °C
 Source: Suassuna de Andrade Ferreira, 2021

4.5. CLASSIFICATION ALGORITHM RESULTS AND DISCUSSIONS

The fault database was used for classification scenario 1. A CSD vector was calculated and used as input for the classification algorithm. The resonance and anti-resonance points of the traces were also considered. The algorithm analyzed each of the 343 instances and classified them into 5 classes: no-fault, axial displacement (AD), radial deformation (RD), disc space variation (DSV), or shorted turns (ST). Figure IV.9 shows the confusion matrices obtained for these classifications.

The general performance of this classification was 93% when only CSD values were used as input. The performance increased to 99.7% when resonance and anti-resonances were considered as input. In all the classification scenarios, 10-fold cross-validation was used to train the algorithm. The confusion matrix shows the percentage of instances classified in each class, along with the total number of instances corresponding to this percentage.

CSD vector
Classified as:

		No-fault	AD	RD	DSV	ST
True class	No-fault	100% (49)	0	0	0	0
	AD	1% (1)	99% (128)	0	0	0
	RD	0	0	100% (70)	0	0
	DSV	32% (23)	0	0	68% (49)	0
	ST	0	0	0	0	100% (23)

(a)

Resonances and anti-resonances
Classified as:

		No-fault	AD	RD	DSV	ST
True class	No-fault	100% (49)	0	0	0	0
	AD	0	99% (129)	0	0	0
	RD	0	0	100% (70)	0	0
	DSV	0	0	0	99% (71)	1% (1)
	ST	0	0	0	0	100% (23)

(b)

Combined input
Classified as:

		No-fault	AD	RD	DSV	ST
True class	No-fault	100% (49)	0	0	0	0
	AD		100% (129)	0	0	0
	RD	0	0	100% (70)	0	0
	DSV	0	0	0	99% (71)	1% (1)
	ST	0	0	0	0	100% (23)

(c)

Figure IV.9 Confusion matrices for fault database classification (classification scenario 1) using the following as input: (a) CSD vector values, (b) resonance and anti-resonance points (frequency and amplitude) and (c) combined input
Source: Suassuna de Andrade Ferreira, 2021

The temperature database was then used to test the classification algorithm (classification scenario 2), with the CSD vector and a combination of CSD vector values and resonance and anti-resonance points as input. Since classification with only the resonance points did not differ from the combination of inputs, this classification was omitted from thenceforward. The algorithm was expected to classify the data without having previously been trained for temperatures other than 20 °C. Figure IV.10 shows the confusion matrices obtained for this new test. The general performance of the SVM method dropped to 71% when the CSD vector was used. However, the performance of the classifier using the resonance and anti-resonance points dropped to 40%. These confusion matrices were also divided into four additional matrix lines, according to the temperature of the measurements classified.

The confusion matrices shown in Figure IV.10 corroborate the hypothesis that the algorithm is not always capable of distinguishing faults from temperature variation. As the matrices divided by temperature show, significant problems occurred when the temperature dropped below -10 °C, that is, a shift of -30 °C from the reference temperature (20 °C). The measurements from -40 °C to -20 °C were misclassified as axial displacement, disc space variation, or shorted turns faults, depending on the input used for classification.

To overcome the misclassification problem, the SVM algorithm needs to be trained with FRA measurements at different temperatures, to learn as many different patterns as possible. In classification scenario 3, both the fault database and the temperature database are considered when training the SVM algorithm. For this classification scenario, the training and testing datasets included 70% and 30% of the complete dataset, respectively; that is, 70% of the data was used to train the classification algorithm, with the remaining 30% left for testing and validation. Afterward, the datasets were stratified to ensure the ratio of temperature and fault data was maintained from the initial complete dataset into the divided training and testing sets.

CSD vector
Classified as:

True class	Classified as:					Temperature:	Shift from reference (20 °C):
	No-fault	AD	RD	DSV	ST		
No-fault	71% (30)	10% (4)	0	19% (8)	0	-40 °C to 40 °C	[-60 to +20] °C
No-fault	100% (16)	0	0	0	0	20 °C to 40 °C	[0 to +20] °C
No-fault	93% (13)	0	0	7% (1)	0	-10 °C to 10 °C	[-30 to 10] °C
No-fault	8% (1)	33% (4)	0	58% (7)	0	-40 °C to -20 °C	[-60 to -40] °C

(a)

Combined input
Classified as:

True class	Classified as:					Temperature:	Shift from reference (20 °C):
	No-fault	AD	RD	DSV	ST		
No-fault	40% (17)	5% (2)	0	0	55% (23)	-40 °C to 40 °C	[-60 to +20] °C
No-fault	88% (14)	12% (2)	0	0	0	20 °C to 40 °C	[0 to +20] °C
No-fault	21% (3)	0	0	0	79% (11)	-10 °C to 10 °C	[-30 to 10] °C
No-fault	0	0	0	0	100% (12)	-40 °C to -20 °C	[-60 to -40] °C

(b)

Figure IV.10 Confusion matrices using temperature database to test the SVM classification algorithm (classification scenario 2) with the following as input: (a) CSD vector values and (b) combined input with CSD vector and resonances and anti-resonances
Source: Suassuna de Andrade Ferreira, 2021

The SVM's general performance, using the combined databases (fault and temperature databases) and the CSD vector as input, was once again 93.9%. Its performance returned to 99.1% when resonances and anti-resonances were used in combination with the CSD vector. This indicates that once temperature is considered in the training dataset, the classification algorithm performs as well as when only faults are used in the classification. This was true for all inputs considered, confirming the importance of a large database of measurements that consider different temperatures in the training dataset.

In this study, measurements at different temperatures were possible because the laboratory winding model allowed a number of possibilities for FRA measurements. With real transformers, measuring a wide range of temperatures may not be feasible. One possible solution to this problem is to improve automated interpretation by using computational simulation environments to help generate a database of frequency responses that includes different fault and temperature conditions. Further research into this possibility should be considered.

4.6. CONCLUSIONS

This paper addresses the interpretation of FRA measurements at different temperatures using machine-learning applications. A laboratory winding model specially designed for FRA measurements was used as the testing equipment. The model allows the introduction of mechanical and electrical faults and, hence, frequency response under different conditions can be assessed. Tests were performed in a climatic chamber, allowing the temperature to vary from $-40\text{ }^{\circ}\text{C}$ to $40\text{ }^{\circ}\text{C}$. The influence of the temperature on an SVM algorithm classification was reported.

As already reported in the literature, temperature affected the measurements. Among other things, variations in capacitance values were noted, probably due to moisture dynamics related to changes in the insulation temperature. The results also showed that when temperature is not considered in the training set of the machine learning algorithm, the classification can be compromised. In fact, at least 30% of the tested measurements were misclassified on the first attempt, with the error of classification as high as 60%, depending on the input data for the classification algorithm. The misclassification occurred predominantly in a group with temperature shifts of more than $30\text{ }^{\circ}\text{C}$.

Temperature measurements need to be included in the training set to overcome the misclassification problem and restore SVM performance. The SVM classifications were

performed using the following as classifier input: (a) CSD index values; (b) trace resonance and anti-resonance frequencies and amplitudes; and (c) a combination of (a) and (b). The CSD was calculated over a frequency window that swept the entire frequency range to obtain a vector of CSD index values.

Confusion matrices were used to get a picture of the SVM performance. They show that the algorithm misclassifies different temperature measurements as an axial displacement, disc space variation or short-circuited turns faults, corroborating the need to include different measurement conditions in the training datasets of machine learning algorithms. The improvement in the database when measurements that consider other factors influencing FRA traces are included needs to be acknowledged. This is one of the contributions of this research.

CHAPTER V
REPRODUCING TRANSFORMER'S FREQUENCY RESPONSE FROM FEM SIMULATION
AND PARAMETERS OPTIMIZATION

Article to be submitted to a peer review journal

REPRODUCING TRANSFORMER'S FREQUENCY RESPONSE FROM FEM SIMULATION AND PARAMETERS OPTIMIZATION

Abstract

Frequency Response Analysis (FRA) is being employed worldwide as one of the main methods for condition assessment in transformers due to its capability to detect changes inside transformers. Nonetheless, the objective interpretation of FRA measurements is still a challenge for the industry. This is mainly attributable to the lack of complete data from the same or similar units. A large database of FRA measurements can contribute to improving automatic classification algorithms and lead to a more objective interpretation. Due to their destructive nature, mechanical deformations cannot be performed on real transformers to collect data from different scenarios. The use of simulation and laboratory transformers models is necessary. This research proposes a new method using Finite Element Method simulation and lumped element circuit to obtain FRA traces from a laboratory model at healthy and faulty states, along with an optimization method to improve capacitive parameters from estimated values. The results show that measured and simulated FRA traces are in good agreement. Furthermore, the faulty FRA traces were analyzed using automatic classification algorithms, and the results have shown good classification for short-circuit faults, while axial displacements were only well classified at their greatest extents. This supports the use of the proposed method in the generation of faulty frequency response for automatic classification algorithms. The proposed approach is therefore tailored for generating a larger and unique database with industrial importance and academic significance.

5.1. INTRODUCTION

Frequency Response Analysis (FRA) is a well-known monitoring and diagnostic method used in the industry to detect faults in power transformers [85, 113, 114]. This technique is based on interpreting power transformers as an electric circuit comprising inductive, capacitive, and resistive parameters. When a fault occurs inside the transformer, these parameters are differently influenced. For example, short-circuited turns can affect self and mutual inductances, while winding movements can principally affect series capacitances [79]. A comparison between reference measurement (before fault or healthy measurement) and actual measurement (faulty measurement) presents frequency response deviations because of circuit parameters change. These deviations can therefore allow fault identification.

Nonetheless, FRA interpretation is not straightforward. This is because the parameters in frequency response depend on many variables in the transformer design characteristics, such as power and voltage ratios, insulation type, windings type and connections. In this regard, many researchers have been focusing on developing objective interpretation schematics to identify fault type, extent, and location [49, 86, 115, 116]. The main categories of interpretation methods are numerical indices, simulation models and automatic classification algorithms [24].

The use of numerical indices helps quantify the difference between reference and actual measurement. This technique has been applied using numerical index limits to differentiate healthy and faulty transformers [22, 51, 86] and as input to automatic classification algorithms [29, 49].

High-frequency simulation models are used to reproduce the frequency response of the power transformer. These models allow the generation of FRA traces at different fault conditions without damage to the physical transformer. The simulations use the Finite Element Method (FEM) [25, 78] and the RLC equivalent circuit method [33, 117] individually or combined [79] to recreate the traces. In addition, the transformer's design data, such as

geometrical dimensions and material properties, are required to obtain the RLC circuit parameters for FEM simulation [33, 109].

The current literature on simulation models explores methods to replicate FRA traces and observe the frequency response once the faults are introduced. New information can be acquired by correlating circuit elements changes, or the geometry changes, in previous and after fault simulations [80]. Moreover, most recent research has also compared the capabilities of simulation models to attain numerical indices values to the ones calculated from measured traces [25]. However, the application of numerical indices from simulation models into automatic classification algorithms is yet to be explored.

Automatic classification algorithms are implemented using numerical indices [29] and, more recently, image processing methods [26] as input for the algorithms. These algorithms are trained and tested to classify faults from frequency responses automatically. Consequently, classification algorithms require an extensive database of fault cases to learn from and be able to classify unseen instances. FRA method has expanded its use worldwide as a main diagnostic method, and even though it has been standardised by different international groups [20, 21], the data available to develop and improve automatic classification algorithms are still scarce [24].

This research has developed a new method for simulating frequency response in transformers using the finite element method (FEM) and lumped circuit elements to contribute to this matter. The approach is based on calculating, estimating, and optimising lumped circuit parameters. The main contributions of this study are:

- A new approach for FEM simulation of frequency response in transformers;
- Lumped elements circuit parameters optimisation;
- A novel approach tailored for generating an infinite and unique database for training classification algorithms with potential impact on FRA interpretation improvements.

5.2. MATERIALS AND METHODS

The methodology employed for the frequency response simulation is based on a laboratory winding model specially designed for FRA measurements. The simulation is first performed using Comsol Multiphysics® software, and later the capacitance parameters are optimized using MATLAB® functions and Comsol Multiphysics®.

5.2.1. LABORATORY WINDING-MODEL

The transformer model consists of two coils, an outer winding (winding 1) and an inner winding (winding 2). A picture and the electrical connections schematics for the winding model are presented in Figure V.1. The model is specially designed for FRA measurements. Thus, no power or voltage ratings are attributed to it. The insulation present in the winding is uniform, solid, and non-graded. Winding 1 has 300 mm of internal diameter and is composed of 448 turns distributed in 16 sections of 28 turns each. The sections in winding 1 are disposed in top of the other with pressboard paper spacers of 6.14 mm between them. The total height of winding 1 is 515 mm. Winding 2 has 251 mm of internal diameter with 228 turns distributed in three layers of 76 turns each. The total height of winding 2 is 530 mm.

The 16 sections of winding 1 are designed to be interchanged and therefore allow the introduction of faults in the winding model. For example, short-circuits can be introduced by connecting the terminals of any section. Axial displacements can be created by displacing the entire winding 1, while radial deformation can be performed by exchanging the winding sections for deformed ones, preserving the model's integrity [49].

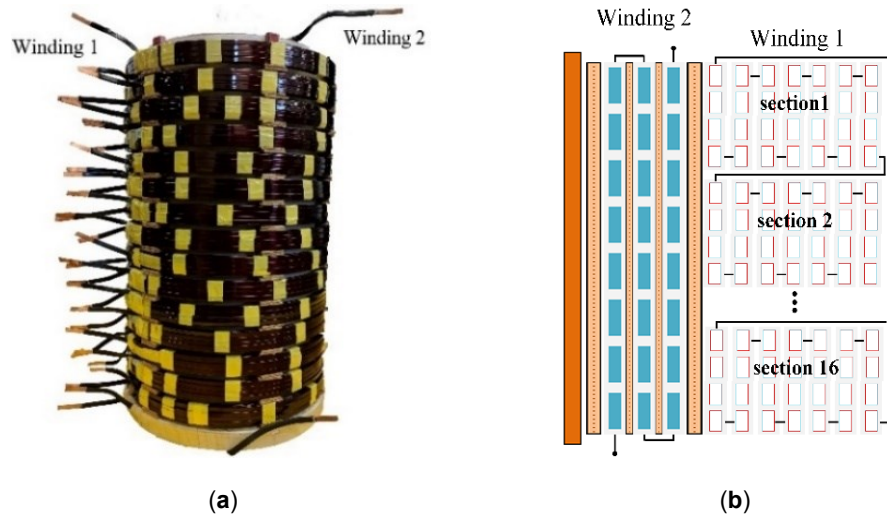


Figure V.1 Winding- model used for simulation and measurement purposes: (a) model's picture and (b) connections schematic
 Source: Suassuna de Andrade Ferreira, 2022

5.2.2. FINITE ELEMENT METHOD SIMULATION

The FEM simulation is performed in three steps. First, a geometric model is developed based on the laboratory winding-model dimensions. Then, the windings are defined using the magnetic fields and electrostatic physics available in Comsol Multiphysics®. These physics are used to associate the geometric sections to the correspondent number of turns and excitation of the coils, as well as the equations that define the study. Finally, an equivalent electric circuit obtains the winding's frequency response.

Figure V.2 presents the 2D axis-symmetric and a cut-view of the 3D form. A 2D axis-symmetric geometry can be used to represent the model, and this simplification saves computational effort while the final frequency response is not affected.

The FEM simulation considers the skin and proximity effects. Any increase in the frequency is reflected in the current density in the conductors due to these effects. As shown in Figure 3, at 60 Hz, the current density is primarily uniform in the conductor. As the frequency increases, the current density increases near the edges of the conductors.

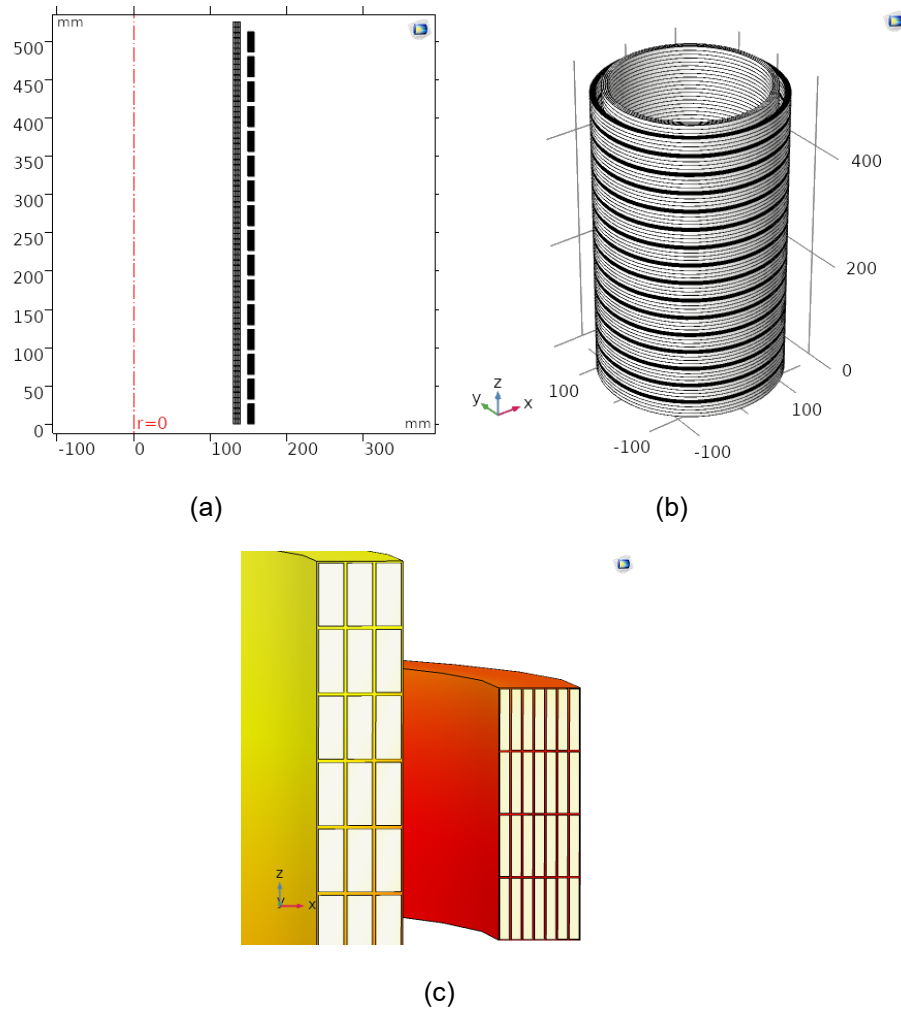


Figure V.2 Geometric model created for simulation of the frequency response (a) 2D axisymmetric geometry, (b) rotational form of 2D axisymmetric model and (c) detail of conductors and insulation from windings 1 and 2
 Source: Suassuna de Andrade Ferreira, 2022

The magnetic field and electrostatic physics in *Comsol Multiphysics*® use Ohm's law to calculate the lumped element parameters. These parameters are then introduced in the electrical circuit physic to calculate the frequency response, similar to the measurement setup presented in Figure V.4. A voltage signal of 10 V over a sweep of frequencies is applied to the electric circuit through the input terminal (V_{in}), and the measured voltage is obtained at the output terminal (V_{out}). The open circuit measurement was preferred due to its extensive applicability in FRA interpretation methods. While winding 1 is under measurement, winding 2 is kept open, according to the FRA measurements standards [20].

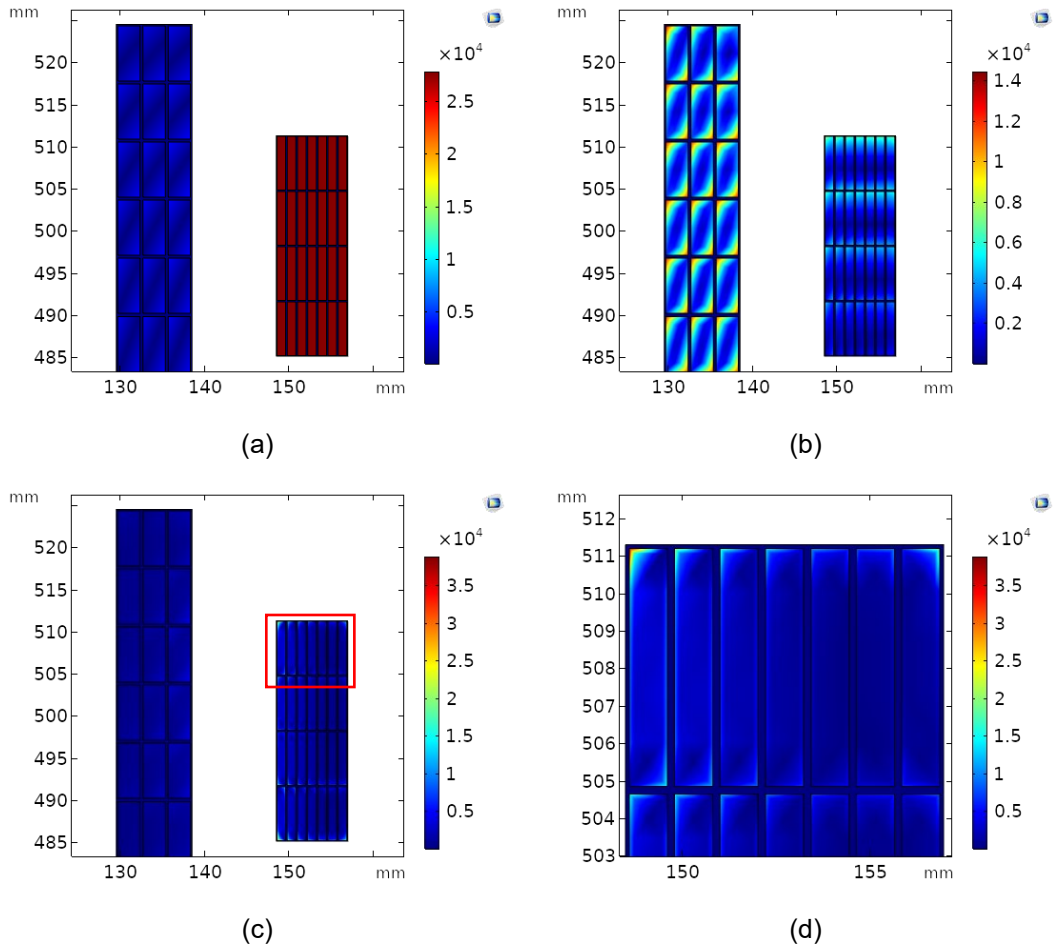


Figure V.3 Current density in the conductors' section area at (a) 60 Hz, (b) 10 kHz and (c) 1 MHz, (d) zoomed portion at 1 MHz
Source: Suassuna de Andrade Ferreira, 2022

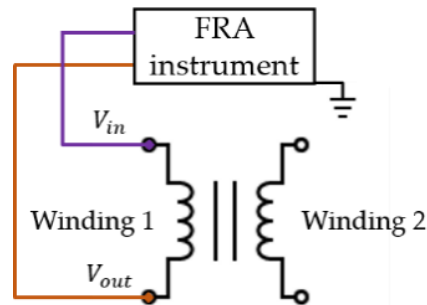


Figure V.4 FRA measurement schematic for winding 1 open circuit measurement
Source: Suassuna de Andrade Ferreira, 2022

5.2.3. OPTIMIZATION OF CIRCUIT PARAMETERS

An optimisation method is used to attain the best fit between measured and simulated curves. The optimisation is performed using MATLAB® function `fminsearch`. `Fminsearch` uses the Nelder-Mead simplex algorithm, described in [118]. Initially, the algorithm makes a simplex evaluation around the initial estimated values (x_0), adding 5% to each of the initial estimations ($x_0(i)$) at a time. Following, the algorithm modifies the simplex repeatedly until the method finds the minimum of the desired function. For this research, the mean square error is used as the function to be minimised, and the capacitance values (C_{s1} , C_{s2} and C_{12}) are the variables (x). The optimisation adjusts the capacitance values at each interaction. It recalculates the simulated frequency response and the mean square error between measured and new simulated curves until the error is minimal. The optimization ends once $|f(x(i)) - f(x(i + 1))| < 10^{-4}$, which means the error function has reached a local minima.

5.2.4. EVALUATION OF SIMULATION MODEL

Different faults are introduced to evaluate the simulation model created, and comparisons between simulated and measured frequency responses are performed. Two extents of axial displacement fault and two of short-circuit fault are added. These two fault types are sufficiently different and diversified to exploit the capabilities of the simulated model. As seen in the literature and the simulation process, axial displacements influence series and interwinding capacitances. Meanwhile, short-circuit fault influences winding inductances and resistances [85, 119]. The simulation of radial displacements could not be carried out using the 2D axisymmetric model. A 3D model would be required.

The axial displacement fault is created by inserting spacers at the bottom of winding 1 to displace it relative to winding 2, resulting in a loss of magnetic coupling between the windings. The short-circuit fault is created by shorting sections of winding 1. At first, winding 1

has the turns of section 2 (from top to bottom) shorted, with a total of 28 shorted turns; later, sections 2 and 3 are short, with 56 shorted turns.

Since the further objective of simulation frequency response results in the development of a database for training automatic classification algorithms, and the primary input used for these algorithms are numerical indices, the analysis of the deviations using the CSD numerical index is also done. The CSD index is widely used for its good performance in evaluating deviations in FRA traces, given its monotonicity, linearity, and sensitivity [29, 56, 77]. The CSD index is calculated from equation (V.1),

$$\text{CSD} = \sqrt{\frac{\sum_{i=1}^N [(X(i)-\bar{X}) - (Y(i)-\bar{Y})]^2}{N-1}}, \quad (\text{V.1})$$

$$\bar{X} = 1/N \sum_{i=1}^N X(i) \quad \text{and} \quad \bar{Y} = 1/N \sum_{i=1}^N Y(i),$$

where X and Y are the references and current frequency response vectors, $X(i)$ and $Y(i)$ are the i^{th} elements of these vectors, and N is the number of data points in vectors X and Y at the frequency band under evaluation.

The frequency band used for CSD calculation is selected to avoid the dependency of the transformer's structures in FRA traces. The sweep window method proposed in [31] is then applied. The method uses a frequency window (WS) determined from the number of data points per decade ($f_{p/d}$) in the trace, using equation (V.2). The window is then swept over the complete frequency range in pre-determined steps. The index is calculated for each window, and a vector of CSD values is obtained.

$$WS = 10 + 6 \left(\frac{f_{p/d} - 200}{200} \right). \quad (\text{V.2})$$

5.3. SIMULATED FREQUENCY RESPONSE OF WINDING MODEL

The 16-sections lumped element circuit shown in Figure V.5 is used to obtain the frequency response trace for the winding model from the FEM simulation. Due to the winding model specifications, a 16 sections circuit is used comprising series inductances and resistances from winding 1 (L_1 and R_1 , respectively) and winding 2 (L_2 , R_2 , respectively), along with series capacitances (C_1 and C_2), inter-winding capacitances (C_{12}) and ground capacitances (C_{g1} and C_{g2}).

The parameters of the circuit model are differently calculated. The inductances and series resistances are calculated directly from its geometry parameters and physics equations in FEM simulation. The series capacitances can be estimated by different methods, such as geometrical parameters and insulation materials [33, 109]. Since the individual winding measurements were available for this study, the series capacitances for each winding are estimated from individual winding frequency response measurements. A preliminary simulation with only one winding at a time is produced to obtain the series capacitance. This simulation provides the individual windings inductance values. The capacitances are then estimated using equation (V.3), and the resonance frequency values obtained from the individual winding measurements presented in Figure V.6a.

$$f_{\text{res}} = \frac{1}{2\pi \sqrt{L_i C_i}}, \quad (\text{V.3})$$

where f_{res} is the resonance frequency, L_i and C_i are the inductance and capacitance respectively.

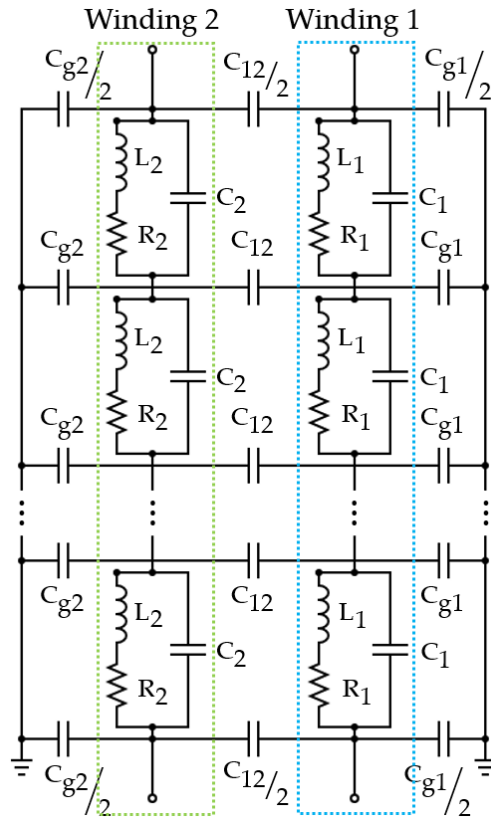


Figure V.5 Lumped element circuit used to obtain the simulated frequency response for the winding-model
 Source: Suassuna de Andrade Ferreira, 2022

Meanwhile, the inter-winding capacitance is estimated from the capacitive inter-winding FRA measurement presented in Figure V.6b and using equation (V.4). This equation is obtained from the transfer function of the measurement presented in equation (V.5) and uses a 50 Ω measurement impedance for the measuring instrument. The connections for a capacitive interwinding measurement are observed in Figure V.7.

$$C_{12} = \frac{50 \sin(\varphi)}{10^{CIW_{dB}/20} 2\pi f}, \quad (V.4)$$

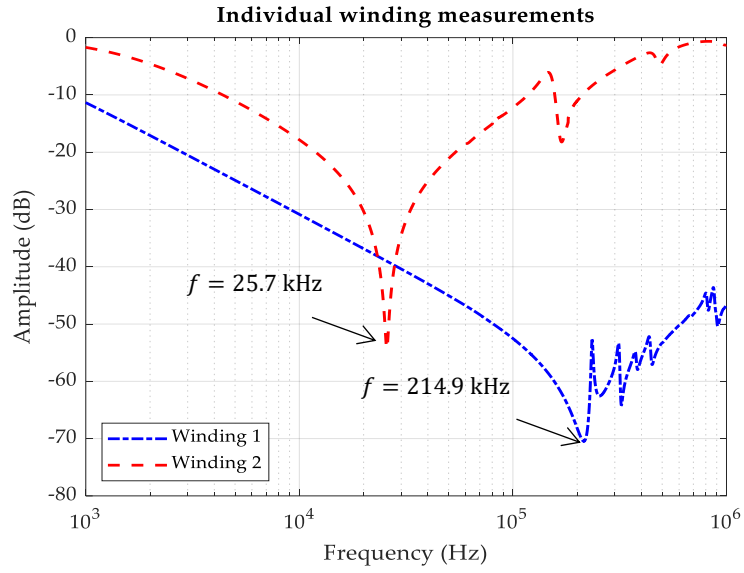
$$CIW_{dB} = 20 \log_{10} \left(\frac{V_{out}}{V_{in}} \right), \quad (V.5)$$

Later, all these capacitances are optimized to obtain a better fit between simulated and measured FRA traces. Thus, the simulation method can also be applied when sufficient information about the insulation of the transformer windings is unavailable. The estimated

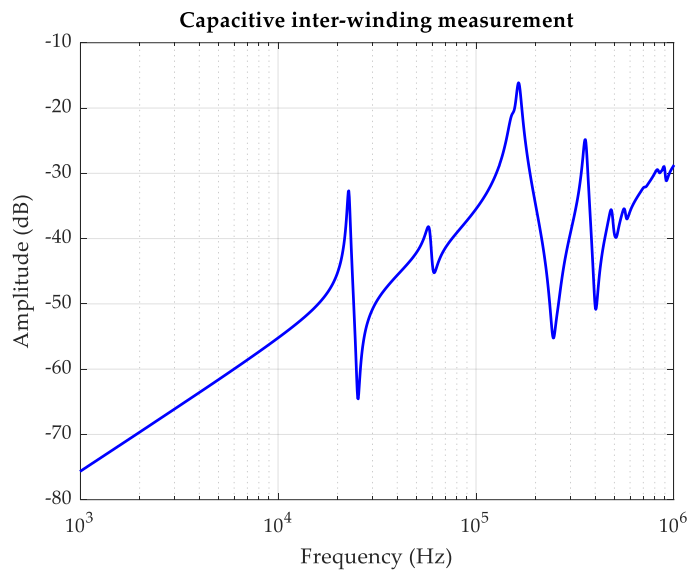
capacitance values, presented in Table V.1, are then introduced into the electric circuit to calculate the model's frequency response. The ground capacitances are small and negligible for this winding model since there is no ground structure near the windings. The measurements are taken inside a Faraday cage with larger dimensions than the winding height. Thus, to complete the electrical circuit presented in Figure V.5, the ground capacitances are considered as $C_{g1} = C_{g2} = 1 \times 10^{-16}$ F.

The initial frequency response obtained from the electrical circuit using the estimated parameters from Table V.1 is shown in Figure V.8. As it can be observed, the curves have similar trends, and the main resonances and anti-resonances are present in the simulated frequency response. However, the absolute error between the curves increases, especially at the resonance points. The mean square error for the curves presented in Figure V.8 is 23.20. This indicates that although the simulation and circuit models represent well the frequency response of the laboratory winding model, the estimated capacitances can still be adjusted to reach a better fit. Thus, the need to optimize the capacitance values.

The optimization is then performed. After about thirty interactions, the *fminsearch* obtained the new mean square error of 3.23. The final frequency response of the simulation after parameters optimization is presented in Figure V.9. The new optimized capacitance values obtained for the laboratory winding model are presented in Table V.2. In Figure V.9, it can be observed that the main resonances are still present. The error between curves has considerably lowered.



(a)



(b)

Figure V.6 Frequency response measurements (a) individual winding measurements and (b) capacitive interwinding measurement
Source: Suassuna de Andrade Ferreira, 2022

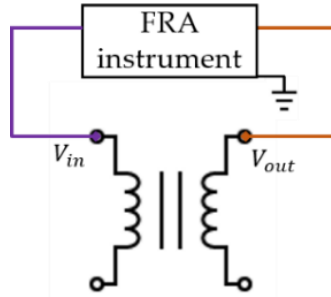


Figure V.7 FRA measurement schematic for interwinding capacitive measurement
Source: Suassuna de Andrade Ferreira, 2022

Table V.1 Initial values for capacitance parameters in frequency response simulation

Winding 1	Winding 2	Inter-winding
$C_{s1} = 2.00 \times 10^{-11}$ F	$C_{s2} = 6.98 \times 10^{-9}$ F	$C_{12} = 5.30 \times 10^{-10}$ F

Source: Suassuna de Andrade Ferreira, 2022

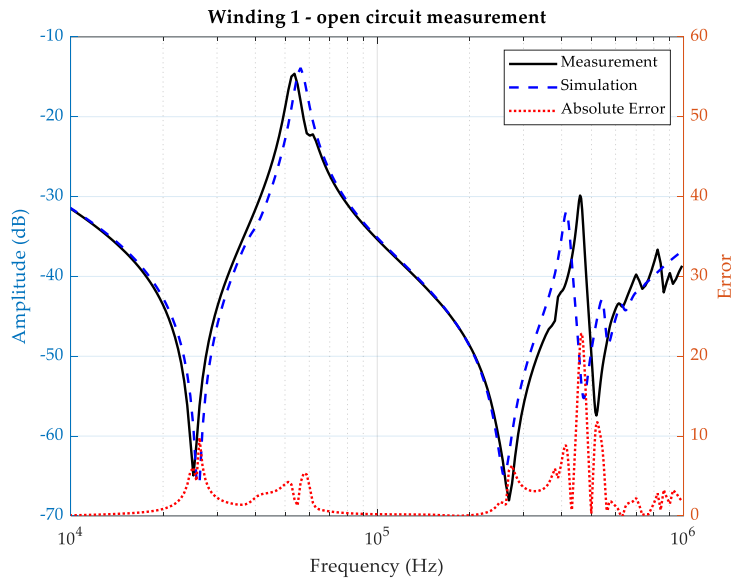


Figure V.8 Frequency response from winding model measurement and simulation using initial estimated values

Source: Suassuna de Andrade Ferreira, 2022

Table V.2 Optimized values for capacitance parameters in frequency response simulation

Winding 1	Winding 2	Inter-winding
$C_{s1} = 1.52 \times 10^{-11}$ F	$C_{s2} = 7.54 \times 10^{-9}$ F	$C_{12} = 5.29 \times 10^{-10}$ F

Source: Suassuna de Andrade Ferreira, 2022

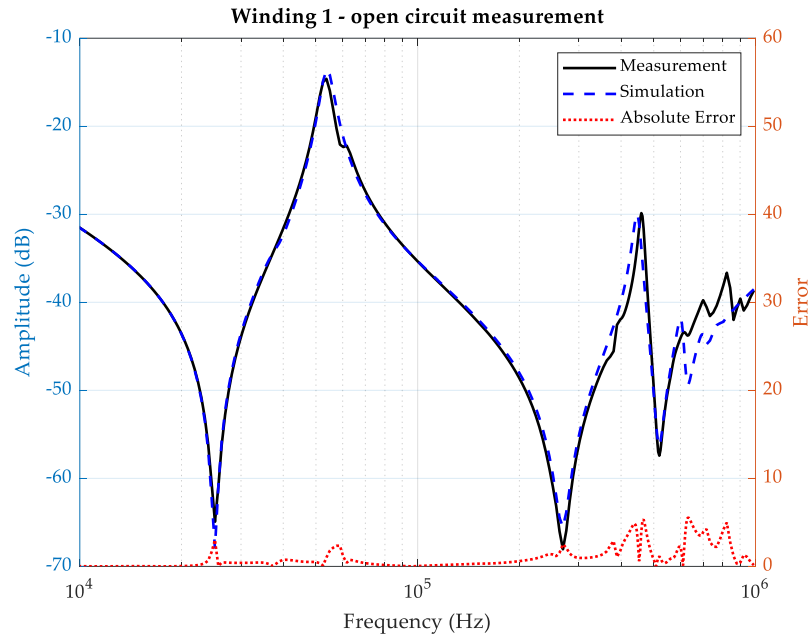


Figure V.9 Frequency response from winding model measurement and simulation using optimized capacitance values
Source: Suassuna de Andrade Ferreira, 2022

5.4. WINDING-MODEL FAULT ANALYSIS AND CLASSIFICATION PERFORMANCE

After the fault's introduction in the winding model, the frequency response obtained from simulation and the CSD index vectors are present in Figure V.10.

In Figure V.10a, it is possible to observe that the simulation has very slight deviations for the first axial displacement level. However, once the displacement increases, it is possible to better recognize the deviations due to the fault. In addition, the CSD values could identify slight deviations even for the lower displacement level, significantly above 400 kHz. The absence of deviations in the simulation's lower axial displacement (AD1) can occur due to the reduced sensibility of the simulation model to capacitance changes. Since the capacitances are the main parameters influenced in this fault, the low displacement levels associated with low capacitive changes might not be well represented in the simulation model.

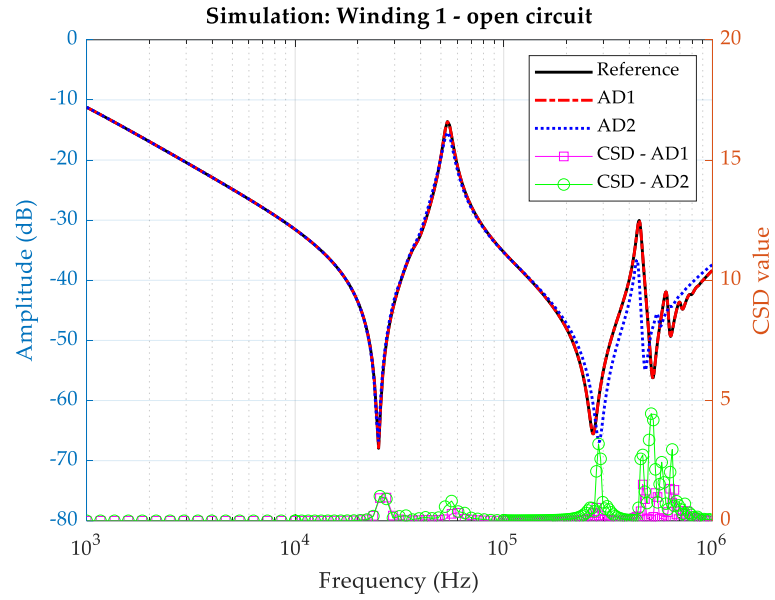
Meanwhile, the first and second fault levels can be distinguished from the reference simulation for the short-circuit fault. As shown in the CSD values presented in Figure V.10b.

Considering that the short-circuit fault has more impact on the capacitive and resistive circuit parameters, it can be noticed that these are also the most sensible parameters of the simulation model developed.

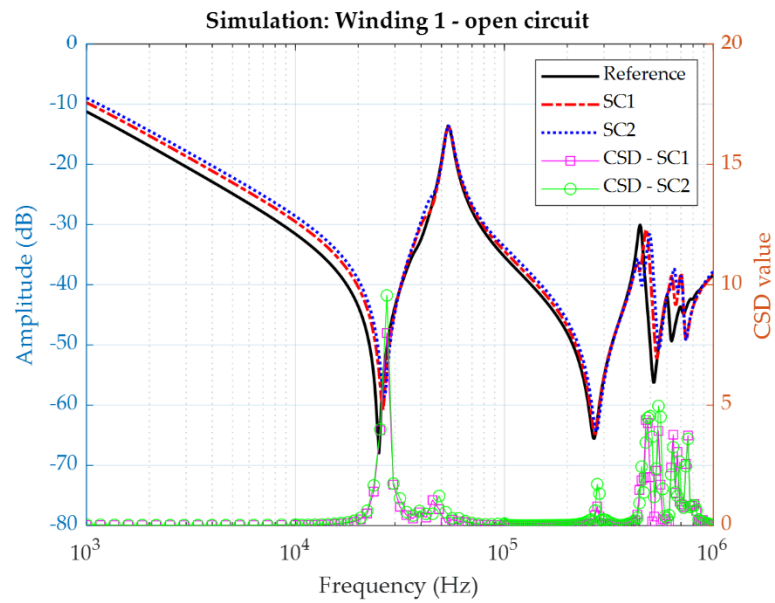
Furthermore, observing the frequency responses presented in Figure V.10, it is noticeable that the first resonance point (around 50 kHz) remains unaltered for any fault applied. This conclusion has previously been noticed in the different measurements performed for the same laboratory winding model [49], and this study shows that the simulation also reproduced the pattern. From the FEM simulation, it is possible to observe that this is the frequency of high energy density in the frequency range considered for any of the faults simulated.

The energy density can also be used to calculate the inductance of the model and further be applied in identifying faults, as presented in [78]. The simulation method can also apply new approaches for diagnostic by inductance changes. Preliminarily, the energy density of the model can be observed, and its variation due to the different faults can be identified, as shown in Figure V.11.

Finally, to evaluate the faulty simulation's ability to be used in automatic classification algorithms, the model support vector machine algorithm developed in [56] is tested using the five FRA traces presented in Figure V.10 from reference and faulty traces. For this analysis, the classification algorithm is trained using an extensive database, including axial displacements, short-circuits and other faults at different extents. The reference and the four faulty traces obtained from the simulation model developed in this research are used as a testing dataset. The algorithm used can detect and identify the different faults with a performance accuracy of 93,9%. The results for the classification of the simulated traces are presented in Table V.3.



(a)



(b)

Figure V.10 Winding model frequency response simulated for: (a) axial displacement and (b) short-circuit faults
Source: Suassuna de Andrade Ferreira, 2022

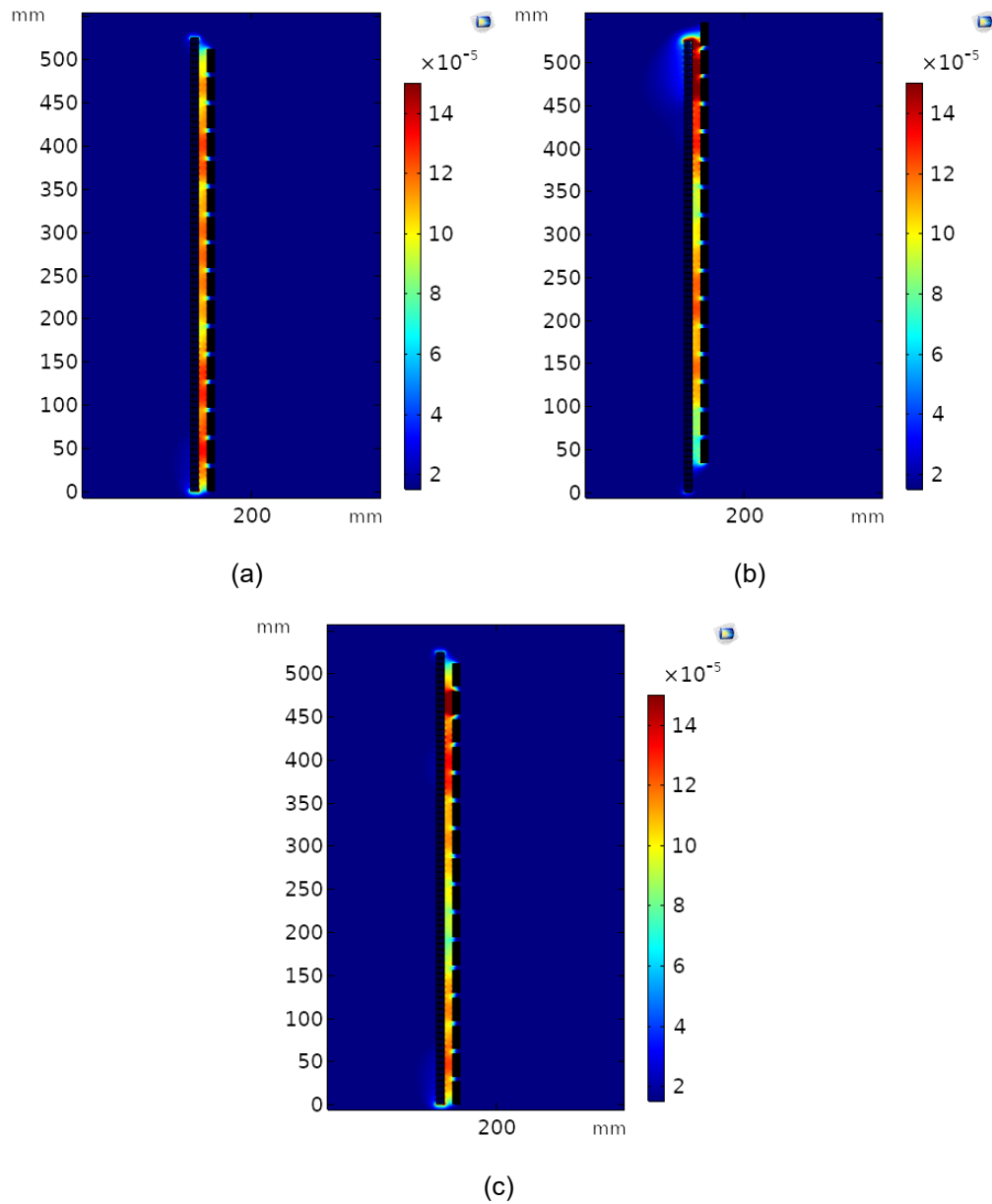


Figure V.11 Energy density distribution (J/m^3) for winding model simulation at 50 kHz for: (a) reference (no-fault), (b) axial displacement (AD2) and (c) short-circuit (SC1) faults
Source: Suassuna de Andrade Ferreira, 2022

From Table V.3, it is possible to observe that the reference and short-circuits fault are well classified in the algorithm. At the same time, the axial displacement was not always well classified, especially for the lower level of displacement. As already seen in Figure V.10, this fault level did not present enough deviations to be identified by the classification algorithm.

Moreover, this article presents an analysis opposite to what would ideally be usual regarding the databases used for training and testing the classification algorithms. This is due to a still limited amount of data from the simulations. Despite the capability of the simulation method, it is still necessary to expand the simulations to obtain other faults and extents and other transformers' design data. The research presented in this study is a proof-of-concept.

Table V.3 Automatic classification using support vector machine algorithm [56] and FRA traces obtained from simulation

Actual class	Classified as
No-Fault	No-Fault
Axial Displacement 1	No-Fault
Axial Displacement 2	Axial Displacement
Short-Circuit 1	Short-Circuit
Short-Circuit 2	Short-Circuit

Source: Suassuna de Andrade Ferreira, 2022

5.5. CONCLUSIONS

This paper reports a new method for frequency response simulation with optimization of capacitance parameters to fit measurement and simulation traces. The method's main objective is to access transformers' frequency response to develop and improve FRA interpretation techniques.

The proposed simulation method uses FEM to obtain inductive and resistive transformer parameters and the Nelder-Mead simplex algorithm to optimize estimated values for the capacitive parameters. Later, the parameters are integrated into lumped electrical circuit elements, and the circuit's transfer function is calculated to obtain the model's frequency response. The results indicate good agreements between the measured and simulated traces.

The evaluation of faulty simulated traces has demonstrated that while the method can reproduce short-circuit faults that classification algorithms can detect, the axial displacement faults are only well represented by the simulation method at the highest levels of displacement.

Due to its destructive nature, faulty measurements cannot be performed in real transformers. Using a laboratory model combined with simulation methods appears to be an interesting approach to contribute to the development of automatic and objective FRA interpretation algorithms. The proposed approach opens the door for obtaining infinite fault measurements on a single unit and generating a larger database of frequency responses. The method can further improve automatic fault classification algorithms by improving training databases.

CHAPTER VI

CONCLUSION

6.1. SUMMARY AND MAJOR FINDINGS

This research reports on frequency response interpretation using numerical indices, machine learning algorithms and FEM simulations. The FRA measurements and simulations are performed based on a laboratory transformer model. This model was specially designed so FRA measurements, under different circumstances, can be evaluated. It has removable sections and is designed and manufactured to enable short-circuits and mechanical deformations (axial or radial), allowing reproducibility and repeatability of frequency response measurements.

The main results obtained in the research are:

- The determination of good indices for evaluation of mechanical deformation severity showed that while all the indices were able to identify the highest levels of deformations in the frequency range of interest (400 kHz to 700 kHz), the best overall results of this study were obtained with the CSD, given its monotonic behaviour, linear increase with fault severity and sensitivity, even to the smallest deformations.
- The study of machine learning classifiers for fault diagnostics was very promising. The RBF, SVM and k-NN networks performed well when classifying faults using the CSD index and targeted frequency bands as input. SVM using polynomial ($p=3$) kernel function and k-NN with five neighbours have presented the best performance for the parameters optimization analysis.
- The study of the impact of temperature in automatic fault classification has shown that when the temperature parameter is not considered in the training set of the

machine learning algorithm, the classification can be compromised. At least 30% of the tested measurements were misclassified on the first attempt. The misclassification occurred predominantly in a group with temperature shifts of more than 30 °C from the reference temperature (20 °C).

- Finally, the proposed simulation method uses FEM to obtain inductive and resistive transformer parameters and the Nelder-Mead simplex algorithm to optimize estimated values for the capacitive parameters. These parameters are integrated into lumped electrical circuit elements, and the circuit's transfer function is calculated to obtain the model's frequency response. Results show a good match between measured and simulated FRA traces. Moreover, the short-circuit and axial displacements were introduced in the simulated model and analyzed using automatic classification algorithms. The classification algorithm presented good performance for short-circuit classification, while axial displacement was well classified at its greatest extents.

6.2. RESEARCH CONTRIBUTIONS

The following papers were produced under the course of development of the PhD research. The papers summarize the main results obtained in the research.

Three journal papers:

1. Regelii S. de A. Ferreira, Patrick Picher, Hassan Ezzaidi, Issouf Fofana, "Frequency Response Analysis Interpretation using Numerical Indices and Machine Learning: A Case Study based on a Laboratory Model" IEEE Access Volume 9, p. 67051-67063, April 2021.

2. Regelii S. de A. Ferreira, Patrick Picher, Hassan Ezzaidi, Issouf Fofana, "A Machine-Learning Approach to Identify the Influence of Temperature on FRA Measurements" *Energies* 2021, Volume 14, p. 5718, September 2021.

3. Regelii S. de A. Ferreira, Patrick Picher, Issouf Fofana, Hassan Ezzaidi, Christophe Volat, Fethi Meghnefi and Vahid Behjat, "Reproducing Transformer's Frequency Response from FEM Simulation and Parameters Optimization", this paper is under final review by the authors before submission.

And four conference papers:

1. R. M. Youssouf, R. S. A. Ferreira, F. Meghnefi, H. Ezzaidi, P. Picher and I. Fofana, "Frequency Response of Transformer Winding: A Case Study based on a Laboratory Model", 2018 CEIDP (Conference on Electrical Insulation and Dielectric Phenomena), October 21-24, 2018, Cancun, Mexico.

2. R. S. A. Ferreira, H. Simard, P. Picher, V. Behjat, I. Fofana et H. Ezzaidi, "Case study for assessing the integrity of a service-aged transformer repair using Frequency Response Analysis (FRA)", 2019 Congress CIGRÉ Canada, September 16-19, 2019, Montreal Canada.

3. Regelii S. A. Ferreira, Hassan Ezzaidi, Issouf Fofana, Patrick Picher, "Transformers Fault Identification by Frequency Response Analysis using Intelligent Classifiers", 2021 ISH (22nd International Symposium on High Voltage Engineering), November 21-25, 2021, Xi'an, China.

4. R. S. A. Ferreira, A. Sengupta, P. Picher, I. Fofana and H. Ezzaidi, "Influence of Transformer Structures on the Frequency Response Analysis: A Laboratory Case Study", 2021 CEIDP (Conference on Electrical Insulation and Dielectric Phenomena), December 12-15, 2021, Vancouver, Canada.

6.3. FUTURE OF THE RESEARCH AND RECOMMENDATIONS

For the continuity of this research topic and to address further aspects of FRA interpretation, some topics of attention are suggested:

- The development of a three-phase transformer model that is closer to a real transformer (including tank and core aspects) should enable a variety of possibilities to be added to this research, such as the impact of winding connections and the study of core faults in FRA measurements;
- The study of faults localization in the windings;
- The advance in FEM modelling to allow better reproduction of the model's capacitive parameters and improve the results of faults affecting these variables;
- The evolution of simulation methods to include other types of faults and temperature variations;
- The development of a large number of simulations results to support of the training of classification algorithms based on simulated FRA traces, which include but are not limited to different faults with different fault severities and at several different locations along the transformer windings;
- The study of the methods to generate mathematically calculated displacements to reproduce temperature variation in transformer's insulation media, so the temperature displacements can be determined ahead and introduced in training datasets of automatic classification algorithms;
- The study of real-case transformers can improve the algorithms proposed in this research and direct the results to more generalized conclusions.

REFERENCES

- [1] CIGRE WG A2.20, "Guide on economics of transformer management," *Brochure 248*, 2004.
- [2] J. F. Araujo, E. G. Costa, F. L. M. Andrade, A. D. Germano, and T. V. Ferreira, "Methodology to Evaluate the Electromechanical Effects of Electromagnetic Forces on Conductive Materials in Transformer Windings Using the Von Mises and Fatigue Criteria," *IEEE Trans Power Delivery*, vol. 31, no. 5, pp. 2206-2214, 2016, doi: 10.1109/TPWRD.2016.2579165.
- [3] CIGRE Working Group A2.18, "Life management techniques for power transformer," *Brochure 227*, 2003.
- [4] S. Tenbohlen *et al.*, "Results of a Standardized Survey about the Reliability of Power Transformers," presented at the 20th International Symposium on High Voltage Engineering, Buenos Aires, Argentina, August 27 - September 01, 2017.
- [5] CIGRE Technical Brochure 642, "Transformer Reliability Survey," 2015.
- [6] M. M. Islam, G. Lee, and S. N. Hettiwatte, "A review of condition monitoring techniques and diagnostic tests for lifetime estimation of power transformers," *Electr Eng*, Article in Press pp. 1-25, 2017, doi: 10.1007/s00202-017-0532-4.
- [7] M. Duval, "A review of faults detectable by gas-in-oil analysis in transformers," *IEEE Electr Insul Mag*, vol. 18, no. 3, pp. 8-17, 2002, doi: 10.1109/MEI.2002.1014963.
- [8] H. Malik, A. Azeem, and R. K. Jarial, "Application research based on modern-technology for transformer Health Index estimation," in *International Multi-Conference on Systems, Signals & Devices*, 20-23 March 2012 2012, pp. 1-7, doi: 10.1109/SSD.2012.6198012.
- [9] G. V. R. Xavier, H. S. Silva, E. G. d. Costa, A. J. R. Serres, N. B. Carvalho, and A. S. R. Oliveira, "Detection, Classification and Location of Sources of Partial Discharges Using the Radiometric Method: Trends, Challenges and Open Issues," *IEEE Access*, vol. 9, pp. 110787-110810, 2021, doi: 10.1109/ACCESS.2021.3102888.
- [10] I. Fofana, H. Hemmatjou, and F. Meghnefi, "Effect of thermal transient on the polarization and depolarization current measurements," *IEEE Trans Dielectr Electr Insul*, vol. 18, no. 2, pp. 513-520, 2011, doi: 10.1109/TDEI.2011.5739457.
- [11] M. Florkowski and J. Furgał, "Modelling of winding failures identification using the frequency response analysis (FRA) method," *Electr Power Syst Res*, vol. 79, no. 7, pp. 1069-1075, 2009, doi: 10.1016/j.epsr.2009.01.009.
- [12] S. M. Islam, "Detection of shorted turns and winding movements in large power transformers using frequency response analysis," in *IEEE Power Engineering Society Winter Meeting*, 23-27 Jan. 2000, vol. 3, pp. 2233-2238, doi: 10.1109/PESW.2000.847703.
- [13] K. Ragavan and L. Satish, "Localization of changes in a model winding based on terminal measurements: Experimental study," *IEEE Trans Power Delivery*, vol. 22, no. 3, pp. 1557-1565, 2007, doi: 10.1109/TPWRD.2006.886789.
- [14] L. Satish and S. K. Sahoo, "Locating faults in a transformer winding: An experimental study," *Electr Power Syst Res*, vol. 79, no. 1, pp. 89-97, 2009, doi: 10.1016/j.epsr.2008.05.020.
- [15] E. P. Dick and C. C. Erven, "Transformer diagnostic testing by frequency response analysis," *IEEE Trans. Power Appar. Syst.*, vol. PAS-97, no. 6, pp. 2144-2153, 1978, doi: 10.1109/TPAS.1978.354718.
- [16] CIGRE Technical Brochure 342, "Mechanical-Condition Assessment of Transformer Windings Using Frequency Response Analysis (FRA)," 2008.
- [17] P. Picher, S. Tenbohlen, M. F. Lachman, A. Scardazzi, and P. Patel, "Current state of transformer FRA interpretation," *Proceeding of the 4th International Colloquium "Transformer Research and Asset Management"*, 2017.

- [18] E. Rahimpour, J. Christian, K. Feser, and H. Mohseni, "Transfer function method to diagnose axial displacement and radial deformation of transformer windings," *IEEE Trans Power Delivery*, vol. 18, no. 2, pp. 493-505, 2003, doi: 10.1109/TPWRD.2003.809692.
- [19] E. Rahimpour, M. Jabbari, and S. Tenbohlen, "Mathematical Comparison Methods to Assess Transfer Functions of Transformers to Detect Different Types of Mechanical Faults," *IEEE Trans Power Delivery*, vol. 25, no. 4, pp. 2544-2555, 2010, doi: 10.1109/TPWRD.2010.2054840.
- [20] IEC 60076-18, "Measurement of frequency response," 2012.
- [21] IEEE Std C57.149-2012, "IEEE Guide for the Application and Interpretation of Frequency Response Analysis for Oil-Immersed Transformers," 2013, doi: 10.1109/IEEESTD.2013.6475950.
- [22] The Electric Power Industry Standard of People's Republic of China, "Frequency Response Analysis on Winding Deformation of Power Transformers," DL/T 911-2016.
- [23] D. A. K. Pham, T. M. T. Pham, H. Borsi, and E. Gockenbach, "A new diagnostic method to support standard frequency response analysis assessments for diagnostics of transformer winding mechanical failures," *IEEE Electr Insul Mag*, vol. 30, no. 2, pp. 34-41, 2014, doi: 10.1109/MEI.2014.6749571.
- [24] CIGRE Technical Brochure 812, "Advances in the interpretation of transformer Frequency Response Analysis (FRA)," 2020.
- [25] S. Tenbohlen, M. Tahir, E. Rahimpour, B. Poulin, and S. Miyazaki, "A new approach for high frequency modelling of disk windings," *CIGRE, A2-214*, 2018.
- [26] A. Moradzadeh, H. Moayyed, B. Mohammadi-Ivatloo, G. B. Gharehpetian, and A. P. Aguiar, "Turn-to-Turn Short Circuit Fault Localization in Transformer Winding via Image Processing and Deep Learning Method," *IEEE Transactions on Industrial Informatics*, pp. 1-1, 2021, doi: 10.1109/TII.2021.3105932.
- [27] A. A. Reykherdt and V. Davydov, "Case studies of factors influencing frequency response analysis measurements and power transformer diagnostics," (in), *IEEE Electr Insul Mag*, vol. 27, no. 1, pp. 22-30, 2011, Art no. 5699444, doi: 10.1109/MEI.2011.5699444.
- [28] M. Bagheri, B. T. Phung, and T. Blackburn, "Influence of temperature and moisture content on frequency response analysis of transformer winding," *IEEE Trans Dielectr Electr Insul*, vol. 21, no. 3, pp. 1393-1404, 2014, doi: 10.1109/TDEI.2014.6832288.
- [29] M. Bigdeli, P. Siano, and H. H. Alhelou, "Intelligent Classifiers in Distinguishing Transformer Faults Using Frequency Response Analysis," *IEEE Access*, vol. 9, pp. 13981-13991, 2021, doi: 10.1109/ACCESS.2021.3052144.
- [30] M. Bigdeli, M. Vakilian, and E. Rahimpour, "Transformer winding faults classification based on transfer function analysis by support vector machine," *IET Electr Power Appl*, vol. 6, no. 5, pp. 268-276, 2012, doi: 10.1049/iet-epa.2011.0232.
- [31] M. Tahir and S. Tenbohlen, "Novel calculation method for power transformer winding fault detection using Frequency Response Analysis," in *5th International Colloquium "Transformer Research and Asset Management"*, 2019.
- [32] S. M. Al-Ameri *et al.*, "Understanding the Influence of Power Transformer Faults on the Frequency Response Signature using Simulation Analysis and Statistical Indicators," *IEEE Access*, pp. 1-1, 2021, doi: 10.1109/ACCESS.2021.3076984.
- [33] N. Abeywickrama, Y. V. Serdyuk, and S. M. Gubanski, "High-frequency modeling of power transformers for use in frequency response analysis (FRA)," *IEEE Trans Power Delivery*, vol. 23, no. 4, pp. 2042-2049, 2008, doi: 10.1109/TPWRD.2008.917896.
- [34] A. Franzen and S. Karlsson, "Failure Modes and Effects Analysis of Transformers," Royal Institute of Technology - School of Electrical Engineering, Stockholm, Sweden, 2007.

- [35] W. H. Tang and Q. H. Wu, *Condition Monitoring and Assessment of Power Transformers Using Computational Intelligence*. Springer, 2011, p. 202.
- [36] W. Lech and L. Tyminski, "Detecting Transformer Winding Damage - The Low Voltage Impulse Method," *Electrical Review*, vol. 18, 1966.
- [37] M. H. Samimi, S. Tenbohlen, A. A. S. Akmal, and H. Mohseni, "Evaluation of numerical indices for the assessment of transformer frequency response," *IET Generation, Transmission and Distribution*, vol. 11, no. 1, pp. 218-227, 2017, doi: 10.1049/iet-gtd.2016.0879.
- [38] M. H. Samimi and S. Tenbohlen, "FRA interpretation using numerical indices: State-of-the-art," *Int J Electr Power Energy Syst*, Review vol. 89, pp. 115-125, 2017, doi: 10.1016/j.ijepes.2017.01.014.
- [39] S. w. Fei and X. b. Zhang, "Fault diagnosis of power transformer based on support vector machine with genetic algorithm," *Expert Systems with Applications*, vol. 36, no. 8, pp. 11352-11357, 2009, doi: 10.1016/j.eswa.2009.03.022.
- [40] X. Mao, Z. Wang, P. Crossley, P. Jarman, A. Fieldsend-Roxborough, and G. Wilson, "Transformer winding type recognition based on FRA data and a support vector machine model," *High Voltage*, vol. 5, no. 6, pp. 704-715, 2020, doi: 10.1049/hve.2019.0294.
- [41] A. J. Ghanizadeh and G. B. Gharehpetian, "ANN and cross-correlation based features for discrimination between electrical and mechanical defects and their localization in transformer winding," *IEEE Trans Dielectr Electr Insul*, vol. 21, no. 5, pp. 2374-2382, 2014, doi: 10.1109/TDEI.2014.004364.
- [42] R. S. A. Ferreira, H. Simard, P. Picher, V. Behjat, I. Fofana, and H. Ezzaidi, "Case study for assessing the integrity of a service-aged transformer repair using Frequency Response Analysis (FRA)," presented at the 2019 CIGRE Canada Conference, Montréal, Québec, 2019.
- [43] R. Youssouf, R. Ferreira, F. Meghnefi, H. Ezzaidi, I. Fofana, and P. Picher, "Frequency Response of Transformer Winding: A Case Study based on a Laboratory Model," in *2018 IEEE Conference on Electrical Insulation and Dielectric Phenomena (CEIDP)*, 2018: IEEE, pp. 271-274.
- [44] Z. Wang, J. Li, and D. M. Sofian, "Interpretation of Transformer FRA Responses - Part I: Influence of Winding Structure," *IEEE Trans Power Delivery*, vol. 24, no. 2, pp. 703-710, 2009, doi: 10.1109/TPWRD.2009.2014485.
- [45] D. M. Sofian, Z. Wang, and J. Li, "Interpretation of Transformer FRA Responses - Part II: Influence of Transformer Structure," *IEEE Trans Power Delivery*, vol. 25, no. 4, pp. 2582-2589, 2010, doi: 10.1109/TPWRD.2010.2050342.
- [46] X. Mao, Z. Wang, P. Jarman, and A. Fieldsend-Roxborough, "Winding Type Recognition through Supervised Machine Learning using Frequency Response Analysis (FRA) Data," in *ICEMPE 2019 - 2nd International Conference on Electrical Materials and Power Equipment, Proceedings*, 2019, pp. 588-591, doi: 10.1109/ICEMPE.2019.8727354.
- [47] S. M. Saleh, S. H. El-Hoshy, and O. E. Gouda, "Proposed diagnostic methodology using the cross-correlation coefficient factor technique for power transformer fault identification," *IET Electr Power Appl*, vol. 11, no. 3, pp. 412-422, 2017, doi: 10.1049/iet-epa.2016.0545.
- [48] R. Wimmer, S. Tenbohlen, M. Heindl, A. Kraetge, M. Krüger, and J. Christian, "Development of algorithms to assess the FRA," presented at the 15th International Symposium on High Voltage Engineering, Ljubljana, Slovenia, 2007.
- [49] R. S. D. A. Ferreira, P. Picher, H. Ezzaidi, and I. Fofana, "Frequency Response Analysis Interpretation Using Numerical Indices and Machine Learning: A Case Study Based on a Laboratory Model," *IEEE Access*, vol. 9, pp. 67051-67063, 2021, doi: 10.1109/ACCESS.2021.3076154.

- [50] P. M. Nirgude, D. Ashokraju, A. D. Rajkumar, and B. P. Singh, "Application of numerical evaluation techniques for interpreting frequency response measurements in power transformers," *IET Sci. Meas. Technol.*, vol. 2, no. 5, pp. 275-285, 2008, doi: 10.1049/iet-smt:20070072.
- [51] J. C. G. Arispe and E. E. Mombello, "Detection of Failures Within Transformers by FRA Using Multiresolution Decomposition," *IEEE Trans Power Delivery*, vol. 29, no. 3, pp. 1127-1137, 2014, doi: 10.1109/TPWRD.2014.2306674.
- [52] K. Pourhossein, G. B. Gharehpetian, E. Rahimpour, and B. N. Araabi, "A probabilistic feature to determine type and extent of winding mechanical defects in power transformers," *Electr Power Syst Res*, vol. 82, no. 1, pp. 1-10, 2011, doi: 10.1016/j.epsr.2011.08.010.
- [53] K. P. Badgujar, M. Maoyafikuddin, and S. V. Kulkarni, "Alternative statistical techniques for aiding SFRA diagnostics in transformers," *IET Generation, Transmission & Distribution*, vol. 6, no. 3, pp. 189-198, 2012, doi: 10.1049/iet-gtd.2011.0268.
- [54] M. H. Samimi, S. Tenbohlen, A. A. Shayegani Akmal, and H. Mohseni, "Improving the numerical indices proposed for the FRA interpretation by including the phase response," *Int J Electr Power Energy Syst*, vol. 83, pp. 585-593, 2016, doi: 10.1016/j.ijepes.2016.04.044.
- [55] M. Bagheri, B. T. Phung, T. Blackburn, and A. Naderian, "Influence of temperature on frequency response analysis of transformer winding," in *31st Electrical Insulation Conference, EIC*, Ottawa, Canada, 2013, pp. 40-44, doi: 10.1109/EIC.2013.6554198.
- [56] R. Suassuna de Andrade Ferreira, P. Picher, H. Ezzaidi, and I. Fofana, "A Machine-Learning Approach to Identify the Influence of Temperature on FRA Measurements," *Energies*, vol. 14, no. 18, p. 5718, 2021.
- [57] J. W. Kim, B. K. Park, S. C. Jeong, S. W. Kim, and P. G. Park, "Fault diagnosis of a power transformer using an improved frequency-response analysis," *IEEE Trans Power Delivery*, vol. 20, no. 1, pp. 169-178, 2005, doi: 10.1109/TPWRD.2004.835428.
- [58] M. Heindl, S. Tenbohlen, A. Kraetge, M. Krüger, and J. Velásquez, "Algorithmic determination of pole-zero representations of power transformers' transfer functions for interpretation of FRA data," presented at the 16th International Symposium on High Voltage Engineering, Cape Town, South Africa, 2009.
- [59] E. Rahimpour and D. Gorzin, "A new method for comparing the transfer function of transformers in order to detect the location and amount of winding faults," *Electr Eng*, vol. 88, no. 5, pp. 411-416, 2006, doi: 10.1007/s00202-005-0294-2.
- [60] R. S. A. Ferreira, H. Ezzaidi, I. Fofana, and P. Picher, "Transformers Fault Identification by Frequency Response Analysis using Intelligent Classifiers," presented at the 22nd Symposium on High Voltage Engineering (ISH 2021), Xi'an, China, 21-25 November 2021, 2021.
- [61] P. Karimifard, G. B. Gharehpetian, and S. Tenbohlen, "Determination of axial displacement extent based on transformer winding transfer function estimation using vector-fitting method," *Eur Trans Electr Power*, vol. 18, no. 4, pp. 423-436, 2008, doi: 10.1002/etep.194.
- [62] M. Tahir, S. Tenbohlen, and M. Samimi, "Evaluation Of Numerical Indices For Objective Interpretation Of Frequency Response To Detect Mechanical Faults In Power Transformers," *21st International Symposium on High Voltage Engineering*, 2019.
- [63] M. H. Samimi, S. Tenbohlen, A. A. S. Akmal, and H. Mohseni, "Effect of Different Connection Schemes, Terminating Resistors and Measurement Impedances on the Sensitivity of the FRA Method," *IEEE Trans Power Delivery*, vol. 32, no. 4, pp. 1713-1720, 2017, doi: 10.1109/TPWRD.2016.2572160.
- [64] M. H. Samimi, A. A. Shayegani Akmal, H. Mohseni, and S. Tenbohlen, "Detection of transformer mechanical deformations by comparing different FRA connections," *International Journal of Electrical Power & Energy Systems*, vol. 86, pp. 53-60, 2017 2017, doi: <https://doi.org/10.1016/j.ijepes.2016.09.007>.

- [65] S. A. Ryder, "Diagnosing transformer faults using frequency response analysis," *IEEE Electr Insul Mag*, vol. 19, no. 2, pp. 16-22, 2003, doi: 10.1109/MEI.2003.1192032.
- [66] The Electric Power Industry Standard of People's Republic of China, "Frequency Response Analysis on Winding Deformation of Power Transformers," DL/T 911-2004.
- [67] W. C. Sant'Ana *et al.*, "A survey on statistical indexes applied on frequency response analysis of electric machinery and a trend based approach for more reliable results," *Electr Power Syst Res*, vol. 137, pp. 26-33, 2016/08/01/ 2016, doi: <https://doi.org/10.1016/j.epsr.2016.03.044>.
- [68] G. M. Kennedy, A. J. McGrail, and J. A. Lapworth, "Using Cross-Correlation Coefficients to Analyze Transformer Sweep Frequency Response Analysis (SFRA) Traces," in *2007 IEEE Power Engineering Society Conference and Exposition in Africa - PowerAfrica*, 16-20 July 2007 2007, pp. 1-6, doi: 10.1109/PESAFR.2007.4498059.
- [69] J.-W. Kim, B. Park, S. C. Jeong, S. W. Kim, and P. Park, "Fault diagnosis of a power transformer using an improved frequency-response analysis," *IEEE Trans Power Delivery*, vol. 20, no. 1, pp. 169-178, 2005.
- [70] T. Y. Ji, W. H. Tang, and Q. H. Wu, "Detection of power transformer winding deformation and variation of measurement connections using a hybrid winding model," *Electr Power Syst Res*, vol. 87, pp. 39-46, 2012/06/01/ 2012, doi: <https://doi.org/10.1016/j.epsr.2012.01.007>.
- [71] W. H. Tang, A. Shintemirov, and Q. H. Wu, "Detection of minor winding deformation fault in high frequency range for power transformer," in *IEEE PES General Meeting*, 25-29 July 2010 2010, pp. 1-6, doi: 10.1109/PES.2010.5589573.
- [72] V. Behjat and M. Mahvi, "Statistical approach for interpretation of power transformers frequency response analysis results," *IET Sci. Meas. Technol.*, vol. 9, no. 3, pp. 367-375, 2015, doi: 10.1049/iet-smt.2014.0097.
- [73] S. Miyazaki, M. Tahir, and S. Tenbohlen, "Detection and quantitative diagnosis of axial displacement of transformer winding by frequency response analysis," *IET Generation, Transmission & Distribution*, vol. 13, no. 15, pp. 3493-3500, 2019, doi: 10.1049/iet-gtd.2018.6032.
- [74] D. M. Sofian, "Transformer FRA Interpretation for Detection of Winding Movement," Ph.D., University of Manchester, England, 2007.
- [75] J. Velasquez, D. Kolb, M. A. Sanz-Bobi, and W. Koltunowicz, "Identification of transformer-specific frequency sub-bands as basis for a reliable and automatic assessment of FRA results," presented at the Conference on Condition Monitoring and Diagnosis (CMD), Tokyo, Japan, 6-11 September, 2010.
- [76] J. Velasquez, "Intelligent monitoring and diagnosis of power transformers in the context of an asset management model," Ph.D., Department of electrical engineering, Polytechnic University of Catalonia, 2011.
- [77] M. Tahir and S. Tenbohlen, "Transformer Winding Condition Assessment Using Feedforward Artificial Neural Network and Frequency Response Measurements," *Energies*, vol. 14, no. 11, p. 3227, 2021, doi: 10.3390/en14113227.
- [78] P. Mukherjee and S. K. Panda, "Diagnosing disk-space variation in transformer windings using high-frequency inductance measurement," *IEEE Trans Power Delivery*, 2022, doi: 10.1109/TPWRD.2022.3148598.
- [79] A. Abu-Siada, M. I. Mosaad, D. Kim, and M. F. El-Naggar, "Estimating Power Transformer High Frequency Model Parameters Using Frequency Response Analysis," *IEEE Trans Power Delivery*, Article vol. 35, no. 3, pp. 1267-1277, 2020, Art no. 8818329, doi: 10.1109/TPWRD.2019.2938020.
- [80] S. K. Sahoo and L. Satish, "Discriminating changes introduced in the model for the winding of a transformer based on measurements," *Electr Power Syst Res*, vol. 77, no. 7, pp. 851-858, 2007, doi: 10.1016/j.epsr.2006.07.007.

- [81] K. H. Ibrahim, N. R. Korany, and S. M. Saleh, "Effects of power transformer high-frequency equivalent circuit parameters non-uniformity on fault diagnosis using SFRA test," *Ain Shams Engineering Journal*, vol. 13, no. 4, p. 101674, 2022/06/01/ 2022, doi: <https://doi.org/10.1016/j.asej.2021.101674>.
- [82] V. Larin, "Internal short-circuits faults localization in transformer windings using FRA and natural frequencies deviation patterns," *CIGRE SC A2 Colloquium, Cracow, Poland*, 2017.
- [83] V. Larin, D. Matveev, and A. Y. Volkov, "Application of natural frequencies deviations patterns and high-frequency white-box transformer models for FRA interpretation," *CIGRE paper A2-209*, 2018.
- [84] S. Miyazaki, Y. Mizutani, T. Okamoto, Y. Wada, and C. Hayashida, "Abnormality diagnosis of transformer winding by frequency response analysis (FRA) using circuit model," in *Proceedings of 2012 IEEE International Conference on Condition Monitoring and Diagnosis, CMD 2012*, 2012, pp. 273-276, doi: 10.1109/CMD.2012.6416429.
- [85] A. Abu-Siada, N. Hashemnia, S. Islam, and M. Masoum, "Understanding power transformer frequency response analysis signatures," *IEEE Electr Insul Mag*, vol. 29, no. 3, pp. 48-56, 2013, doi: 10.1109/MEI.2013.6507414.
- [86] M. Bigdeli, D. Azizian, and G. B. Gharehpetian, "Detection of probability of occurrence, type and severity of faults in transformer using frequency response analysis based numerical indices," *Measurement: Journal of the International Measurement Confederation*, Article vol. 168, 2021, Art no. 108322, doi: 10.1016/j.measurement.2020.108322.
- [87] B. A. Thango, A. F. Nnachi, G. A. Dlamini, and P. N. Bokoro, "A Novel Approach to Assess Power Transformer Winding Conditions Using Regression Analysis and Frequency Response Measurements," *Energies*, vol. 15, no. 7, p. 2335, 2022.
- [88] A. De and N. Chatterjee, "Impulse fault diagnosis in power transformers using self-organising map and learning vector quantisation," *IEE Proceedings: Generation, Transmission and Distribution*, Conference Paper vol. 148, no. 5, pp. 397-405, 2001, doi: 10.1049/ip-gtd:20010462.
- [89] G. M. V. Zambrano, A. C. Ferreira, and L. P. Calôba, "Power transformer equivalent circuit identification by artificial neural network using frequency response analysis," in *IEEE Power Engineering Society General Meeting, PES*, Montreal, Canada, 2006.
- [90] S. M. Piryonesi and T. E. El-Diraby, "Role of Data Analytics in Infrastructure Asset Management: Overcoming Data Size and Quality Problems," *Journal of Transportation Engineering, Part B: Pavements*, vol. 146, no. 2, p. 04020022, 2020, doi: doi:10.1061/JPEODX.0000175.
- [91] C. McCormick. "RADIAL BASIS FUNCTION NETWORK (RBFN) TUTORIAL." <https://chrisjmcormick.wordpress.com/2013/08/15/radial-basis-function-network-rbfn-tutorial/> (accessed 10 May, 2022).
- [92] L. Hamel, *Knowledge Discovery with Support Vector Machines* (Wiley Series on Methods and Applications in Data Mining). Hoboken, New Jersey, USA: John Wiley & Sons, Inc., 2009.
- [93] Z. Zhao, C. Yao, C. Tang, C. Li, F. Yan, and S. Islam, "Diagnosing Transformer Winding Deformation Faults Based on the Analysis of Binary Image Obtained from FRA Signature," *IEEE Access*, Article vol. 7, pp. 40463-40474, 2019, Art no. 8674767, doi: 10.1109/ACCESS.2019.2907648.
- [94] H. Tarimoradi and G. B. Gharehpetian, "Novel Calculation Method of Indices to Improve Classification of Transformer Winding Fault Type, Location, and Extent," *IEEE Transactions on Industrial Informatics*, vol. 13, no. 4, pp. 1531-1540, 2017, doi: 10.1109/TII.2017.2651954.
- [95] M. F. Lachman, V. Fomichev, V. Rashkovsky, and A. Shaikh, "Frequency response analysis of transformers: visualizing physics behind the trace," *Proceedings of the Seventy-Eighth Annual International Conference of Doble Clients*, Sec. T-14, 2011.

- [96] A. Moradzadeh and K. Pourhossein, "Application of Support Vector Machines to Locate Minor Short Circuits in Transformer Windings," in *2019 54th International Universities Power Engineering Conference (UPEC)*, 3-6 Sept. 2019 2019, pp. 1-6, doi: 10.1109/UPEC.2019.8893542.
- [97] V. Nurmanova, M. Bagheri, A. Zollanvari, K. Aliakhmet, Y. Akhmetov, and G. B. Gharehpetian, "A New Transformer FRA Measurement Technique to Reach Smart Interpretation for Inter-Disk Faults," *IEEE Trans Power Delivery*, Article vol. 34, no. 4, pp. 1508-1519, 2019, Art no. 8682123, doi: 10.1109/TPWRD.2019.2909144.
- [98] P. Picher, C. Rajotte, and C. Tardif, "Experience with frequency response analysis (FRA) for the mechanical condition assessment of transformer windings," in *31st Electrical Insulation Conference, EIC*, Ottawa, Canada, 2013, pp. 220-224, doi: 10.1109/EIC.2013.6554237.
- [99] M. Tahir, S. Tenbholen, and S. Miyazaki, "Analysis of Statistical Methods for Assessment of Power Transformer Frequency Response Measurements," *IEEE Trans Power Delivery*, vol. 36, no. 2, pp. 618-626, 2021, doi: 10.1109/TPWRD.2020.2987205.
- [100] S. Tenbohlen, S. Coenen, M. Djamali, A. Müller, H. M. Samimi, and M. Siegel, "Diagnostic Measurements for Power Transformers," *Energies*, vol. 9, no. 5, 2016, doi: 10.3390/en9050347.
- [101] J. Liu, Z. Zhao, C. Tang, C. Yao, C. Li, and S. Islam, "Classifying Transformer Winding Deformation Fault Types and Degrees Using FRA Based on Support Vector Machine," *IEEE Access*, vol. 7, pp. 112494-112504, 2019, doi: 10.1109/ACCESS.2019.2932497.
- [102] S. S. Haykin, *Neural Networks: A Comprehensive Foundation*. Prentice Hall, 1999.
- [103] V. Kecman, T.-M. Huang, and M. Vogt, "Iterative Single Data Algorithm for Training Kernel Machines from Huge Data Sets: Theory and Performance," in *Support Vector Machines: Theory and Applications*, L. Wang Ed. Berlin, Heidelberg: Springer Berlin Heidelberg, 2005, pp. 255-274.
- [104] M. H. Samimi, S. Tenbohlen, A. A. S. Akmal, and H. Mohseni, "Dismissing Uncertainties in the FRA Interpretation," *IEEE Trans Power Delivery*, vol. 33, no. 4, pp. 2041-2043, 2018, doi: 10.1109/TPWRD.2016.2618601.
- [105] R. S. d. A. Ferreira, P. Picher, H. Ezzaidi, and I. Fofana, "Frequency Response Analysis Interpretation using Numerical Indices and Machine Learning: A Case Study based on a Laboratory Model," *IEEE Access*, pp. 1-1, 2021, doi: 10.1109/ACCESS.2021.3076154.
- [106] M. Tahir and S. Tenbohlen, "Novel calculation method for power transformer winding fault detection using Frequency Response Analysis," presented at the 5th International Colloquium "Transformer Research and Asset Management", 2019.
- [107] "Weka: Machine Learning Software." <https://www.cs.waikato.ac.nz/ml/weka/> (accessed 15th July, 2021).
- [108] S. Bernhard, P. John, and H. Thomas, "An Efficient Method for Gradient-Based Adaptation of Hyperparameters in SVM Models," in *Advances in Neural Information Processing Systems 19: Proceedings of the 2006 Conference*: MIT Press, 2007, pp. 673-680.
- [109] E. Bjerkan, "High frequency modeling of power transformers," Trondheim, 2005.
- [110] T. Tsutaoka, M. Ueshima, T. Tokunaga, T. Nakamura, and K. Hatakeyama, "Frequency dispersion and temperature variation of complex permeability of Ni-Zn ferrite composite materials," *J Appl Phys*, vol. 78, no. 6, pp. 3983-3991, 1995, doi: 10.1063/1.359919.
- [111] I.-K. Suh, H. Ohta, and Y. Waseda, "High-temperature thermal expansion of six metallic elements measured by dilatation method and X-ray diffraction," *Journal of Materials Science*, vol. 23, no. 2, pp. 757-760, 1988/02/01 1988, doi: 10.1007/BF01174717.
- [112] N. Abeywickrama, "Effect of dielectric and magnetic material characteristics on frequency response of power transformers," Ph.D., Chalmers University of Technology, 2007.

- [113] Y. Liu *et al.*, "A study of the sweep frequency impedance method and its application in the detection of internal winding short circuit faults in power transformers," *IEEE Trans Dielectr Electr Insul*, vol. 22, no. 4, pp. 2046-2056, 2015, doi: 10.1109/TDEI.2015.004977.
- [114] S. Alsuhaibani, Y. Khan, A. Beroual, and N. H. Malik, "A Review of Frequency Response Analysis Methods for Power Transformer Diagnostics," *Energies*, vol. 9, no. 11, p. 879, 2016.
- [115] R. Khalili Senobari, J. Sadeh, and H. Borsi, "Frequency response analysis (FRA) of transformers as a tool for fault detection and location: A review," *Electr Power Syst Res, Review* vol. 155, pp. 172-183, 2018, doi: 10.1016/j.epsr.2017.10.014.
- [116] K. V. S. Narasimha Swamy and U. Savadamuthu, "Sweep frequency response based statistical approach for locating faults in transformer windings using sliding window technique," *Electr Power Syst Res*, vol. 194, p. 107061, 2021/05/01/ 2021, doi: <https://doi.org/10.1016/j.epsr.2021.107061>.
- [117] P. Saji, A. Muhammed, and V. V, "Estimating The Effect of Axial Displacement on Equivalent Circuit Parameters of Transformer Winding Using Finite Element Method," in *2021 IEEE 5th International Conference on Condition Assessment Techniques in Electrical Systems (CATCON)*, 3-5 Dec. 2021 2021, pp. 311-316, doi: 10.1109/CATCON52335.2021.9670500.
- [118] J. C. Lagarias, J. A. Reeds, M. H. Wright, and P. E. Wright, "Convergence Properties of the Nelder--Mead Simplex Method in Low Dimensions," *SIAM Journal on Optimization*, vol. 9, no. 1, pp. 112-147, 1998, doi: 10.1137/s1052623496303470.
- [119] S. Miyazaki, Y. Mizutani, H. Suzuki, and M. Ichikawa, "Abnormality Diagnosis of Transformer Winding by Frequency Response Analysis (FRA) Using Circuit Model," in *IEEE International Conference on Condition Monitoring and Diagnosis (CMD)*, Bali, Indonesia, 23-27 September 2012, pp. 964-967.